Dissertation

Submitted to the

Combined Faculties for the Natural Sciences and for Mathematics

of the Ruperto-Carola University of Heidelberg, Germany

For the degree of

Doctor of Natural Sciences

Presented by

Marta Fratini, M.Sc.

Born in: Rome, Italy

Oral-examination: 18th of September 2018

Biophysical determinants of virus-cell interaction at the single particle level.

Referees:

Prof. Dr. Ralf Bartenschlager

Dr. Steeve Boulant

To my parents

Table of Contents

Acknowledgements

Looking back at this PhD in many years from now, some people might think:
"OK, that was just a PhD, what the fuss is all about?"

Yes, perhaps I will think this as well. Perhaps. Perhaps I will forget all this anger I had towards those who behaved unfairly and rudely to me. Perhaps I will forget those who tried to claim credit for things they did not do. Perhaps I will forget those who tried to push me down and thought I was weak. Perhaps I will forget all of this.

But I am sure I will keep strong in my mind all the precious scientists and friends that have walked with me these years, who gave me support, excellent ideas and new perspectives, who are, to me, an amazing proof that science can still be pure and the result of a collaborative, team-working effort, to look closer at the perfection of our nature and everything that surround us.

For this I would like to first thank my supervisors Dr. Steeve Boulant and Dr. Ada Cavalcanti-Adam, who gave me this big chance to work in here, in Heidelberg. I want to thank them in first place, for being "good humans", to consider their students really as students, as people who want to learn, grow and understand how to really do science. I want to thank them for being excellent scientific mentors, teaching me all about my project, for their immense patience to repeat steps that were not clear to me, and for challenging me at the right moment. Thank you for building up this project together, from zero, for feeding my enthusiasm with long discussions and excellent questions. In particular, thank you, Ada, for welcoming me in your department without never judging the limited experience I had at that time and for believing in my potential; thank you for being always so kind and patient when things were not working. Importantly, thank you for introducing me to this exciting topic of mechanobiology and surface chemistry that became the field I would like to pursue in the future. And of course a big thank you goes to Steeve. Thank you, Steeve, for giving me a chance, thank you for your strongly dedicated supervision, thank you for sitting next to me at my bench during my first days in the lab, for being patient and teaching me every single step of the experiments, thank you for being always available for discussing problems and experiments and also for

being pushy and asking with no mercy for data and figures (and I admit I have learnt with time to appreciate also this!).
Although, sometimes, having two supervisors was tiring -double meetings, double retreats, double experiment requests- I feel lucky with your guidance and I will cherish it.
A big thanks goes also to my TAC committee members, Prof. Dr. Ralf Bartenschlager, who is also chairman in my defense committee, and Dr. Volker Lohman. Thank you for taking care of my annual progress all over this PhD, for providing excellent suggestions and feedback. I would also like to acknowledge Dr. Freddy Frischknecht and Dr. Petr Chlanda for being immediately so enthusiastic and positive about being part of my defense committee.

Thank you to all my lab members and lab students who were with me for so long and listened to all my never ending jokes, complains, questions on how to do a western blot and comments on how important is to wash coverlips using a piranha solution. Thank you guys for your patience and for your support all over these years.
In particular a big special thanks goes to Pranav, a dear friend and colleague. Thank you Pranav for always supporting me, thank you for believing in my project, especially those days where I could not hold it anymore, thank you for every constructive (and often destructive!) discussion about my experiments, on how to improve them and getting new ideas; thank you for often joining me during my exhaustive microscopy sessions, to push me to stay longer at night when I was tired and I wanted to go home and also to force me to leave when my cells were all dead but still I was trying to acquire data. Thank you also for all our philosophical discussions on the meaning and purpose of life, often ending up with dirty jokes and tons of laughs. Most of all thank you for your loyal and transparent friendship. I wish you all the best for your career and life with Janvhi.
Thank you to Popi for sharing so much together over these years. Thank you for introducing me to this initially mysterious (to me) world of interferon β and λ, for always listening extremely carefully to my talks and for supporting me all those moments I though I was not moving forward. And of course thank you for welcoming me in the Greek community, and for introducing me to the amazing Cretan music, Cretan goats and Cretan Raki. Thank you for all the dancing adventures we shared, thank you for dreaming together about our future, thank you for facing together this last stressful phase of our

PhD. And also thank you for all the fights we faced during these years; I know we were just a bit lost in a country that is not our home.
Thank you also to Markus, the Bavarian guy with Mediterranean soul; such mixtures are difficult to find. I won't forget that every time I was asking you for help or suggestions, you were always replying: "you can always ask". This is also very difficult to find.
A special thanks goes also to Luis, the Spanish little doctor whose awkward jokes and laughs and love adventures will stay in the history of our lab.
And of course I want also to thank Megan. Thank you, Megan, for being a reference point for all us students in the lab, thank you for always be willing to provide help and suggestions; most of all, thank you for always bringing big smiles and positive attitude in the lab, also when things were not as we wished.

During these years I had the big chance to work with so many scientists, and among them I really want to acknowledge Dr. Charlotta Funaja. Dear Charlotta, your collaboration was the most enthusiastic and productive I ever had. Thank you for providing your kind and professional assistance; your help pumped up my work and gave me the amazing chance to finally look with my eyes at the phenotype I was working on.
A big thanks goes also to Dr. Vibor Laketa. Thank you, Vibor, for being always available for any kind of problem I had with the spinning disc, especially during my early start, thank you for being always kind and helpful; people like you are not easy to find. And of course, I would like to acknowledge Nikos, for helping me with German translation, for scientific help and for being my supporter in pushing Panos to quit smoking!

But during these years I was lucky to meet also many extraordinary people outside my lab. And first, of course, is you, Dimi. We shared so much all over these years that it is difficult for me to describe our friendship. We lived together for almost 5 years, you are a dear friend, a true friend, a perfect flatmate, and also a motivating coach (in this, at least you tried!). Thank you because your passion for your work inspired me to do more, and because your positive attitude helped me to take things easier. Thank you for involving me in your life, sharing friends, food and long night talks, and for being happy in being involved in my life, visiting my home, welcoming my roman friends and meeting my family. Most of all, thank you for making our flat a new home for me. When I moved in Heidelberg, I realized that life would have been hard away from my city, but

after moving with you I felt like being in a new home. Right now I cannot imagine how it would have been to live here without meeting you. Thank you for all, I know our GW27 stays for life. And a big thank you goes also to Marta; thank you Martita for being always so happy to share everything in our flat, thank you for bringing more Mediterranean attitude in the house (especially because finally we can have dinner together at 21pm and not 18pm!), thank you for often feeding us, thank you for our Italian funny talks, and most of all thank you for being a bright and positive personality!

Some people enter in your life as a thunderstorm opens a closed window; this how Jenny entered in my life. Dear Jenny, the year spent with you was the craziest adventure in Heidelberg, you brought madness together with peace, joy and cheeriness. As I learnt from you and Ole, thank you thank you thank you! And when I though my place would have not been the same, Teo arrived! And things could have not been better. Thank you Teo for being enthusiastic of our GW27, and although now I dream about saving Macedonian dogs, thank you for making me part of your life.

A big thanks goes also to Himanshu, the sweetest guy I could meet, thank you Himanshu for our chats during the long tiring working days in TP4, for listening to all my complains about my experiments, to try to calm me down when I was entering my crazy mood. Thank you for being a loyal friend. And also thank you to the girl who joined us, Lavinia. Grazie zucchero per esserci sempre, per calmare le mie paranoie, specie quelle sulla mia trachea, per essere sempre disponibile a parlare, a chiarire, a capire. Grazie perche questi ultimi due anni son stati duri e trovare un' amica e' stata una fortuna. Thank you also to Praa, because although we had bad luck to meet for just a short time, you are a good friend, I am sure that the future will give us more time! And Thank you also to the crazy Anna, thank you for bringing a bit of madness in our group, thank you for introducing me to the amazing Frico and thank you for taking care of me when after getting a flu I thought I was about to die!

Also big thanks go to all my girls who were supporting me from Rome, especially Laura, Elisa Anna and Eli, and Giusy. Thank you for all the never ending calls, for visiting me, for going through this adventure together.

And of course I want to thank the diabolical Gaussian fitter. Thank you, Panos, for your immense, never ending patience, thank you for always smiling, for showing always

interest in everything around me. Thank you for being an example of a passionate scientist, especially those moments where my motivation was dropping down. You know I am not good with words, that is why I asked somebody to help me..."Δεν κόβεται στα δύο η ζωή, είναι κόλαση, παράδεισος μαζί, κι αυτά που έζησα είτε άσχημα είτε όμορφα ήσαν εγώ κι εσύ." Grazie, Panos mou.

Finally, a big huge thanks goes to my family. Grazie papo e mammetta, grazie per avermi sempre supportato, per avermi capita quando stavo nervosa e quando non sono riuscita a tornare a casa tanto spesso, grazie perche ogni volta che torno a casa ed a Santa Marienella sento che tutto e' come prima che voi siete la cosa piu bella. Grazie anche ai due ciccioni, Tommy e Camilla, perche' tutto il tempo passato con voi mi ha insegnato ad affrontare i momenti bui e di solitudine, e grazie anche a zio Paoletto per la sua immensa pazienza e alla nonnetta e a tutti i mie nonni perche' sono le mie radici e li sento con me.

Overall, I want to say to all the people that I met in the lab, in the department, in Heidelberg, and throughout my studies, that I deeply appreciate them for improving me as a person and for giving me experiences that helped me to survive, fight and, hopefully, succeed in this PhD!

List of abbreviations

CME: Clathrin-mediated endocytosis

CCP: Clathrin-coated pit

CCV: Clathrin-coated vesicle

AAV2: Adeno-associate virus serotype 2

VSV: Vesicular Stomatitis Virus

CPV: Canine Parvovirus

IAV: Influenza A virus

HIV: Human Immunodeficiency Virus

SA: sialic Acid

JAM A: Junctional Adhesion Molecule A

PI(4-5)P2: phosphatidylinositol-4,5-bisphosphate

PI(3,4)P2: phosphatidylinositol-3,4-bisphosphate

PI(3)P: phosphatidylinositol-3-phosphate

Tf: Transferrin

TfR: Transferrin receptor

LDL: low-density lipoprotein

LDLR: low-density lipoprotein receptor

CLC: Clathrin light chain

MOI: Multiplicity of infection

BAR domain: Bin/Amphiphysin/Rvs domain

ENTH domain: Epsin N-terminal homology domain

Hsc70: heat shock cognate 71 kDa protein

SNX9: sorting nexin 9

NHS: n-hydroxysuccinimide ester

N3: azide function

Si: Silane

PEG: PolyEthylene Glycol

cRGDfk: cyclo(Arg-Gly-Asp-Phe-propargyl)

CuAAC : Cu(I)-mediated azide-alkyne cycloaddition

PFA: paraformaldehyde

SDCLM: spinning disk confocal laser microscopy

EM: electron microscopy

TEM: transmission electron microscopy

SEM: scanning electron microscopy

FIB SEM: Focused ion beam SEM

CLEM: Correlative light-electron microscopy

STED microscopy: Stimulated emission depletion microscopy

TIRF microscopy: total internal reflection fluorescence microscopy

DLS: dynamic light scattering

AFM: Atomic force microscopy

List of Figures

Abstract

Clathrin-mediated endocytosis (CME) is one of the major endocytic pathways among eukaryotic organisms. Importantly, this pathway is also hijacked by many pathogens, such as viruses, in order to enter and infect cells. Since the first identification of Clathrin-coated endocytic vesicles, in 1964, CME has been thoroughly characterized and more than 50 proteins have been described to be part of this pathway. Nevertheless, which protein plays a main regulatory function during initiation and which factors are involved in inducing CME activation upon virus binding and internalization is still a matter of debate. Studying the early determinants of virus-cell early interaction and CME recruitment represents an extremely challenging topic due to the fact that such events take place in an extremely narrow time window and are spatially unpredictable. In this work, I describe a novel method to covalently immobilize virus particles onto glass surfaces in order to study early host-pathogens interactions. To specifically address the role of the mechanical vs receptor-mediated properties of viruses in inducing CME activation, latex beads of several sizes were immobilized using the same established approach.

By combining surface chemistry, click chemistry and several microscopy techniques (fluorescence live microscopy, super resolution microscopy and electron microscopy) it was possible to unveil new details of early virus–cell interaction. In particular, I could confirm that CME recruitment is dependent on the size of the cargo. Specifically, sizes between 80 to 300 nm in diameter, can favor CME activation independently from receptor binding (mechanical induction). Surprisingly, it was discovered that the maturation process that leads to the formation of Clathrin-coated vesicles (CCVs) is independent from cargo internalization and that the size of the CCVs is imprinted on the Clathrin coat at the early cargo-cell interaction. These results could not be unveiled with canonical cell biology techniques. Interestingly, recruitment of CME can be favored on nanoparticles whose size is below the critical diameter to support mechanical induction (< 80 nm), by artificially inducing receptor engagement/clustering.

Taken together these results demonstrate the presence of a fine-tuning between mechanical induction and receptor activation during early virus-cell interaction; this

balance plays a major role in virus infection. The established method can be applied in future studies in the field of virology and endocytosis aiming at understanding how different pathogens favor their internalization using certain pathways, which proteins play a major role in endocytosis initiation and which early factors (mechanical VS receptor-mediated) play a role in activating one pathway over the other.

Zusammenfassung

In eukaryotischen Zellen, stellt die Clathrin-abhängige Endozytose (engl. Clathrin-Mediated Endocytosis (CME)) einen der wichtigsten Aufnahmewege dar. Diese Maschinerie wird von vielen Pathogenen wie z.B. Viren in Anspruch genommen um die Zelle zu infizieren. Seit der ersten Entdeckung von Clathrin-ummantelten endozytotischen Vesikeln im Jahre 1964, wurde CME umfangreich untersucht und mehr als 50 Proteine werden mit diesem Prozess in Verbindung gebracht. Jedoch ist es umstritten, welche regulatorischen Faktoren dabei involviert sind. Es ist auch unklar, welche Faktoren bei der Virusbindung und Internalisierung durch CME involviert sind. Das Erfassen von Faktoren, welche für die frühe Virus-Zell-Interaktionen und die Rekrutierung der Clathrin-Maschinerie wichtig sind, stellt eine große Herausforderung dar. Grund dafür ist, dass diese Ereignisse in einem kurzen Zeitrahmen stattfinden und räumlich nicht vorhersehbar sind. In dieser Arbeit beschreibe ich ein neues Verfahren um Viruspartikel kovalent auf einer Glasoberfläche zu fixieren um frühe Wirt-Pathogen-Interaktionen zu studieren. Um spezifisch zwischen mechanischer oder rezeptorvermittelter Induktion von CME durch Viren zu unterscheiden, wurden Latex-Kugeln verschiedener Größen auf der Oberfläche mit der oben erwähnten etablierten Methode fixiert.

Die Kombination von Oberflächen-Chemie, Klick-Chemie und verschiedenen mikroskopischen Methoden (Fluoreszenzmikroskopie, hochauflösender Mikroskopie und Elektronenmikroskopie) ermöglichte weitere Einblicke in die frühen Virus-Zell-Interaktionen. Ich konnte bestätigen, dass die Rekrutierung der Clathrin-Maschinerie von der Größe der Fracht abhängt. Im genaueren wird bei einer Größe von 80 bis 300 nm Durchmesser die Aktivierung von CME unabhängig von der Rezeptorbindung ausgelöst (mechanische Induktion). Erstaunlicherweise ist der Reifungsprozess, der zur Ausbildung von Clathrin-umhüllten Vesikeln (engl. Clathrin-coated vesicle (CCV)) führt, unabhängig von der Frachtinternalisierung und die Information der CCV Größe wird während der frühen Fracht-Zell-Interaktion in der Clathrinhülle festgeschrieben. Diese Ergebnisse konnten zuvor nicht mit herkömmlichen zellbiologischen Methoden erfasst werden. Wenn die Größe der Partikel unter der Ausschlussgrenze für mechanische Induktion liegt

(< 80 nm), kann interessanterweise die Rekrutierung von CME für diese Nanopartikel durch künstliche Rezeptorstimulierung/Rezeptorclustering eingeleitet werden. Zusammenfassend konnte dargestellt werden, dass bei früher Virus-Zell-Interaktion eine Feinabwägung zwischen mechanischer Induktion und Rezeptoraktivierung stattfindet, welche eine große Rolle für die Virusinfektion spielt. Die hier etablierten Methoden können in zukünftigen Studien in den Forschungsfeldern der Virologie und Endozytose angewandt werden, um zu verstehen, wie verschiedene Pathogene ihre Internalisierung durch Inanspruchnahme verschiedener Endozytosewege begünstigen. Dabei kann weiter untersucht werden, welche Proteine bei der Aktivierung der Endozytose eine Rolle spielen und welche frühen Faktoren bei der Unterscheidung zwischen mechanischer und rezeptorvermittelten Endozytose wichtig sind.

1 Introduction

1.1 Clathrin mediated endocytosis

1.1.1 Endocytosis

The cell plasma membrane represents a physical barrier that confines the cell environment from the extracellular environment. Despite its role as physiological barrier, the cell membrane shows high order dynamics that regulate cell response and cell adaptation to its environment. The process of endocytosis represents the rearrangement of the cell lipid bilayer by forming vesicles that are internalized into the cell; in this way, nutrients and metabolites can be internalized inside the cytosol. Moreover, through the recurrent formation and release of vesicles, lipids and proteins from the plasma membrane are continuously recycled, contributing in the cell membrane homeostasis maintenance. However, cell endocytosis does not only regulates nutrient uptake and cell membrane homeostasis, but is also involved in regulating cell response to its environment; many studies have shown that endocytosis is involved in the recycling of cell receptors, cell signaling, cell adhesion and cell migration[1]. Importantly, many pathogens have evolved mechanisms to evade cell immune response and be internalized inside the cells through endocytosis.

In the cell we can distinguish two main endocytic pathways: phagocytosis and pinocytosis (Figure 1). Through phagocytosis, cells generate large vesicles (phagosomes, more than 250 nm in diameter) to internalize big structures such as bacteria or cell debris[2,3]. Upon cargo binding/ recognition, cells generate long extracellular protrusions, which embrace the cargo and fuse to each other forming a big vesicle. Phagocytosis is mainly used by blood cells, macrophages and neutrophils, mainly to clear microorganisms from infected tissues.

Through pinocytosis, cells internalize fluids and small particles using four main mechanisms: macropinocitosis[4,5], Clathrin-mediated endocytosis (or receptor-mediated endocytosis)[6,7], caveolin-mediated endocytosis[8,9] and Clathrin and caveolin independent endocytosis[10]. A part from macropinocitosis, which forms membrane extensions to

internalize molecules and/or fluids, all the other mechanisms generate inward vesicles at the cell membrane that are smaller than 200 nm in diameter. Clathrin mediated endocytosis (CME) is involved in several cellular mechanisms, it represents the most studied process among the pinocytic pathways[6,7] and is the most evolutionary conserved among eukaryotic organisms[11].

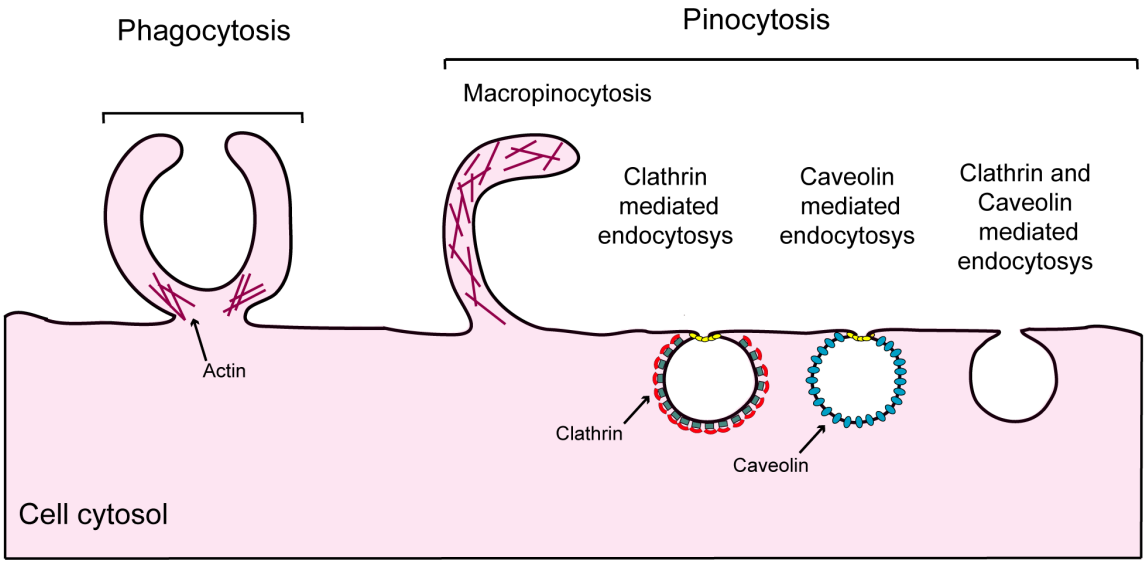

Figure 1: Cellular endocytic mechanisms. Schematic representation of the main endocytic pathways in eukaryotic cells.

1.1.2 Clathrin-mediated endocytosis

Clathrin coated vesicles were first identified by Roth and Porter in 1964[12]. In their studies, the authors were investigating the yolk protein uptake into mosquito oocytes; interestingly, at the oocyte cortex, they observed the presence of vesicles that exhibited a characteristic, well-defined, "coat". These vesicles were therefore called "bristle-coated"[12]. Many similar observations were made in the following years. By looking at isolated vesicles, Kanaseki and Kadota in 1969 identified the typical "basket" shape of Clathrin-coated vesicles, whose geometry was made of hexagonal and pentagonal structures[13]. For this reason they called those vesicles 'vesicles in a basket'. It was only in 1975 that Barbara Pearse purified and characterized those coated vesicles from pig brain[14]. In her work, she demonstrated that those vesicles have a diameter of 70 to 100 nm and that their coat was composed by many copies of just one protein of 180 kDa, that

she called "Clathrin"[14]. By observing Clathrin structures in unroofed cells (cells adhering on a substrate whose upper part is removed by mechanical/chemical treatment while the basal membrane stays intact) the typical geometrical pattern, made of hexagon and pentagon, of Clathrin-coated vesicles was afterwards confirmed[15] (Figure 2 A).

Subsequent structural studies clarified the Clathrin structure. Clathrin is composed by three heavy chains who interact with a light chain; these three heterodimers together represents the main Clathrin unit, that due do its peculiar structure was called triskelion (which comes from the Greek word *triskelion* "a three-legged structure")[16,17] (Figure 2 B). During Clathrin cages assembly, the legs of different triskelia interact within each other giving rise to pentagons and hexagon structures; every vertex is made by a triskelion whose three legs interact with other triskelia to interconnect every vertex[18,19,20] (Figure 2 B). A Clathrin coat composed only by hexagons has a flat shape; addition of pentagons, introduces coat bending (necessary for CCPs formation)[15,20]. Although it has been shown that Clathrin molecules are continuously and quickly exchanged (turnover every 2 sec) at all stages of CCPs[21], how the triskelia rearrangements from hexagon to pentagon take place at the molecular level is not yet completely clear. EM studies further demonstrated that the Clathrin lattice exhibits really high polymorphism; they can form large flat arrays but also highly curved CCPs, confirming a strong flexibility of triskelia assembly. The "legs" of each triskelion are composed of 42 alpha helical zig-zags characterized by a pronounce bendability[18] (Figure 2 B); Clathrin baskets can assemble into smaller or bigger vesicles by changing the angle of interaction between legs from two different triskelia[18]. Although CCVs have a canonical size of 90-120 nm, bigger cargos can induce the formation of larger Clathrin vesicles[22,23], indicating that the legs of triskelion can adapt their curvature depending of the size of the cargo[18,20]. Currently the role of Clathrin light chains is still a matter of debate. Nevertheless, different studies have shown that light chains have no role in Clathrin assembly or triskelia interactions[24,25].

Mammalian and yeast cells share many similarities in the CME pathway, as well as many differences[7,26]: in this thesis I will focus my work on mammalian CME.

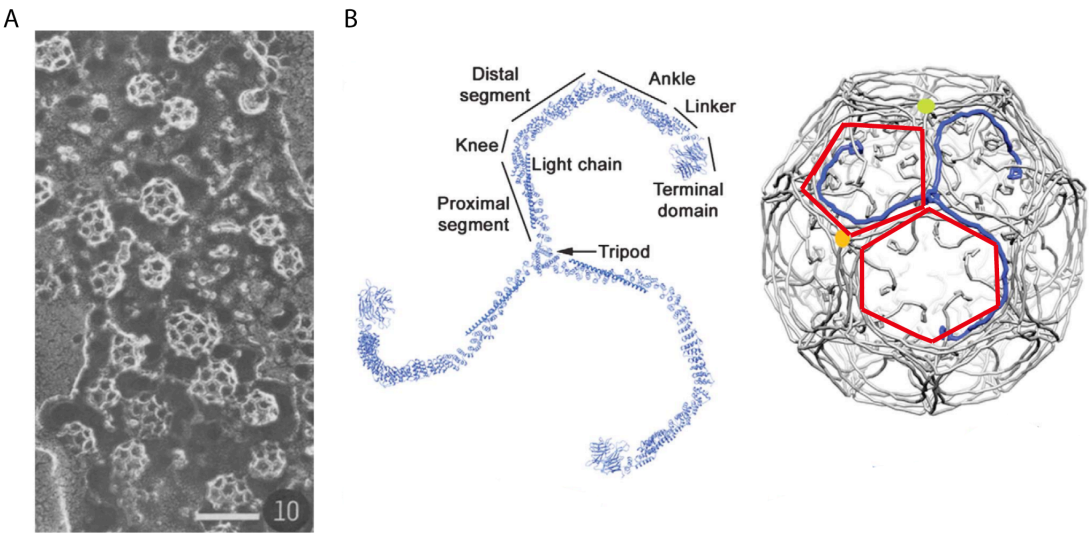

Figure 2. Clathrin cages and Clathrin triskelia. A) Electron microscopy pictures of empty Clathrin cages isolated from brain. Scale bar 100 nm. Adapted from Heuser et al., 1980. B) (Left part) Structure of a Clathrin triskelion and (right part) triskelia organization into Clathrin cages; hexagon and pentagon structures are highlighted in red. Adapted from Xing et al., 2010.

1.1.3 Steps of Clathrin-mediated endocytosis

During CME initiation, a specific signaling at the cell membrane (i.e. receptor activation, cargo binding) induces the recruitment of adaptor proteins. Clathrin can not bind lipids and therefore its recruitment to the cell membrane is mediated by adaptor proteins. The assembly polypeptide 2 (AP2) is the major adaptor protein in mammalian cells[27,28] and it is one of the first adaptor proteins to be recruited to the plasma membrane (Figure 3). AP2 recruitment is mediated by its interaction with the phosphatidylinositol-4,5-bisphosphate (PI(4-5)P2) at the cell membrane[28–30] and signaling/sorting motifs at the cytosolic tails of cell receptors/cargo molecules[31–34]. Once the pathway is initialized, an early Clathrin-coated structure starts to assemble (Figure 3) and is referred to the field as a Clathrin coated pit (CCP). Afterwards many other protein adaptors and curvature effectors are recruited to stabilized and promote pit growth and invagination of the cell membrane[7]. When a Clathrin-coated vesicle (CCV) is mature, dynamin, a large GTPase protein, is recruited to the "neck" which still connects the vesicle with the cell membrane, leading to the release of the CCV into the cell cytosol[35] (Figure 3). The whole process takes place in a time range of about a minute. Although CME has been deeply characterized in the past 40 years, still the main regulators of each step and which proteins are involved in the transition among each stage, remain unclear.

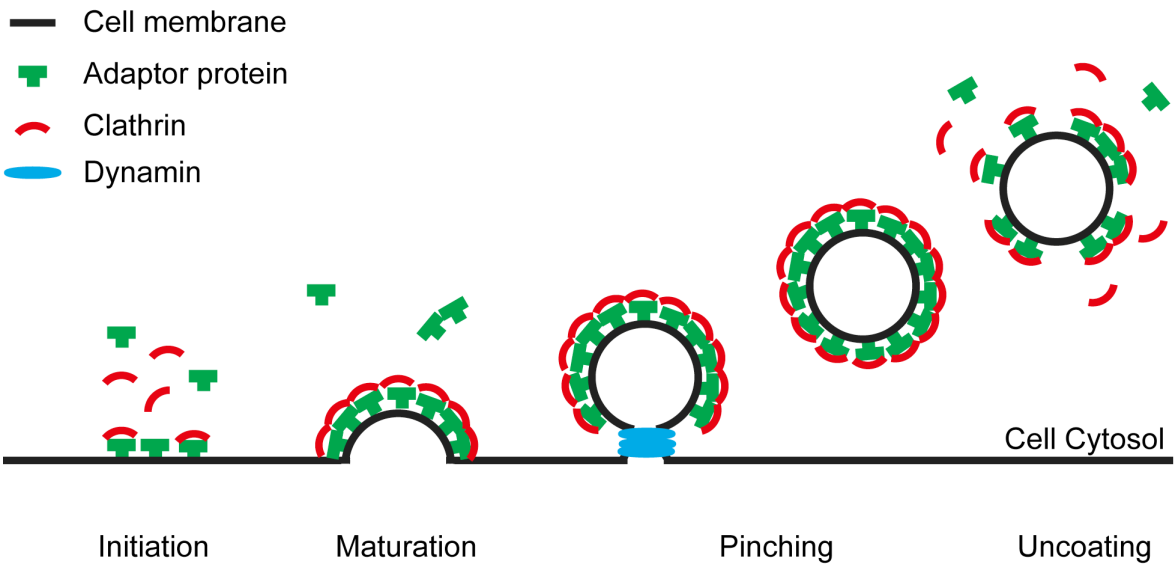

Figure 3. CME stages. Schematic representation of the different steps of CME; initiation, maturation, pinching and uncoating.

1.1.4 Initiation: many candidates but no assignment yet.

1.1.4.1 Role of Adaptors and BAR proteins: who comes first?

As mentioned before, Clathrin alone is not able to directly bind the cell membrane components and therefore, CCP initiation needs protein adaptors[36]. Due to their function to recruit Clathrin at the cell membrane, adaptor proteins have been considered optimal candidates for being main initiators. AP2, in particular, is a heterotetramer consisting of α, β2, μ2, and σ2 subunits which form a structure having a core unit with two protrusions[20,28,37] (Figure 4 A). This adaptor protein interacts with lipids at the cell membrane[28,30,38], Clathrin[39,40] and cargos [31,32,34,41] (Figure 4 A), and represents the most conserved adaptor protein among eukaryotic organisms[42]. Due to its highly structured Clathrin/adaptors/cargo/lipids interaction network, AP2 was considered an optimal candidate in the hunt of a master initiator (Figure 4 A). Nevertheless, early studies on the AP2 recruitment at nascent CCPs ruled out any potential role of AP2 as the main initiator[43,44]. Moreover, further studies identified the curvature-inducing containing proteins FCHO1/2 (from FCH, a conserved domain among the proteins, and BAR, a conserved domain among curvature-inducing proteins, see next section) as early assembly units of CME[45]. FCHO1 and FCHO2 are proteins that contain BAR domains

which recognize membrane curvature[46]. Henne and colleagues, demonstrated through live-cell microscopy that FCHO1 is recruited to the nascent CCPs before Clathrin[45]. Moreover, knocking down FCHO1/2 expression in cells, strongly inhibited CCPs nucleation, while, if AP2 was depleted, FCHO1/2 could still be recruited to the cell membrane[45]. These results, however, were contradicted a few years after. Further investigations, supported by the advancement of live imaging microscopy techniques and single molecule tracking analysis, revealed that the binding of two AP2 molecules and one Clathrin triskelion at the cell membrane determines CCPs initiation[47]. Moreover the role of FCHO 1/2 was demonstrated to be involved in the CME maturation process rather than initiation[47]. Finally, a recent study[48] based on single mutations at the AP2 subunits, demonstrated that blocking AP2 interaction with PI(4-5)P2 by mutating either the α or β2 PI(4-5)P2 -binding motifs strongly reduces the pit initiation rate, Clathrin polymerization and pit maturation. These results suggest a critical role for AP2 in favoring CME initiation and maturation in mammalian cells[48]. A parallel study from the same year employed structural analysis, EM and fluorescence imagining to further examining the recruitment of AP2 to the cell membrane[49]. In their work, Ma and colleagues, demonstrated that early clusters of FCHO1/2 and Eps15, an adaptor protein, interact with AP2 molecules at the cell membrane thereby inducing conformational changes in AP2 that reinforce its interaction with the cell membrane, favoring cargo binding and further AP2 recruitment (Figure 4 B). Therefore, although AP2 might play a major role in CME initiation, its interaction at the cell membrane appears to be favored by different factors, generating a complex network of proteins involved in initiating CME.

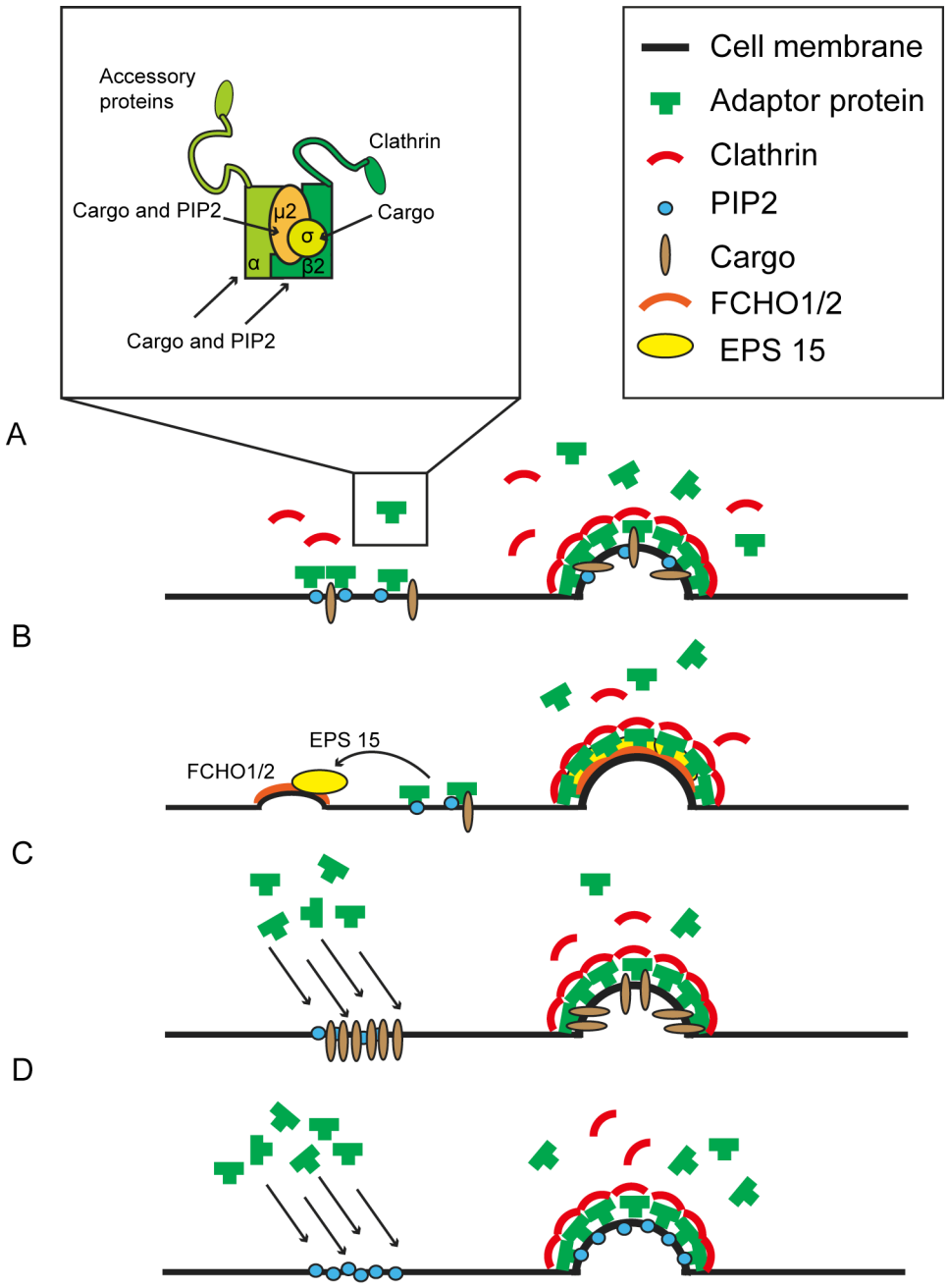

Figure 4. Potential CME initiators. A) (Upper part) schematic structure of AP2 subunits. Adapted from Kadlecova et al., 2016. Black arrows indicate the interaction partners of each subunit. (Lower part) AP2 is considered as one of the main candidates for CME initiation; through its interaction with cargo molecules and PIP2 it was shown to favor CCPs nucleation. B) Cluster of FCHO1 and EPS15 have been proposed to induce AP2 recruitment and CME initiation. C) Cargo may play a role in favoring AP2 recruitment and CME initiation. D) Clustering of lipids, such as PIP2, have been suggested to induce CCPs nucleation; how lipids composition is regulated in specific cell area is not known yet.

1.1.4.2 Role of cargo in initiation

As described for AP2, the role of cargo in CCPs nucleation and maturation is a matter of debate. Although it is reasonable to believe that the interaction between cargos and cell receptors may activate CME recruitment, scientific evidence suggests a different view. Low-density lipoprotein (LDL) and transferrin (Tf) are well characterized cargos which are internalized by the Clathrin machinery[43,50], and are widely used as markers to study cargo internalization by CME. By looking at fluorescently labeled LDL and Tf it was observed that internalization was taking place after co-localization with already preformed CCPs; such cargos therefore do not induce CME recruitment but rather "hijack" preformed Clathrin structures[22]. Moreover, the same authors showed that CCPs co-localizing with LDL or Tf were afterwards directly committing to mature CCVs[22]. Those results led to the belief that cargo might play a role in CCPs maturation rather than initiation. Further studies validated this hypothesis; Loerke and coworkers showed that overexpression of transferrin receptor (TfR) did not lead to an increase of CCPs nucleation events, but it resulted in a higher fraction of CCPs that reach maturation stage[51]. Less than a year after, Liu and collegues created a system to study the role of cargo in CCPs initiation and maturation[52]; using TfR conjugated with a biotin module, they subsequently added streptavidin to the media and induced the clustering of TfR. In their work they demonstrated that the induction of TfR clustering increases CCPs density and initiation rate. TfR is constitutively internalized by CME, meaning that no signaling is associated with CME recruitment[53]; these results therefore demonstrated, conversely to what Loerke and colleagues published a bit earlier, that cargo clustering by itself can affect CME initiation (Figure 4 C).

Finally,in a recent study, the role of cargo in CME initiation was highlighted again by altering the AP2-cargo interaction[48]. AP2 subunits σ2 and μ2 contain cargo-binding motif [31–34]; DNA mutation in such domains causes a general inhibition of cargo internalization and a strong reduction of CCP nucleation rate[48]. These results strongly support a crucial role of cargo–AP2 interaction in CCPs nucleation (Figure 4 C).

In summary, the investigation of the role of cargo in favoring CCPs initiation brought different results and opposite conclusions; nevertheless it is important to consider that different cargos may play different role in favoring Clathrin machinery recruitment and

that an absolute classification of the role of cargo in CME initiation might not be possible.

1.1.4.3 Role of lipids

Lipids at the cell membrane play an important role in CME. It was demonstrated that many early adaptor proteins as well as late binding proteins sequentially interact with the different phosphoinositides (PIP) at the cell membrane favoring pit nucleation, maturation and pinching[54]. Specifically, PI(4-5)P2 plays a crucial role for CME initiation since it specifically interacts with protein adaptors that in turn recruit Clathrin, such as AP2[29]. Artificial removal of PI(4-5)P2 from the cell membrane abolishes CCP nucleation and induces instant disassembly of Clathrin structures[55]. Despite the essential role of PIPs for CME initiation, how and if they regulate CCP nucleation it is not yet known[56] (Figure 4 D). Although the development of new systems to investigate the role of lipids in cellular process[57–59] studying the potential regulation role of lipids in CME still represents a challenging field.

In conclusion, it is not possible to exclude that several mechanisms/factors, rather than only one main initiator, might cooperate together in favoring CME initiation.

1.1.5 Maturation

By studying the dynamics of CCPs through live-cell microscopy using fluorescent markers such as AP2 or Clathrin, it is possible to observe that the fluorescence signal grows over time until reaching a plateau; this stage corresponds to the maturation process of the CCP which culminates in the formation of a CCV. Afterwards the fluorescence signal rapidly decreases until disappearing, which coincides with the release of the CCV into the cytosol (Figure 5 A).

After the initial CCP nucleation, many other endocytic proteins are recruited to the nascent CCP favoring its maturation into a CCV (Figure 5 B). Understanding which protein come first and which role it plays has been a challenging topic for many years. An excellent study from Taylor and colleagues provided detailed information on the temporal recruitment of endocytic proteins to the nascent CCPs giving a better understanding of the maturation process[60]. In this work, they used a previously established method that exploits pH-sensitive fluorophores to detect vesicle pinching at

the cell membrane. Using this approach it was possible to specifically and temporally mark the beginning and the end of each CCPs[61]. The recruitment of 34 proteins at nascent CCPs was then investigated, with a time resolution of 2 sec[60]. After initiation, CCPs are characterized by further recruitment of Epsin and the FBAR proteins FCHO1/2 (Figure 5 B). The main role of these early proteins is to stabilize and promote CCP invagination. Epsin favors CCPs maturation by directly interacting with Clathrin and with the actin binding protein Hip1R, providing a bridge between the coat and the actin network[62]. Moreover, Epsin provides direct membrane bending by the insertion of an amphiphatic helix into the cell membrane bilayer[63] (for details of membrane bending mechanism mediated by Epsin see the next section). FCHO1/2 favors CCP invagination by sensing and inducing cell membrane curvature; these proteins exhibit a typical "banana" shape which interacts with the lipid bilayer favoring its bending[64] (for details see next section). Afterwards, further proteins that favor membrane bending and vesicle constriction are recruited, such as the NBAR proteins endophilin2 and Amphiphysin[6,7,60] (Figure 5 B). NBAR proteins provide high membrane curvature (140 degrees for NBAR while 80 degrees are provided by F BAR proteins)[65] by inserting their amphiphytic helices into the lipid bilayer [66,67] (for details see next section).

The role of actin in mammalian CME is still controversial. In has been shown that during maturation actin binding proteins are recruited and show two bursts, one right before the vesicle scission and one after scission[60]. However, the same study showed that actin is not needed in all CCPs[60], but in some circumstances its recruitment becomes crucial for pit maturation and vesicle constriction, such as in the case of large cargos or high membrane tension[68–70]. Actin recruitment at CCPs is mediated by the Hip1R protein, which connects the CCPs with actin filaments by interacting with Clathrin light chains and F-actin[71,72].

The maturation process of CCPs is strictly regulated by local changes in the lipid composition at the cell membrane[54] (Figure 5 A); such changes define the sequential recruitment of several proteins involved in CCV formation. While initiation depends on the presence of PI(4,5)P2, which favors recruitment of AP2[29] and early maturation proteins such as FCHO1/2[45] and epsin[63,73], maturation is characterized by conversion of this lipid into to PI(3,4)P2. The late protein endophilin, interacts and recruits the 5-

phosphatase synaptojanin p170[74,75] that promotes conversion of PI(4,5)P2 into PI(3,4)P2[76]. Local enrichment of PI(3,4)P2 in turn acts as signal for recruitment of specific late-maturation proteins such as SNX9, which is a curvature protein that aid further constriction of the CCV and directly interact with dynamin[77,78].

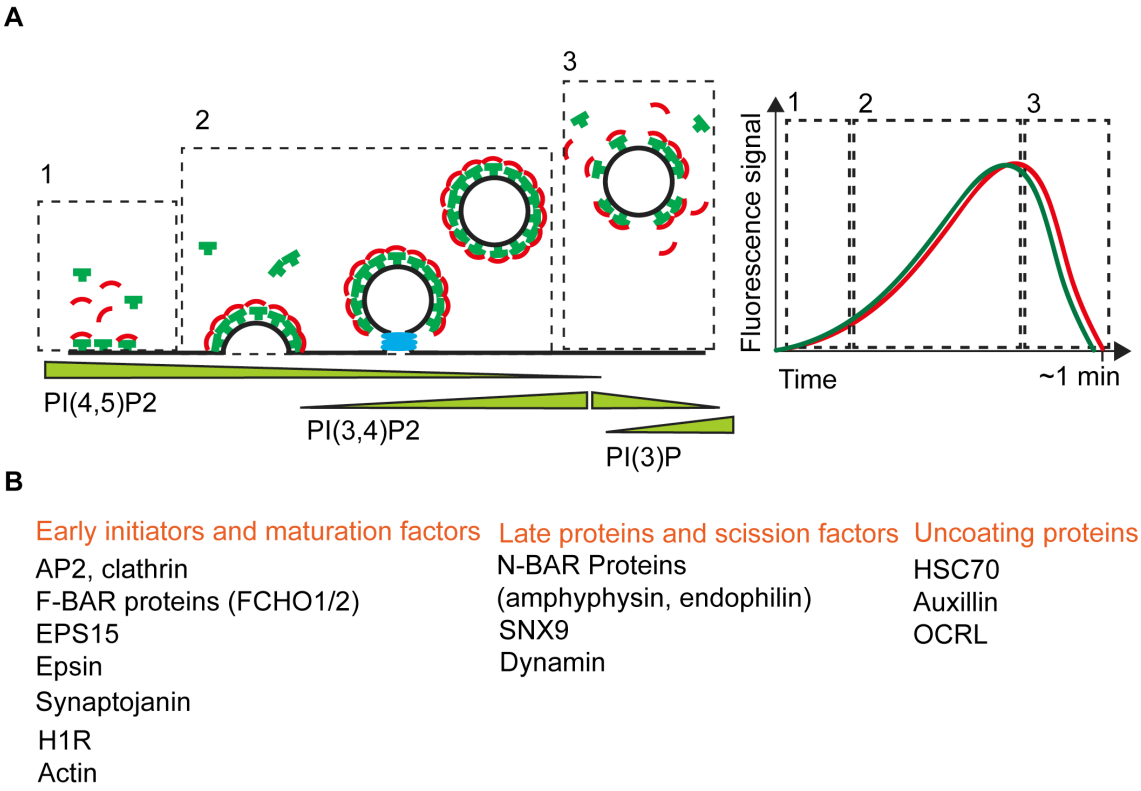

Figure 5. Maturation of CCPs into CCVs. A) (Left part) CCPs growth can be divided into three steps, highlighted with dashed rectangles and labeled 1, 2 and 3; PI(4,5)P2 conversion at each step is depicted in green. (Right part) Schematic representation of the fluorescence intensity profile over time of AP2 and Clathrin from a canonical CCP. From the fluorescence curve it is possible to identify the same three steps of CCPs growth (also depicted with dashed rectangles and labeled 1,2 and 3). B) List of the main proteins involved in early and late maturation of CCPs, scission and uncoating

1.1.6 Scission and uncoating

Recruitment of Dynamin finally provides the scission of CCVs[35,60]. Dynamin is a GTPase protein and was discovered by Shpetner & Vallee in 1989[79]. There are three isoforms of Dynamin, 1, 2 and 3; Dynamin 1 and 3 are mainly expressed in the brain while Dynamin 2, is ubiquitously expressed. Dynamin consists of two GTPase domains and two PI(4-5)P2 binding domain (PH domain) opposite to each other and connected by

a flexible region[35]. Dynamin can self-polymerize into rings-like polymers having the PH domain facing the membrane and GTPase domain facing outside[80–82]. Although it is well accepted that Dynamin polymer-rings constrict the neck of CCPs by binding GTP and favoring vesicle scission, the mechanism is still controversial[83]. Additionally, it is now clearer that other factors such as membrane tension and insertion of amphipathic helix from NBAR proteins and ENTH domain containing proteins collaborate together in energetically favoring vesicle scission[84,85] (for details see next Section).

The enrichment of PI(3,4)P2 during maturation also induces the recruitment of the uncoating proteins Auxillin and HSC70 which together induce the depolymerization of the Clathrin coat at the CCV after scission[86]. Finally, after pinching the PI(3,4)P2 in the vesicle is converted in PI(3)P by recruitment of the 4-phosphatase (PI4)[87]. Importantly, the phosphatase OCRL is recruited at last stages, promoting degradation of the PI(4,5)P2 leftover in the vesicle[88,89]. All together these events will promote the endosomal trafficking of the vesicle[87].

1.1.7 CCPs populations: abortive, terminal and non-terminal.

1.1.7.1 Abortive CCPs

By analyzing Clathrin-coated structures through live-cell microscopy, it was observed that not all CCPs display the same dynamics. While a fraction of CCPs exhibits the typical lifetime of 1 min, there is a large population of CCPs with extremely short lifetimes (around or less than 5 secs)[22]. The percentage of such short lived CCPs represents 25% of total CCPs[22]; more detailed calculations reveled that this fraction may be higher, up 59 % of total CCPs[51]. Since those short-lived CCPs do not co-localize with dynamin and since fluorescence quantification analysis revealed that they are composed of less than 30 triskelia (not enough to build a CCV)[22], people in the field refers to them as abortive CCPs. Loerke and colleagues performed a deep analysis of CCPs lifetimes in three different cell lines and confirmed that they all contained three different pit populations[51]. One population is referred as long-lived Clathrin coated pits (around 1 min duration) and represents the ~38 % of total CCPs and two subpopulations have shorter time duration (around 15 secs and 5 secs). Pits belonging to the short-lived populations are called “late abortive” and “early abortive” which represent ~21% and ~38 % of total

CCPs, respectively[51]. Abortive pits are described as pits that do not reach the maturation state (Figure 6A); CCPs start to nucleate at the cell membrane and, in the absence of a maturation effector/ signal, they dissemble shortly after[51]. Factors that cause "abortion" of such short lived CCPs are not fully understood. It was proposed that cargo could play a major role in favoring pit maturation; overexpression of Clathrin-specific cargos induces an increase of CCPs that reach the maturation stage[22,52]. Moreover interaction between AP2 and specific cargos favor CCPs nucleation and maturation[48].

1.1.7.2 Terminal and Non terminal-pits

As previously described, "canonical" CCPs display a lifetime of around 1 min, and exhibit a fluorescence signal which grows overtime until reaching a peak and then quickly disappears; these events are called "terminal", since they are characterized by a specific start and end-point. Besides terminal CCPs and short-lived CCPs, using live-cell microscopy it was observed that exist a population of CCPs that shows recurrent maturation events, also called non-terminal CCPs[29,61,90]. After vesicle pinching the signal from canonical CCPs disappears from the cell membrane (Figure 6 B), non-terminal pits instead, display a recurrent release of CCVs. Moreover, after each round of pinching, the non-terminal CCPs are not completely dissembled, but some coat components stay at the plasma membrane, explaining their name "non-terminal" (Figure 6 C). A detailed study from Taylor and collogues[60] showed that adaptor proteins, BAR proteins and scission proteins were recruited in a similar way and with similar dynamics to "terminal" and "non-terminal" CCPs; moreover, they confirmed the recurrent pinching of CCVs in "not-terminal" CCPs. Spots in the cell that show recurrent endocytic events are refereed as "hot-spots". These spots and have been noticed in several cell lines[22,29,90,91]. Although the lifetime of CCPs at the "hot spots" have been shown to be highly heterogeneous, their kinetics, compared to CCPs outside "hotspots", are similar[60,92]. To date, the role of the "hot spots" and the factors that induce their formation are unknown. It has been proposed that they might represent a specialized cell area for recruitment/clustering of cargo and/or receptors[92].

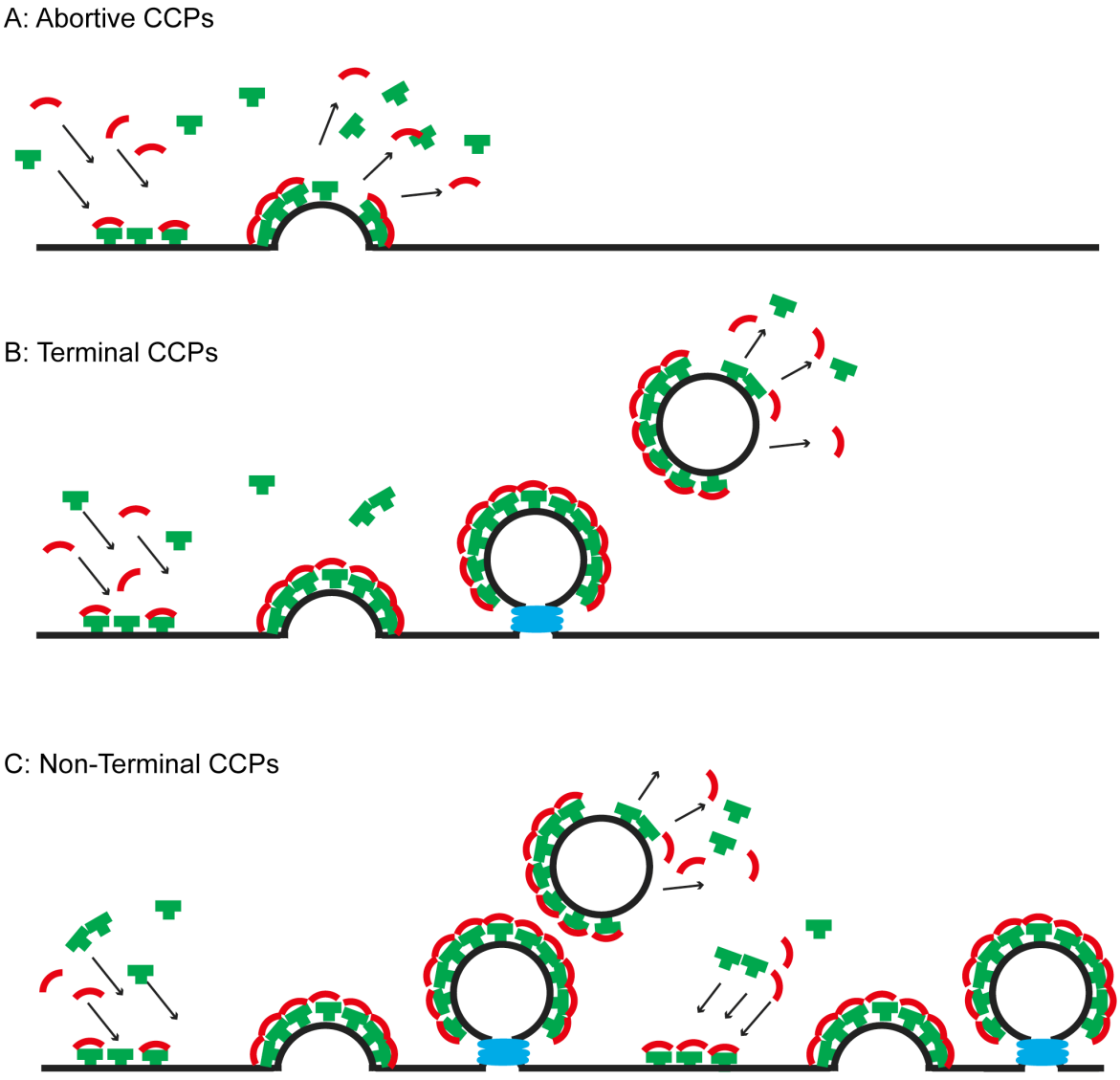

Figure 6. Different populations of CCPs. Schematic representation of A) abortive CCPs, B) terminal CCPs and C) non-terminal CCPs.

1.2 How curvature takes place at the cell membrane

The recruitment of the adaptor proteins and curvature effectors during CCPs maturation helps and/or promotes curvature acquisition of the nascent vesicle. Membrane curvature is a complex process that requires energy and recruitment of specialized proteins. Due to their physical properties, lipid bilayers of mammalian cell membrane tend to avoid any kind of bending; at the same time, generation of highly curved membrane is at the base of many vital cellular processes and is therefore essential for cell survival. For this reason cells have evolved different ways to bend membranes[93,94]. The main mechanisms used by the cells to bend the membranes are mediated by changing in the cell membrane lipid composition, recruitment of protein scaffolds and insertion of protein domains into the lipid bilayer (Figure 7).

1.2.1 Changes in the cell membrane lipid composition

Membrane bending can be generated by changes in the lipid composition at specific spots of the lipid bilayer. Mammalian cell membranes are mainly composed of phospholipids. Phospholipids are made of a two long hydrophobic fatty acid tails and by a hydrophilic head containing a phosphate group; these two components are connected to each other by a glycerol molecule. Because of their amphiphilic characteristic they can assemble into a lipid bilayer. The head of phospholipids can be modified by addition of chemical groups generating different modified-phospholipids; these modifications can favour membrane bending by generating asymmetry in the membrane lipid composition[93,95] (Figure 7 A). Moreover, the presence of different classes of lipids, at the cell membrane can favour membrane asymmetry and therefore curvature[93,95]. The bending energy provided by such mechanism is not enough to provide efficient membrane bending and vesicle invagination. However, lipid modifications can also be responsible for recruitment of specific curvature-inducing proteins at the cell membrane[96].

1.2.2 Scaffolding: protein polymerization and intrinsically curved proteins

The first mechanism through which proteins induce membrane bending is scaffolding. During protein scaffolding, several proteins interact with the lipid bilayer

favouring curvature generation in two main ways. In one way, they interact within each other polymerizing and generating a specific geometrical reticulum/architecture which imposes curvature on the cell membrane. This mechanism is termed indirect scaffolding (Figure 7 B). On the other way, they have an intrinsic curved structure that, by interacting with cell membrane, induces bending; this modality is known as direct scaffolding (Figure 7 C). Clathrin is of course an important example of how scaffolding of proteins can generate membrane bending. The first experiments to demonstrate the ability of Clathrin to induce membrane bending were performed in 1999 in the lab of De Camilli. By incubating Clathrin machinery protein extracts with liposomes and by looking at samples through EM they observed Clathrin buds at liposome membrane[97]. Later structural studies revealed that the curvature imposed on the cell membrane by the Clathrin cages can vary depending on the angle of interaction between the legs of different triskelia; different angles induce the formation of a flatter or of a more curved Clathrin lattice which results in a different pentagon/hexagon ratio and therefore bigger or smaller cages[18,98]. But the final demonstration that Clathrin alone can induce membrane curvature through indirect scaffolding was provided in 2012. Dannhauser and Ungewickell created an *in vitro* system where Clathrin could be artificially recruited on the membrane of large liposome. In their work, the authors showed that Clathrin recruitment induced the formation of Clathrin-coated buds all over the surface of liposomes; the size of these buds was similar to the ones observed *in vivo*. By adding Hsc70, a protein involved in dissociating the Clathrin coat after vesicle pinching, the Clathrin-coated buds were reabsorbed into the liposomes. Through this artificial system it was demonstrated that Clathrin scaffolds assembly provides sufficient bending energy to curve lipid membranes into CCPs and to stabilize them[99].

One other way through which proteins can induce membrane bending is direct scaffolding; such proteins can directly interact with the cell membrane to favour and stabilize curvature by having an intrinsic curved structure (Figure 7C). F-BAR proteins were proved to favour membrane bending by observing that incubation of purified F-BAR domains with liposomes was inducing liposome tabulation; the diameter of the tubules was around 60-100 nm[46,100,101]. Structural analysis of F-BAR proteins revealed a shallow curved shape of these proteins, whose concave interface (called also “banana”

structure) has positively charged residues that interacts directly with membrane lipids inducing curvature[64].

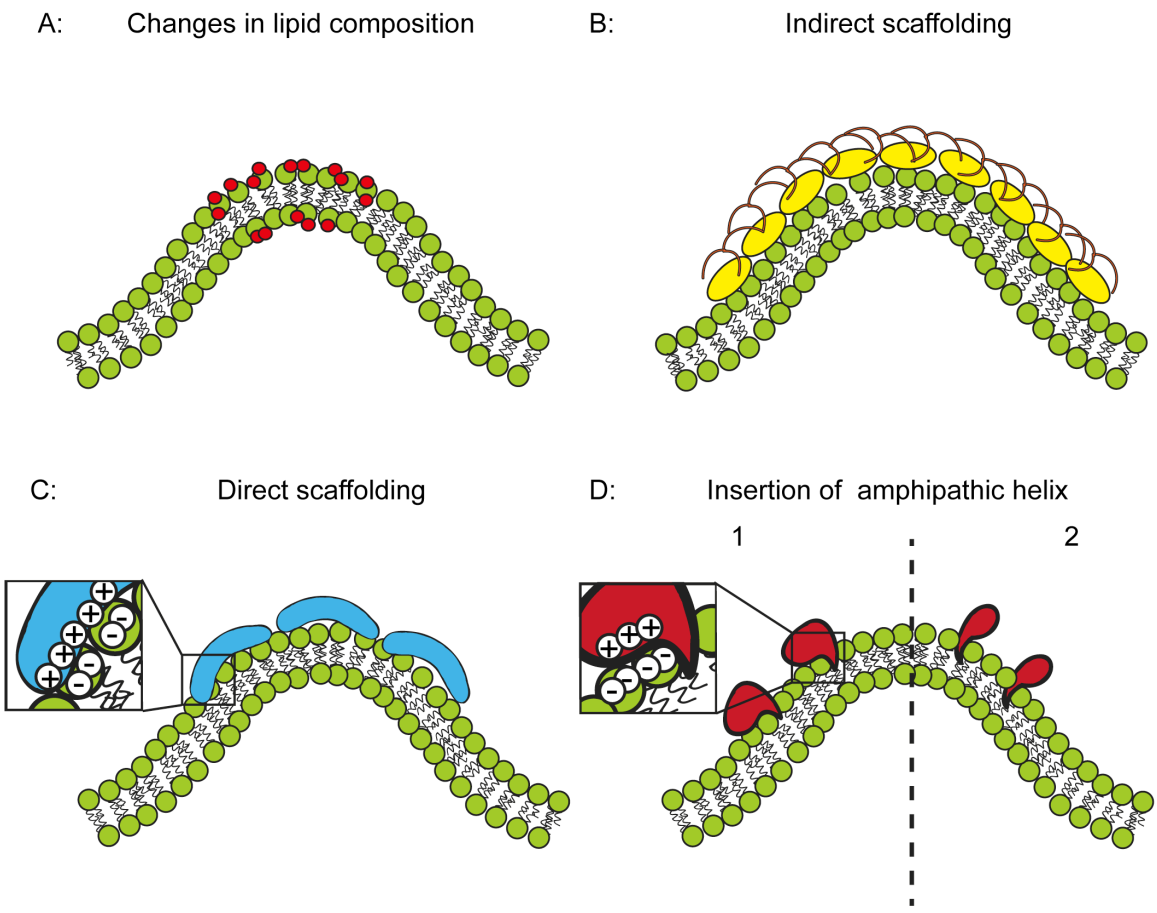

Figure 7. Mechanisms of membrane bending. Schematic representations of different mechanism used by the cell to favor membrane bending. A) Membrane bending mediated by changes in lipid composition at the cell membrane. B) Membrane bending mediated by indirect scaffolding of proteins, which polymerize into geometrical structures around the cell membrane. C) Direct scaffolding of proteins with intrinsic curved shape. D) Membrane bending mediated by insertion of amphipathic helix of proteins into the lipid bilayer

1.2.3 Insertion of amphipathic helix into the lipid bilayer

As mentioned above, some proteins have an intrinsic curved structure that can interact with the lipid bilayer favouring membrane curvature generation. The major class of protein belonging to this category are the BAR proteins. The BAR domain was first identified as a conserved motif in different protein among different organism; BIN1 and Amphiphysins in mammalian cells and Rsv in yeast[102]. The mammalian Amphiphysin

has two isoforms: Amphiphysin 1, mainly expressed in the brain, and Amphiphysin 2, mainly expressed in the muscle. Both isoforms are involved in endocytosis. They are composed of a BAR domain followed by an unfolded region which ends with a SH3 domain[103]. Early structural studies identified an Amphiphysin binding domains for dynamin and synaptojanin, therefore suggesting a crucial role for this protein in dynamin recruitment at mature CCPs and CCVs scission[97]. This result led to the hypothesis that such proteins could play a role in favouring/inducing membrane bending at late stages of CCPs. As it was previously shown for Clathrin, in vitro assays were performed to understand the role of Amphiphysin in membrane curvature. Previous experiments had shown that incubation of liposome with rat brain cytosol extracts and GTPs induced the formation of Clathrin coated constricted buds having dynamin "rings" structures at the neck[104]; however not all the Clathrin buds were actually co-localizing with dynamin[104]. By repeating these experiments in 1999 Takei and colleagues incubated liposome with purified dynamin, Amphiphysin and coat proteins; surprisingly almost all the Clathrin buds co-localized with dynamin and Amphiphysin, suggesting a role for Amphiphysin in connecting dynamin to the Clathrin coated structures[97]. Moreover, incubating purified Amphiphysin with liposome induced massive tabulation, generating tubules 20-60 nm wide[64,105]. Taken together these results highlighted well-defined properties of Amphiphysin in inducing membrane curvature. These studies demonstrated for the first time the role of BAR domains in binding and inducing curvature of lipid bilayer[97]. Afterwards, other endocytic BAR proteins such as endophilin, were identified based on sequence similarities with Amphiphysin; using the same *in vitro* methods, curvature inducing proprieties were confirmed as well[106].

To better understand how curvature if favoured by Amphiphysins, computational analysis were performed and they revealed the presence on an amphipathic helix at the N terminus of the BAR domain[66]. The hydrophobic portion of the helix can be inserted into the lipid bilayer causing membrane asymmetry and therefore curvature[66,67] (Figure 7 D). Proteins with this unique property of inducing curvature were called N-BAR proteins (from N terminal helix BAR Proteins) and they play different role into different cell compartments[107]. Some N-BAR proteins, such as Amphiphysin and endophilin, play a major role in CME inducing curvature of the mature CCPs by inserting their alpha helix

into the lipid bilayer and helping in the recruitment of late proteins such as dynamin, therefore aiding the maturation of CCPs into CCVs[108]. Finally crystallographic analysis revealed that BAR proteins are organized as antiparallel dimers and are characterized by a typical "banana" curved shape[64] whose concave side exhibits many residues with positive charge[95]. Therefore N-BAR proteins can induce membrane bending by acting as protein scaffolds, through their positive-concave face with interacts directly with membrane lipids, and additionally by inserting their alpha helixes into the lipid bilayer[100] (Figure 7 D left part).

One other class of proteins which induce membrane bending by insertion of helices into the lipid bilayer is the Epsin family. Espins consist of three isoforms, among which Epsin 1 and 2 are ubiquitously expressed, mainly involved in CME and localized at the plasma membrane[109]. All Epsins contain a conserved ENTH domain (Epsin N-terminal homology domain) at the N-terminus followed by a region that contain binding motif for several adaptor proteins (Epsin 1 contains binding motif for Clathrin and AP2)[109–111]. The ENTH domain was shown to specifically interact with PI(4-5)P2 at the cell membrane[112]. Detailed crystallographic analysis revealed the presence of an helix at the N terminus of the ENTH domain, called helix 0, with amphipathic properties; as for N-BAR proteins, insertion of the helix 0 into the lipid bilayers provide enough bending energy to curve the cell membrane[63] (Figure 7D right part). Epsins were therefore initially classified as late proteins in CME, as N-BAR proteins, since it was believed that they could promote and stabilize highly curved CCPs into CCVs[85]. Nervertheless, an excellent study from the De Camilli lab, showed a major role of Epsin in maturation of CME[62]. In their study, they generated triple knock out cells (TKO) for all three isoform of Epsin; by performing electron microscopy of TKO cells they observed a strong accumulation of U shape CCPs. Interestingly, through live-cell microscopy they noticed that late proteins such as Dynamin or Endophilin, did not accumulate at the CCPs but they rather had a cytosolic distribution; this result suggested that the U shaped structures were stalled at early stages of CME and not late stages. Therefore these results demonstrated a role of Epsin during the early-middle stages of CME favouring the maturation of CCPs[62].

1.2.4 Membrane bending of CCPs: current models

After understanding how membrane curvature is acquired at the cell membrane during CCPs maturation, the main question that remained was: when does curvature occur in CCPs? Do CCPs start to acquire curvature from early nucleation, or does the Clathrin coat start as a flat array and curvature is acquired after? Many groups struggled and are still trying to find an answer to this question and many studies have been performed. All these efforts contributed to the formulation of two possible models (Figure 8). Initially, through electron microscopy studies performed in the early 1980s, Heuser and colleagues identified a great distribution of flat and curved CCPs on the cell membrane. Because of this result, they hypothesize that Clathrin assembly starts as a flat array of a certain dimension; only afterwards curvature is acquired and increases during the maturation stages[15]. Acquisition of curvature comes along with a switch from hexagons to pentagons in the Clathrin coat[15], mechanism previously proposed by Kanaseki and Kadota in 1969[13].

This model found strong opposition in the following years by the work of Kirchhausen[113]. According to his theory, rearrangement of hexagon into pentagons, favouring bending of an initially flat array, is too expensive from an energetic prospective; therefore he believed that one other model where curvature is constantly acquired would better explain acquisition of curvature. This idea was confirmed by a later study that demonstrated that triskelia legs exhibit a strong rigidity once assembled into cages thereby making it energetically not possible to have rearrangements from hexagon to pentagons[114]. Additionally, it was suggested that the presence of pentagons into Clathrin cages was resulting from artefact generated during EM sample preparation[114]. From these studies, the new model proposed affirmed that CCPs acquire curvature starting from the nucleation step (Figure 8 A)

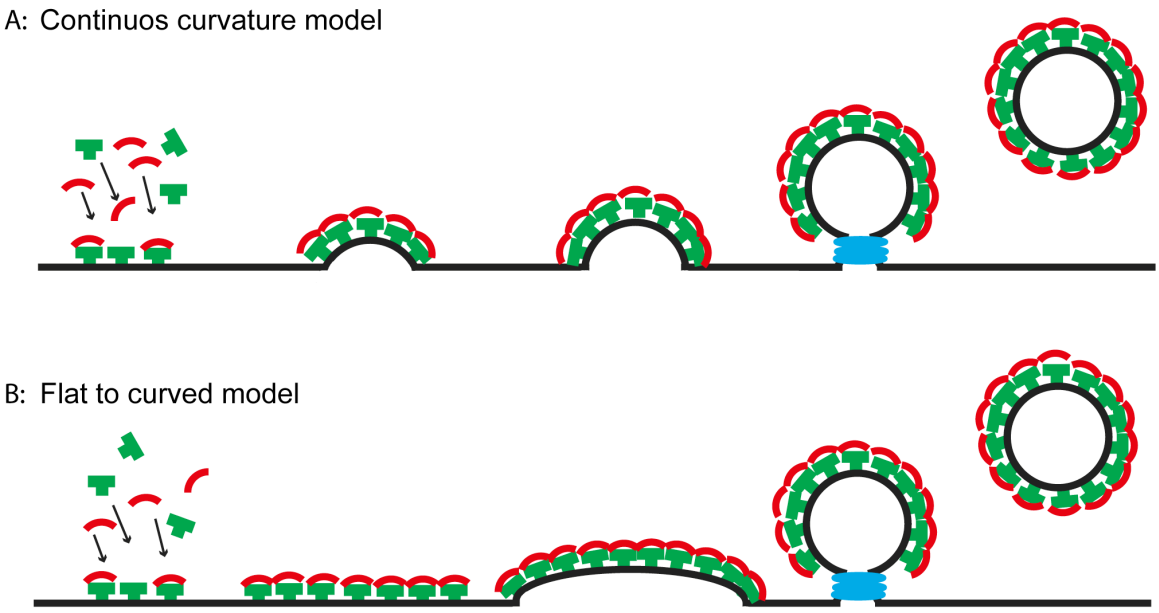

Figure 8. Models of membrane curvature acquisition during CME. Schematic representation of current models on how CCPs acquire curvature**.** A) Continuous curvature model. CCPs are continuously remodeled during maturation. B) Flat to curve model. CCPs nucleate and mature as flat array and afterwards they acquire curvature.

This model was challenged by recent studies that combine fluorescence microscopy, live-cell microscopy and electron microscopy. The advent of correlative light-electron microscopy (CLEM), gave scientists new possibilities to unveil details of CCPs maturation into CCV at high resolution (~nm). Avinoam and colleagues combined fluorescence microscopy with electron tomography to reconstruct the 3D shape of CCPs collected all over the cell membrane[21]. In their work, they observed that the area covered by the Clathrin-coated structures was similar from nascent CCPs to constricted CCPs co-localizing with dynamin. Moreover, they measured the angle of curvature between the CCPs and the cell membrane; interestingly this angle is not stable but increase from nascent to mature CCPs. All these results are compatible with a model where CCPs nucleate as flat arrays; afterwards, during maturation, the flat array starts to acquire curvature keeping its area constant (Figure 8 B). Further bending induces formation of the constriction until dynamin recruitment. This model therefore sheds light on a continuous Clathrin coat rearrangement during CCPs maturation in terms of curvature. This result is compatible the high Clathrin molecule turnover (2 secs) that was measured during pit maturation[21] combined with the high flexibility of Clathrin triskelia in

assembling into hexagonal or pentagonal structures[18,115]. This model is supported by further investigations performed by our group[116]. In this study fluorescence data and CLEM data were combined with mathematical modelling to confirm that CCPs start growing as flat array that later acquire curvature. The flat to curve transition is defined by a change in the AP2/Clathrin ratio that takes place when the Clathrin coat has reached 70% of its complete assembly[116].

All these studies therefore validate the second model (flat to curve CCPs) (Figure 8 B); nevertheless, due to the high plasticity and strong diversity of Clathrin coats, which have been deeply studied and characterize in the last 40 years since its discovery, it was suggested not to consider these two models as exclusive but rather as coexisting possibilities[7]. And in fact a recent work actually demonstrated that this is the case. Scott and colleagues challenged all the previous studies combining CLEM, atomic force microscopy (AFM) and a new imaging technique called polarized TIRF microscopy (pol-TIRF)[117]. This technique is based on the employment of fluorophores that have a polarized evanescent field that differentially emit light depending on their orientation (vertical VS horizontal); by modulating the polarization of the excitation light it is possible to excite only the fluorophores with a certain orientation (vertical or horizontal to the focal plane)[118]. By labeling the cell membrane with a polarized fluorophores they could identified its bending: if the membrane is flat all the fluorophores have horizontal orientation, if the membrane is curved some fluorophores will be horizontal some other vertical. By illuminating the sample with a polarized excitation light and looking at the vertical/ horizontal emission ratio it is possible to define the bending state of the cell membrane at specific spots. In their experimental setup, they performed live imaging using pol-TIRF on cells expressing Clathrin and Dynamin, to visualize CCPs, and a polarized fluorophores on the cell membrane, to get the curvature state at every identified CCPs. To validate the invagination of CCPs visualized by pol-TIRF they combined the fluorescence intensities with CLEM and AFM; in this way they could confirm that the curvature identified by pol-TIRF at a certain CCPs was reflecting the real bending of the cell membrane at that spot. In their work they identified both classes of CCPs; pits that show curvature from the early recruitment during nucleation (according to model 1), and pits that start as flat arrays and acquire curvature during maturation (according to model

2); among these, a big subclass of pits acquired bending before Clathrin reaches its peak, confirming results from previous authors[116].

Taken all together, these studies show that membrane curvature acquisition during CCPs represents a highly variable process that so far could not be classified using one model; probably, there are many other factors that need to be considered as many studies had already underlined. Clathrin turnover, membrane tension, cargo recruitment, accessory proteins and curvature proteins recruitment are all factors that can vary from cell to cell and among different areas of the same cells, defining probably different timing and mechanism of curvature acquisition.

1.2.5 Role of external curvature in inducing CME recruitment

How membrane bending is achieved and which proteins induce and recognize a certain curvature has been a major topic for many years in many research groups. CME is an important example of how curvature plays a major role in cellular function and in the course of time many protein responsible for curvature induction and stabilization have been identified, such as BAR proteins and ENTH proteins. Discovery of these proteins and their mechanism focused afterwards the attention of many scientists on new interesting questions. In particular, as we know that some proteins are recruited to the plasma membrane to actively induce curvature and favour vital process in the cell, could it be possible that certain proteins are recruited as a consequence of membrane deformation, mechanically imposed by the external environment[119]? And can such external mechanical stimuli consecutively favour the activation of certain cellular pathways? This process is called “mechanical induction”, meaning a process where a specific chemical signalling or protein recruitment is induced by mechanical stimuli, such as an imposed external deformation of the cell membrane [119] (Figure 9).

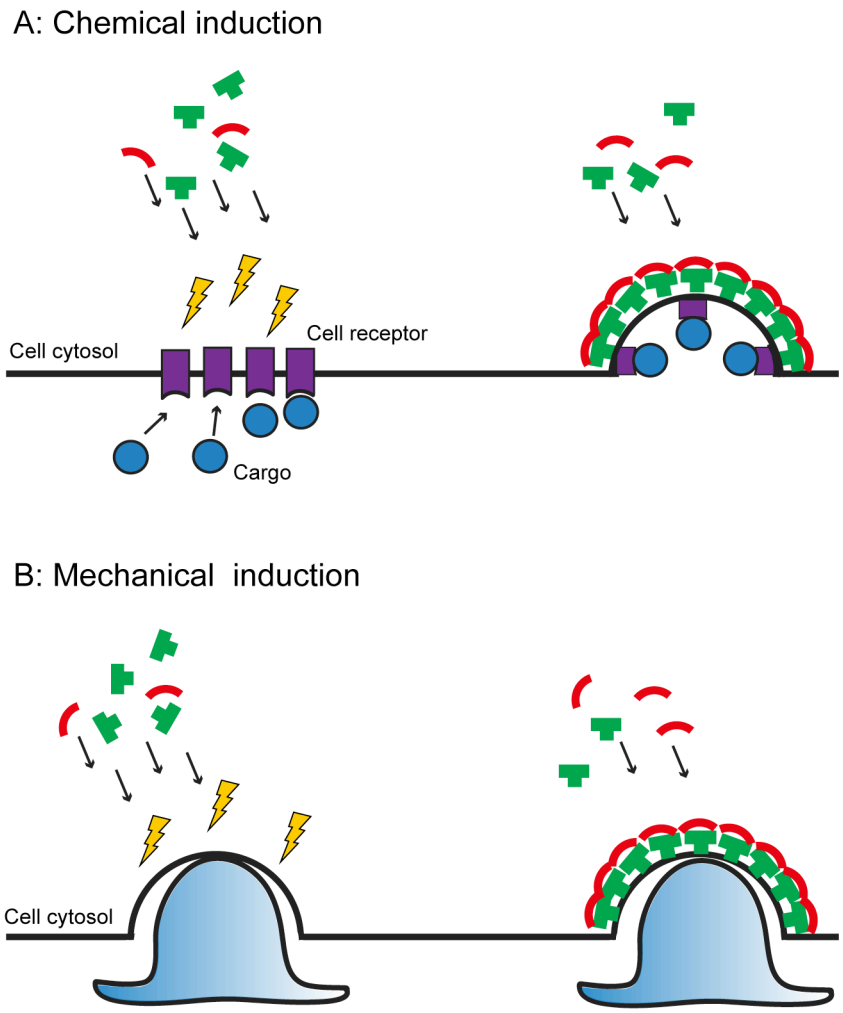

Figure 9. Chemical induction and mechanical induction of CME. A) Chemical induction of CCPs. Activation of specific signaling at the cell membrane, mediated e.g. by receptor-cargo interaction, can favor CME initiation. B) Mechanical induction. The passive curvature of the cell membrane mediated by external objects can favor CME initiation.

One of the major focuses of this field is to understand how and if a certain external stimuli, by inducing membrane passive deformation, can favour recruitment of certain proteins that in turn activate specific molecular pathways. The major limitations in understanding the role of mechanical external stimuli at the cell membrane was initially the lack of specific methods to study this process. In the last years surface chemistry and modified surface synthesis exhibited an important development making possible to study the role of imposed mechanical curvature in cell signalling. One of the first investigations that addressed these questions was performed by Galic and colleagues in 2012[120]. In their work the authors prepared glass surfaces containing nanocones

structures, 200 nm high and 50 nm wide at the base. Cell expressing the N-BAR proteins Nadrin 2 or Amphiphysin were seeded onto the nano-patterned glass coverslips containing stripes 3 um wide covered by nanocones alternated by stripes without nanocones. Interestingly areas of the cells adhering to the nanocones regions were characterized by a well-defined recruitment of both Amphiphysin and Nadrin 2, supporting the hypothesis that external stimuli can induce membrane bending and therefore BAR proteins recruitment. EM sample imaging confirmed membrane bending induced by nanocones. Afterwards the authors looked also at Clathrin and Dynamin recruitment and they noticed a pronounced recruitment as well on nanocones. However, it wasn't until 2017 when a paper from Zhao and co-worker showed how a precise curvature imposed by external mechanical structures induces CME[121]. Glass surfaces containing nanopillars of diameters raging from 50 to 500 nm were generated and cells were seeded on top. Afterwards the authors investigated the recruitment of 10 different CME related proteins. In particular by looking at the recruitment of Dynamin, they noticed a recurrent recruitment above the nanopillars, strongly suggesting the generation of endocytic "hot-spots". The intensity of Clathrin above the structures increases along with the size of the nanopillar and through ion beam and scanning electron microscopy (FIB-SEM) they confirmed the presence of CCPs growing on top of the nanopillars. This work shows how a precise imposed external curvature can induce the activation of cellular pathway such as, in this case, CME[121].

However, considering that nanocones and nanopillars constitute an artificial system, how an external mechanical induction can be imposed at the cell surface? What and "who" is imposing an external curvature? Is this phenomenon really taking place when considering cell in their natural environment? It is important to consider that in most of the cell biology experimental set-ups, we look at cells seeded onto flat surfaces in a 2D dimension; but the "original" environment of cells is much more complex and includes the interaction, for instance, with the complex extracellular matrix protein components. An extremely interesting and recent work revealed that seeding cells on collagen fibers arranged in a 3D environment can induce CME recruitment at the contact surface between fibers and cell membrane; this process is mediated by the curvature imposed by the collagen fibers onto the cell membrane[122]. This was confirmed by EM

images of un-roofed cells, where collagens fibers were covered by Clathrin structures. The role of these areas enriched in CCPs is mediating the anchoring of the cell membrane to the collagen fibers, helping to stabilize tension all over cell surface to favour migration and to stabilize the tension exerted at the cells edges by focal adhesion[122].

Therefore mechanical deformation of the cell membrane is opening a new field of investigations aiming at studying the behaviour of the cells in their natural environment and highlighting a new role of certain cellular pathways in responding to such external mechanical stimuli.

1.3 Virus entry.

1.3.1 Viruses: a general view

Viruses are well known obligate intracellular parasites; this means that they need to gain access inside an organism to replicate and spread. In an extremely simplified model, virus particles can be considered as small nanoparticles composed of a proteinaceous shell, the capsid, which contains the viral genome. Some viruses have their capsid wrapped by the envelope, a lipid membrane deriving from the infected cells, containing viral glycoproteins that help virus internalization. Going over this simplified model, it is possible to appreciate how viruses had evolved a great variability concerning their envelope composition, capsid dimension and architecture, and structure and genome composition. Despite this great variability, the main steps of infection can still be classified into four main stages: attachment to the host cell, the internalization of the particle, replication and translation of virus genome, and release of newly formed virus particles (Figure 10). For the main purposes of this thesis I will focus on the complex process of the early virus-cell interaction during cell attachment. This initial stage, involves several steps and often resulting in virus capsid modifications[123]. Attachment, signaling and endocytosis of the virus particle usually take place together and in a really narrow time window (few minutes) and they vary from virus to virus, therefore it is difficult to clearly describe and classify them. In the following paragraph I will provide some examples of the complexity of this process by describing the early virus–cell interaction of some viruses, highlighting at the end which steps are still not clarified in the field.

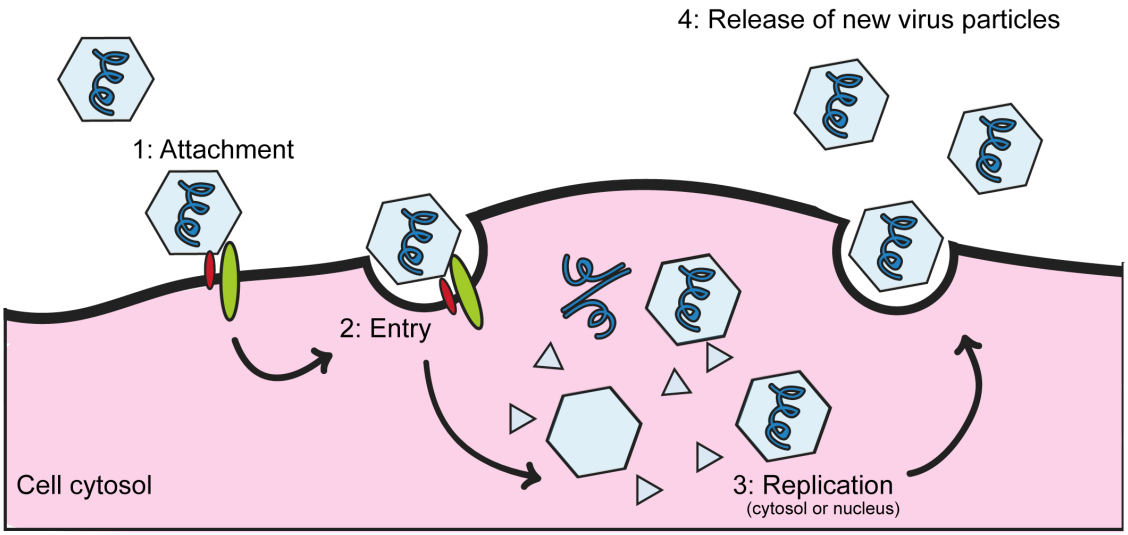

Figure 10. Schematic representation of virus infection. The process of virus infection can be divided in four main steps; 1) attachment of virus particles at the cell surface, 2) virus internalization, 3) virus replication, which can take place either in the cytosol or in the nuclei of the cell and 4) virus particle release.

1.3.2 Early virus – cell interaction: many ways to approach cell surface

Virus attachment is a complex process that involves the interaction between virus capsid or glypoproteins from envelope and specific cell receptors. It is important to differentiate among attachment factors and virus receptors[123]. The formers are molecules that electrostatically interact with virus particles to facilitate their attachment and concentration on the cell surface; these are usually sugar moieties or lipids. The latter define a specific interaction with the virus capsids/glycoprotein, inducing virus modifications, activation of signaling pathways and afterwards penetration. Importantly the specificity of the receptor binding defines the internalization pathway hijacked by the virus and its cell tropism[124]. Interestingly, viruses coming from different families can share similar receptors (such as Adenovirus and Coaxakie virus)[125,126] and at the same time viruses from the same family can use completely different receptors (such as Rinovirus)[127–129]. Moreover it is important to note that not only the specificity of receptors but also the mobility of virus-receptor complex above the cell membrane plays a role in favoring virus entry and in defining the mechanism through which viruses are internalized[130]. Although for many viruses the receptor binding and subsequent cell signaling pathways still need to be clarified, it is well know that viruses have evolved

different mechanisms to be internalized through the cellular endocytic machinery, hijacking several pathway[123,131]. Importantly, one of the main pathways used by viruses to get inside the cell is CME.

Influenza A virus (IAV) after landing on the cell surface shows an highly dynamic motion; the virus "walks" on the cell surface until its movement is arrested and immediately after the particle is internalized by CME[132]. Clathrin is recruited to the virus spot 2-3 minutes after virus binding at the cell surface, mediated by the interaction of the viral glycoprotein Hemagglutinin with Sialic Acid (SA) exposed on glypoproteins and glycolipids at the cell membrane[133]. This observation strongly suggests that IAV directly induces formation of CCPs[132]; however the signaling leading to CME recruitment is still not known.

This mechanism is opposite to the one that been described for canine parvovirus (CPV). Similar to IAV, CPV "walks" on the cell membrane; however instead of stopping on the cell surface, CPV searches an already pre-formed CCPs which it hijacks in order to be internalized[134]. Interestingly, a detailed analysis of CPV-cell receptor binding shows that the virus, after landing on the cells surface, interacts with a limited number of cell receptors; in this way CPV can diffuse on the cell membrane until interacting with a preformed CCPs[134]. A strong virus-cell interaction would probably not confer to the CPV this high mobility at the cell surface, affecting its internalization efficiency[130].

Therefore internalization by CME can display two different options; on one side we have viruses that induce *de novo* formation of CCPs; on the other side we have viruses that hijack pre-formed CCPs in order to gain access inside the cell. These examples show us how intricate the process of early the virus–cell early interaction is and they demonstrate that classification of virus entry based on the entry pathways is more complex than expected. Although the considerable amount of data available on virus attachment and entry, information regarding receptor binding, signaling and recruitment of a specific endocytic pathway for many viruses is still missing or not completely defined**.** This gap of knowledge is mostly due to the transient nature of the virus attachment at the cell surface and to its short duration; after landing at the cell membrane, virus internalization usually takes place within few minutes. We should consider also that these events are highly unpredictable, since we do not know at which cellular spot the

virus will be internalized. Moreover detailed information of virus-cell interaction at the single particle level are still missing. More importantly a method to address how this interaction take place and how this activates a specific endocytic pathway at the single particle level is still missing.

1.3.3 Reoviruses

In my work I used reovirus as a model systems to study early factors involved in virus entry. Reovirus is the prototype virus from the *Reoviridae* family. Their name comes from Respiratory Enteric Orphan virus[135] as they are able to infect both the intestinal and respiratory system, and initially they were associated with no disease (therefore they were "orphan" from symptoms). Nevertheless, it was shown that they can cause symptoms in children[136–138]. Reoviruses are non-enveloped, and have 85 nm icosahedral capsid that includes the viral genome. Their genome is composed of 10 double stranded RNA segments. The genome segments are classified as small, medium and large. The proteins that they encode are classified in numbers according to the genome fragment they belong: sigma (σ, small), mu (μ, medium) and lambda (λ, large).

1.3.3.1 Reovirus capsid

The reovirus viral capsid has two layers: an outer capsid, which defines the virion structure and is released after entry giving rise to the ISVP (infectious sub-viral particle), and a core particle (Figure 11). Reovirus outer capsid has a T=13 icosahedral symmetry[139] and it is composed by 200 copies of μ 1-σ 3 heterodimers arranged into hexagons[139–141] interconnected with 12 pentamers of λ2 subunits[140,142–145]. At the center of each λ2 pentamer there is a trimer of σ1 protein. Both λ2 and σ1 are essential for reovirus attachment and entry[146–149]. The ISVPs are produced once the particles reach the gut and are therefore exposed to trypsin[150,151] or by endosome acidification after virus internalization. ISVPs undergo further modification reaching the state of ISVP*; these particles miss the σ1 proteins and μ1 fragments undergo conformational changes[152,153]. The cleavage on σ1 defines the passage of the particles through the endosome membrane, and the released the core virus into the cytoplasm, where viral protein production and genome replication will take place[154].

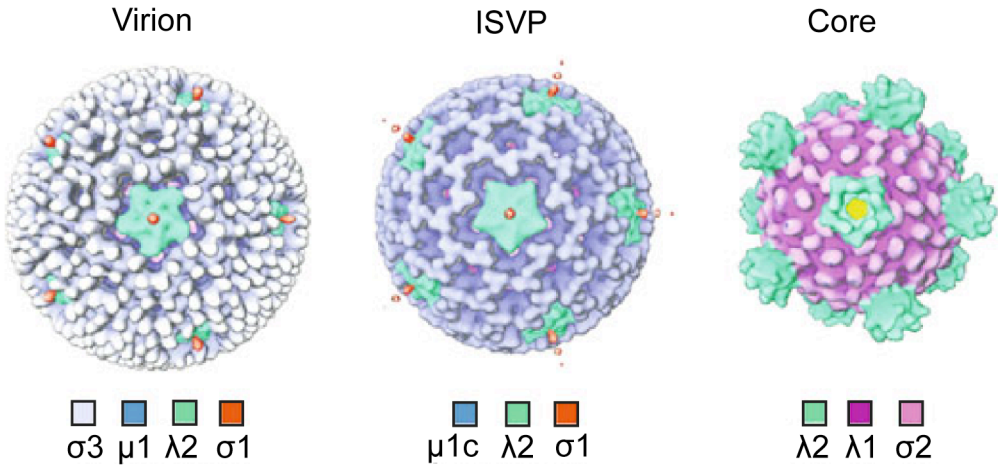

Figure 11. Structure of reovirus Virion, ISVP and Core. Each capsid subunit is highlighted with different colors. Adapted from Dryden at al., 1993.

1.3.3.2 Reovirus entry

Reovirus has three prototype stains: type 1 Lang (T1L), type 2 Jones (T2J) and type 3 Dearing (T3D). Since the attachment slightly differ among these strains, I will focus on T3D attachment, the prototype I used in my work. Surface attachment to the host cell is mediated by the σ1 protein of reovirus virions. Initially, σ1 interacts with the SA on the cell membrane[149]; this step it is essential to mediate the first attachment between the virus and target cell (Figure 12). Besides SA binding, the head of σ1 interacts also with the Junctional Adhesion Molecule A (JAM-A)[146,155] (Figure 12). JAM-A belongs to the immunoglobulin superfamily (IgSF) and it is involved in forming cell-cell tight junction[156] and in leukocyte migration through the endothelial layer[157]. While different serotype of reovirus bind different sugars at the cell membrane, JAM-A is recognized as major attachment factor for all reovirus strains[146,158,159]. Moreover, JAM-A requirement for reovirus infection have been tested both *in vitro* and *in vivo*[146,160]. Although removal of SA from cell membrane by treating cells with neuraminidase reduces T3D attachment to cell surface and therefore infection[161,162] binding of SA is not a requisite for reovirus attachment to JAM-A[146].

Reoviruses are internalized by receptor-mediated endocytosis; this means that after binding to the cell surface, virus particles are internalized by activation/hijacking of

cellular endocytic pathways. JAM-A is a transmembrane receptor, which has two extracellular domains and a small intracellular tail[156,157]; however, it was shown that removal of the cytosolic domain of JAM-A had no effect in reovirus infection[148]. Therefore JAM-A could not mediate activation of the cellular endocytic machinery. Therefore investigations moved forward to find out if a second receptor was involved in reovirus entry. Interestingly, by combining sequence and structural analysis of reovirus capsid proteins, it was discovered that the λ2 subunit exposes KGE and RGD motifs[163], which are well-characterized integrin receptor binding motifs[164]. The role of integrins in reovirus entry was demonstrated by observing that treating cells with blocking antibodies against Integrin Beta 1 reduced infection of reovirus (~50% reduction)[148]. The same authors confirmed this result by showing that Integrin beta1 null cells are less permissive for reovirus infection. In the current model proposed by the Maginnis and coworkers, reovirus infection starts with an early attachment mediated by the interaction between σ1 and the SA at the cell membrane; σ1 further interaction with JAM-A strongly enforce this attachment. Afterwards, λ2 interacts with Integrin Beta1 favoring virus entry through endocytosis[148] (Figure 12).

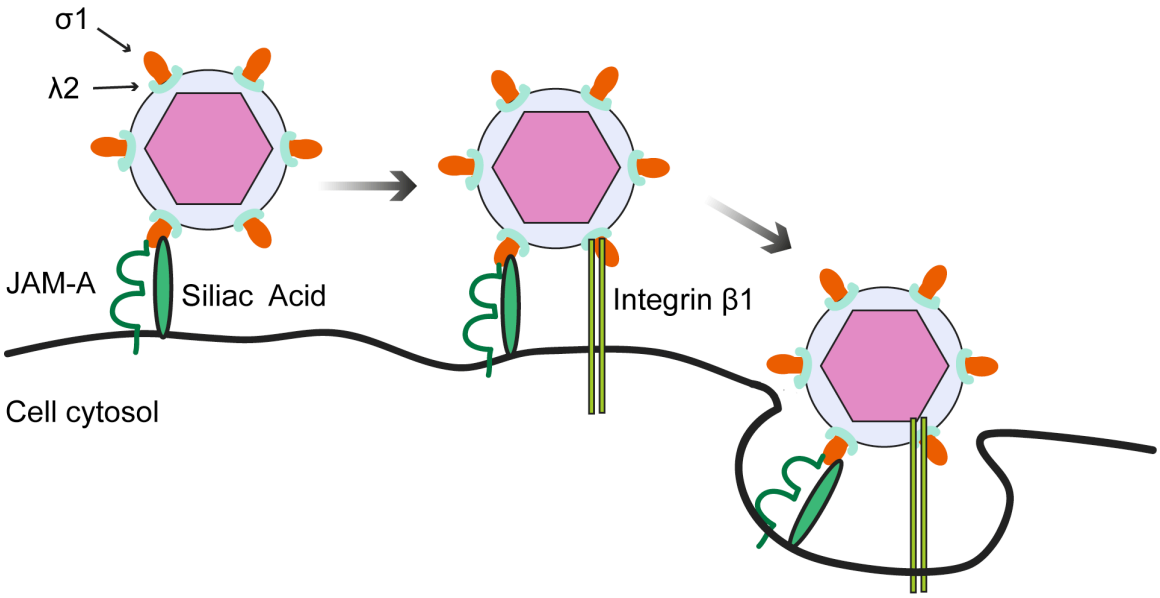

Figure 12. Schematic representation of reovirus entry. Reovirus attachment to the cell membrane is mediated by the interaction between the capsid subunit σ1 with sialic acid molecules and JAM-A receptor. Afterwards integrin β1 receptor is engaged by interacting with the capsid subunit λ2. Finally, virus particles are internalized through endocytosis

It was hypothesized, that a strong virus – receptor interaction, could define a limited diffusion of the virus-receptor complex at the cell membrane and favor activation of cell signaling for endocytic machinery recruitment[130]. Nevertheless, signaling pathways leading to reovirus internalization through endocytosis are not characterized yet. After receptor engagement, reoviruses are internalized by CME. Many studies have shown reovirus co-localization with Clathrin machinery[22,165]. Live-cell imaging of reovirus internalization through CME, show that 15-20 secs after virus attachment, the Clathrin machinery is recruited and the virus particle is internalized[165]; this event is rapid and takes place within a minute[165]. Despite these data, parallel studies suggested that reovirus entry might happen also through caveolae-mediated endocytosis in a cell type dependent manner[166,167]. Nevertheless, as discussed before, cell signaling leading to the activation of one pathway over the other, are not defined yet.

1.4 Nanoparticles uptake

In the last years the strong development of the nanomaterial field started to play a major role in several areas of the scientific research as well as in the biomedicine field. Nanoparticles, in particular, consist of beads of several size (at the nm range) and different composition, which can be extensively and broadly employed for medical purposes. Since cells can easily internalize them, nanoparticles are considered as suitable vectors for drug and gene delivery[168,169]. Another important application is the employment of nanoparticles in the research field and the possibility to coat specific beads with certain ligands to study ligand-receptor interactions and signaling inside/ outside the cell[170–176]. The efficiency of beads-cell interaction and further internalization depends from one side on cell type and cell state[177] and from the other side on nanoparticles characteristics such as composition, charge and size[178]. Considering spherical plain beads (with no coating or charge at the surface) Rejman and colleagues performed a detailed study where they investigated the internalization pathway of polystyrene beads from 50 to 1000 nm in non-phagocytic cells. Using different inhibitors for CME and caveolae-mediate endocytosis, they demonstrated that beads with diameter < 200 nm depended on CME, while beads > 500 nm in diameter were mainly internalized by caveolae[179] (Figure 13). At the same way Chithrani and colleagues analyzed the rate of internalization for gold nanoparticles having sizes from 14 to 100 nm; in their experiments they observed that beads of 45 nm are the ones prevalently internalized by CME[180]. Generally, particles with diameter between 10 and 30 nm can pass through the cell membrane by passive diffusion (Figure 13). Nevertheless, it is important to note that these particles, once suspended into cell media, might electrostatically interact with different proteins (i.e.. FBS) favoring the uptake or speeding up the process; therefore different studies might bring different results[181]. Importantly the charge of the particles can also impact the results; positively charged nanoparticles display a faster rate of internalization compared to neutral or negatively charged beads[182,183]. Positively charged beads may in fact interact with negatively charged molecules at the cell membrane (for instance SA) favoring their internalization. Although charge and interaction with proteins suspended in the cell media may play a role, it is clear that internalization of nanoparticles through one pathway over the other, strongly depends on their size.

However, so far, the mechanism leading to such size dependent mechanism is not clarified yet.

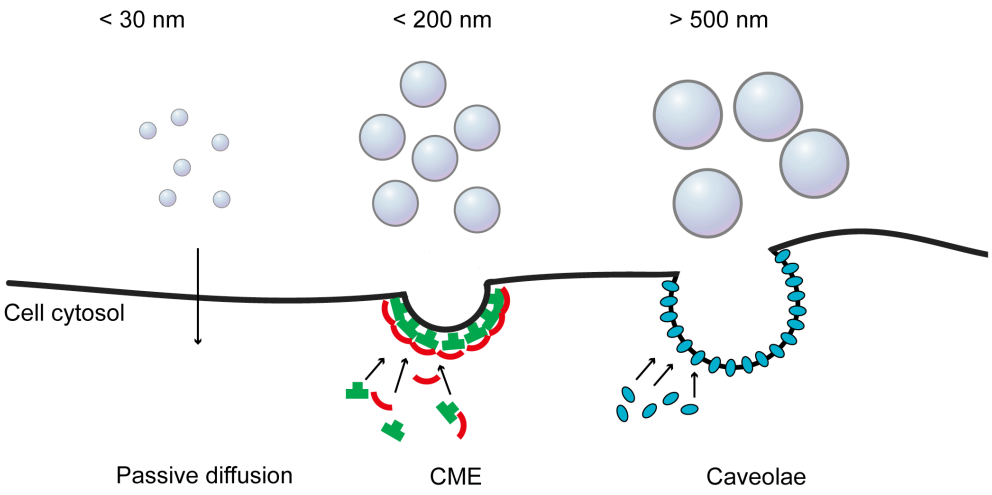

Figure 13. Schematic representation of nanoparticles internalization. Nanoparticles with diameter smaller than 30 nm are mostly internalized thorough passive diffusion at the cell membrane. Diameters smaller than 200 nm are internalized mostly by CME, while diameters greater than 500 nm are mostly internalized by caveolae-mediated endocytosis.

1.5 Aim of the thesis

Despite the great amount on knowledge regarding virus tropism, replication and association with diseases, the early factors that determine virus entry inside the cells are not clarified yet. CME is one of the most characterized endocytic mechanisms among eukaryotic cells and is one of the major pathways hijacked by viruses for their internalization. Nevertheless, which proteins play a regulatory function during initiation, and importantly how CME is activated upon virus binding is still a matter of debate. Virus particles diffuse fast on the cell surface and, once interacting with the Clathrin machinery, their internalization takes place in the range of few minutes.

In order to shed light on the fast and transient virus-Clathrin machinery interaction, the first goal of this thesis was to establish a new method to "freeze" the early interaction between viruses and cell surface. This was achieved by combining surface chemistry and click chemistry to covalently immobilize virus particles onto glass surfaces. Importantly I demonstrated that modified virus particles are still infectious and can interact with cells, proving the efficiency of the method.

The second main aim of this work was to determine the early factors that favor/induce activation of cellular endocytic machinery upon virus binding. Cells expressing marker for CME were seeded on top of virus-coated surfaces; by combining live-cell microscopy, super resolution microscopy and electron microscopy it was possible to unveil early events of virus-cell interaction and define their dynamics at the single molecule level. In particular I, for the first time, addressed the role of mechanical *vs* receptor-mediated proprieties of the virus in inducing CME activation and how these are regulated during early steps of infection. By clicking different viruses onto surfaces it was possible to specifically study the contribution of receptors in inducing CME recruitment and activation. At the same way, by immobilizing beads of several diameters it was addressed the role played by the size and the curvature that virus particles impose at the cell membrane in favoring CME pathway activation.

These aspects could not be investigated with current biological techniques, confirming the relevance of the presented method that can be easily applied to the field of nanotechnology, endocytosis and virology.

2 RESULTS

The text and the figures from the results part have been adapted from Fratini et al., submitted, which corresponds to the manuscript resulting from my PhD research project.

2.1 A new method to study early virus-cell interaction

To study early steps of virus infection and to understand how these affect CME recruitment and virus internalization, I established a new method to investigate early virus-cell interaction. According to this method, virus particles are immobilized onto glass surfaces and afterwards cells are seeded on top; in this configuration, cells can interact with the virus particles but they can not internalize them. The aim of this approach is to "freeze" the early virus–cell interaction and to exert a spatio-temporal control of the Clathrin machinery recruitment above the immobilized viruses (Figure 14).

Before starting working on method establishment, different cell lines were evaluated and, importantly, virus particles were tested for labeling procedure.

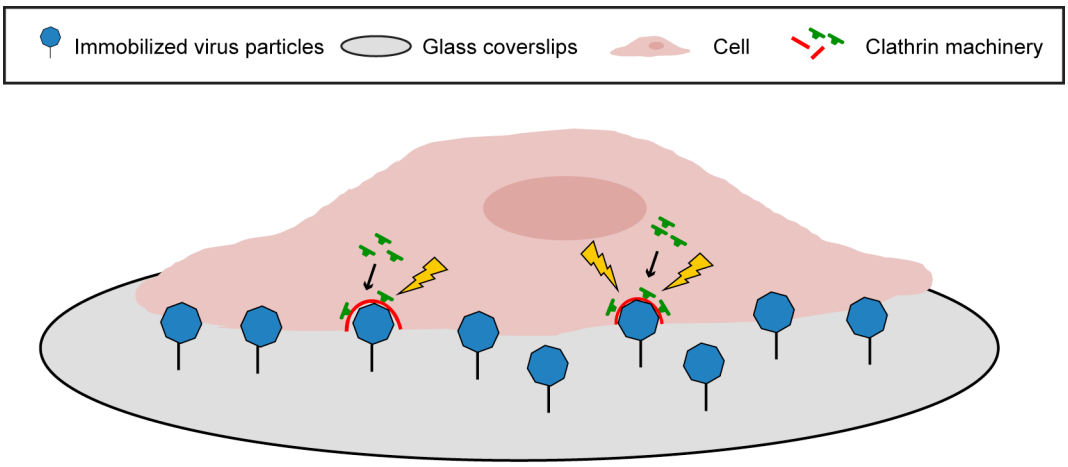

Figure 14. Schematic representation of the approach adopted in this thesis to study early virus-cell interactions. Virus particles are immobilized onto glass surfaces and afterwards cells are seeded on top. This makes it possible to "freeze" the early events of virus-cell interaction without allowing for virus internalization and infection.

The work in this thesis was performed mainly with U373 and BSC1 cells; these cell lines are widely used for studying CME[116,184] and are both susceptible to reovirus

infection[185–187]. Specifically, U373 and BSC1 cells stably expressing AP2-GFP as marker for CME were used; importantly, in contrast to Clathrin, which is involved in coating vesicles at the cell membrane and also in the cell cytosol, the adaptor protein AP2 is recruited only at the cell membrane of the cell. Since there is no cytosolic signal coming from AP2, the signal/ noise ratio at the cell membrane is optimal for imaging through confocal fluorescence microscopy.

2.1.1 Labeling of reovirus particle is compatible with virus infectivity

To visualize virus particles by fluorescence microscopy, virus capsids were labeled with Alexa647 succydimyl ester (NHS). The labeling reaction is based on the strong reactivity of the NHS functions (derived from the fluorophores) towards the free ammines exposed at the virus capsid; the outcome of this reaction is the formation of an amide bond between the fluorophores and virus particles (Figure 15A and B).

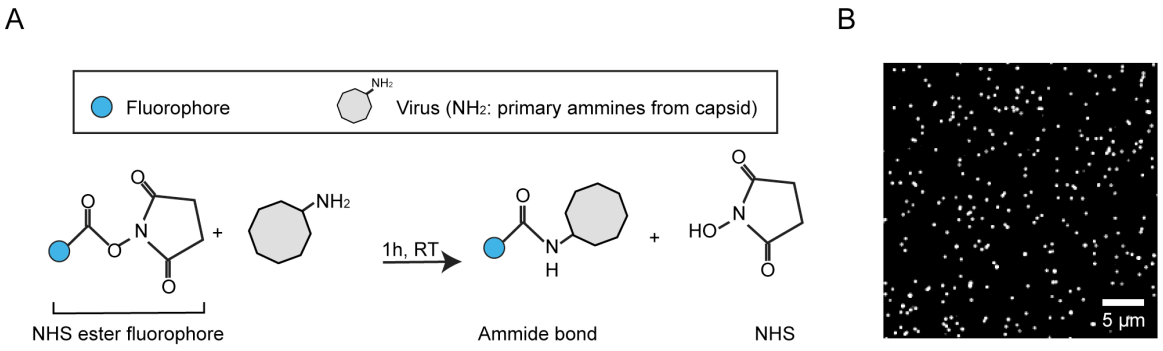

Figure 15. Schematic representation of the virus labeling chemistry. A) NHS fluorophores are incubated with virus particles; these functions react with the free amines groups exposed at the virus capsid forming an amide bond. B) Fluorescence image of label virus particles deposited on glass.

To control for homogenous labeling and aggregation, labeled virus particles were deposited onto glass coverlips and imaged by fluorescence microscopy. Intensity values of virus particles displayed a uniform distribution, demonstrating that the labeling was uniform and that it did not induce virus aggregation (in the case of virus aggregation, fluorescence distribution would have been shifted towards higher fluorescence values) (Figure 16A). To control that the labeling reaction was not affecting virus infectivity, BSC1 cells were infected with same titer of control virus (virus not labeled) and

Alexa647-labeled virus (Alexa647-virus). BSC1 cells were fixed 16-18 h post infection and immunstained against the reovirus non-structural protein μNS, which is a marker for reovirus replication in the cytosol of infected cells[187]. Quantification of the number of infected cells revealed that labeling virus particles had no impact on their infectivity (Figure 16 B). Together these results demonstrate that the labeling procedure produces a uniform distribution on the virus particles, it does not induce virus aggregation and it does not affect virus infectivity.

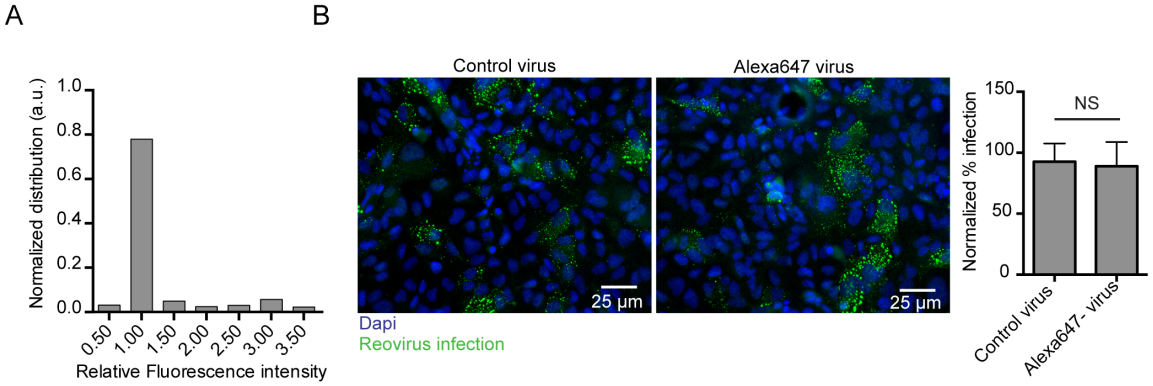

Figure 16. Labeling procedure did not induce virus aggregation and did not affect virus infectivity. A) Fluorescence distribution of Alexa647-virus deposited on glass. B) (Left panel) BSC-1 cells were infected with control virus and Alexa647 virus at MOI 1. 16-18 hours post-infection, cells were fixed and stained for reovirus infection (green). (Right panel) The ratio of infected cells to total number of cells was normalized to cells infected with control virus. Data are shown as mean value ± standard deviation (SD) of three independent replicates.

2.1.2 Immobilizing virus particles on glass surfaces: exploiting electrostatic interactions

After the creation of the labeled virus, I needed to establish the best method to immobilize viruses on a coverslip. I began by investigating the simplest configuration: the electrostatic interactions. This interaction occurs between the negatively charged virus capsids and the positively charged ions of the glass surface inducing the virus particles to adhere at glass coverslips. By using different concentration of viruses, it was possible to reach different viruses distribution onto the glass surfaces (Figure 17).

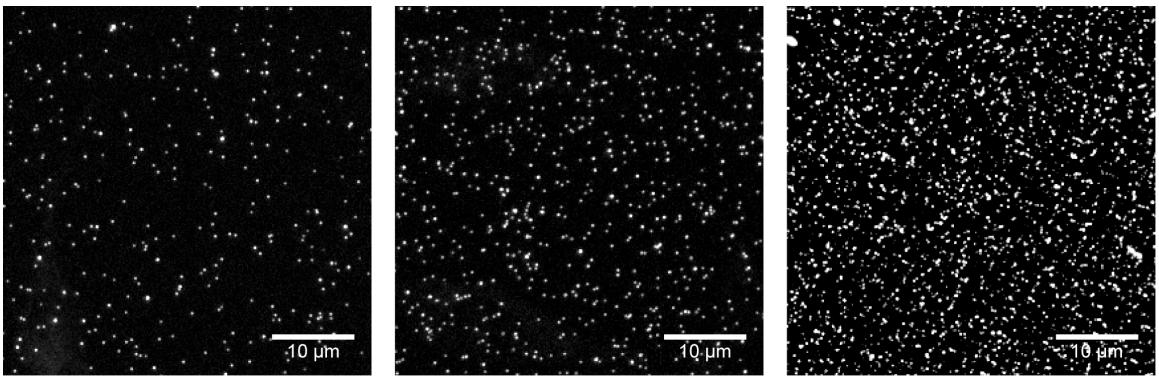

Figure 17. Electrostatically immobilized virus particles. From left to right: fluorescent images of different concentration of virus particles electrostatically immobilized onto glass surfaces (number of virus particles/area is indicated below each picture).

U373 and BSC1 cells stably expressing AP2-GFP were seeded on top of electrostatically immobilized virus particles; the day after cells were fixed and imaged by fluorescence microscopy. The AP2-GFP signal was visible at the cell membrane in the shape of fluorescent dots. Each of these dots represents different stages of CCPs assembled at the cell membrane. However, virus particles located below the adherent cell surface were often completely removed from the glass surface and internalized by cells. Virus uptake was confirmed by immuostaining for reovirus μNS. Additionally, transfection of cells further promoted virus uptake by the cells and subsequent infection (Figure 18). As transfection reagents contain lipid components they are likely affecting the viruses ability to interact with the glass surface. These results indicated that electrostatic interactions were not efficient to stably immobilize virus particles onto the surface of coverslips.

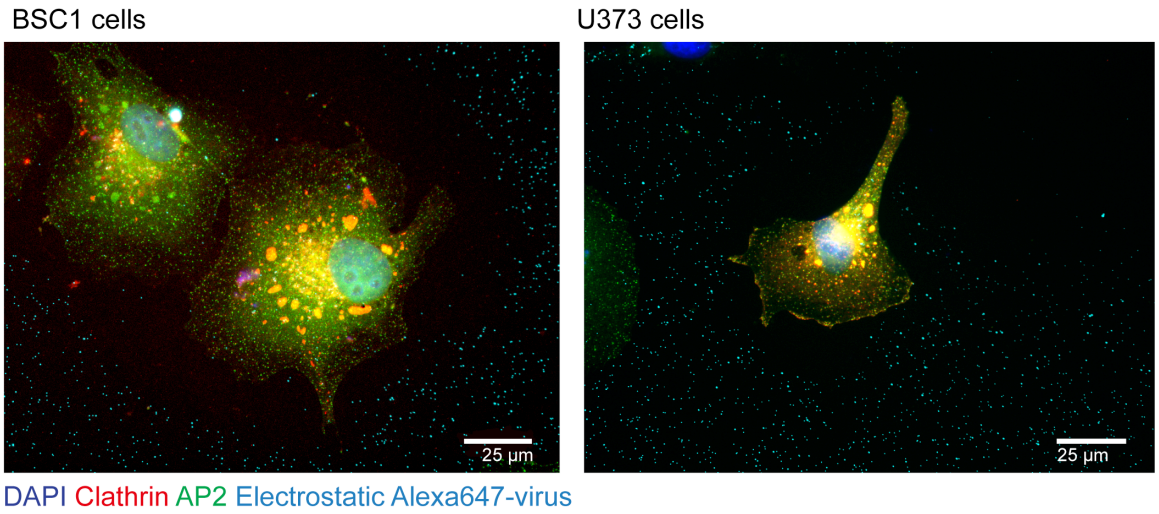

Figure 18. Transfection affects virus immobilization onto glass surfaces. BSC1 and U373 stably expressing AP2-GFP were transfected with Clathrin light chain (CLC). One day after transfection cells are seeded on top of coverslips coated with electrostatically immobilized virus particles. 12 hours post-seeding, cells are fixed and imaged by fluorescence microscopy. During cell adhesion and spread, virus particles are often removed from the glass surface, resulting in cell infection.

2.1.3 Covalent immobilization of virus particles onto glass surfaces

The use of electrostatic interactions did not result in firmly immobilizing particles on the surface of coverslips, indicating that viruses require a covalent and more reproducible immobilization method. As click chemistry fulfills these requirements, virus particles were modified to test this new approach. One of the most used click chemistry approaches is the copper–catalyzed azide-alkyne cycloaddition (CuAAC). In this reaction, an alkyne–molecule A can react with an azide-molecule B, generating a stable A-B complex connected by a triazole ring. The alkyne and azide interaction is highly selective and specific but it strongly depends on the presence of copper as catalyzer[188].To apply this technology to our model, Alexa-647-NHS labeled reoviruses were conjugated with an alkyne function (propargyl-N-NHS ester linker) and afterwards "clicked" onto azide modified surfaces (Figure 19 A). Equal concentrations of Alexa647-NHS ester and alkyne linker were mixed with virus particles generating Alexa647 and alkyne-modified viruses (Alexa647/alkyne-viruses). As described before, the NHS functions from the fluorophores and the alkyne linkers react with free amines exposed at the virus capsid generating a covalent bond. While the fluorophores are essential for visualizing virus particles through

fluorescence microscopy, the alkyne linker serves as functional group for the CuAAC. To control that addition of the alkyne linker was not inducing virus aggregation, Alexa647-viruses and Alexa647/alkyne-viruses were deposited onto glass and imaged by fluorescence microscopy; afterwards intensities values of all virus particles were measured and plotted (Figure 19 B). As shown in Figure 19B, Alexa647-viruses and Alexa647/alkyne-viruses displayed the same regular fluorescence distribution. This result demonstrated that the addition of the alkyne linker did not induce virus aggregation and, moreover, did not affect fluorescence labeling, since intensity values from Alexa647-viruses and Alexa647/alkyne-viruses exhibited same distribution.

To ensure that addition of fluorophores and alkyne linker was not affecting virus size, Scanning Electron Microscopy (SEM) was performed to compare viruses with no modifications (control virus) and Alexa647/alkyne-viruses deposited on glass. By measuring the diameter of each single virus particles, I calculated an average diameter of 79 nm ±16 nm from Alexa647/Alkyne-viruses, which was similar to the average diameter of 77 nm ± 14 nm from control viruses (Figure 19 C). To further confirm this result, dynamic light scattering analysis (DLS), an optical technique that measures the scattering of light within a sample containing suspension of nanoparticles, was used to measure diameter of modified and non-modified virus particles. DLS analysis confirmed that size of Alexa647/alkyne virus is similar to control virus (Figure 19 D). All together these results confirmed that addition of fluorophores and alkyne linker did not induce virus aggregation and did not affect virus size.

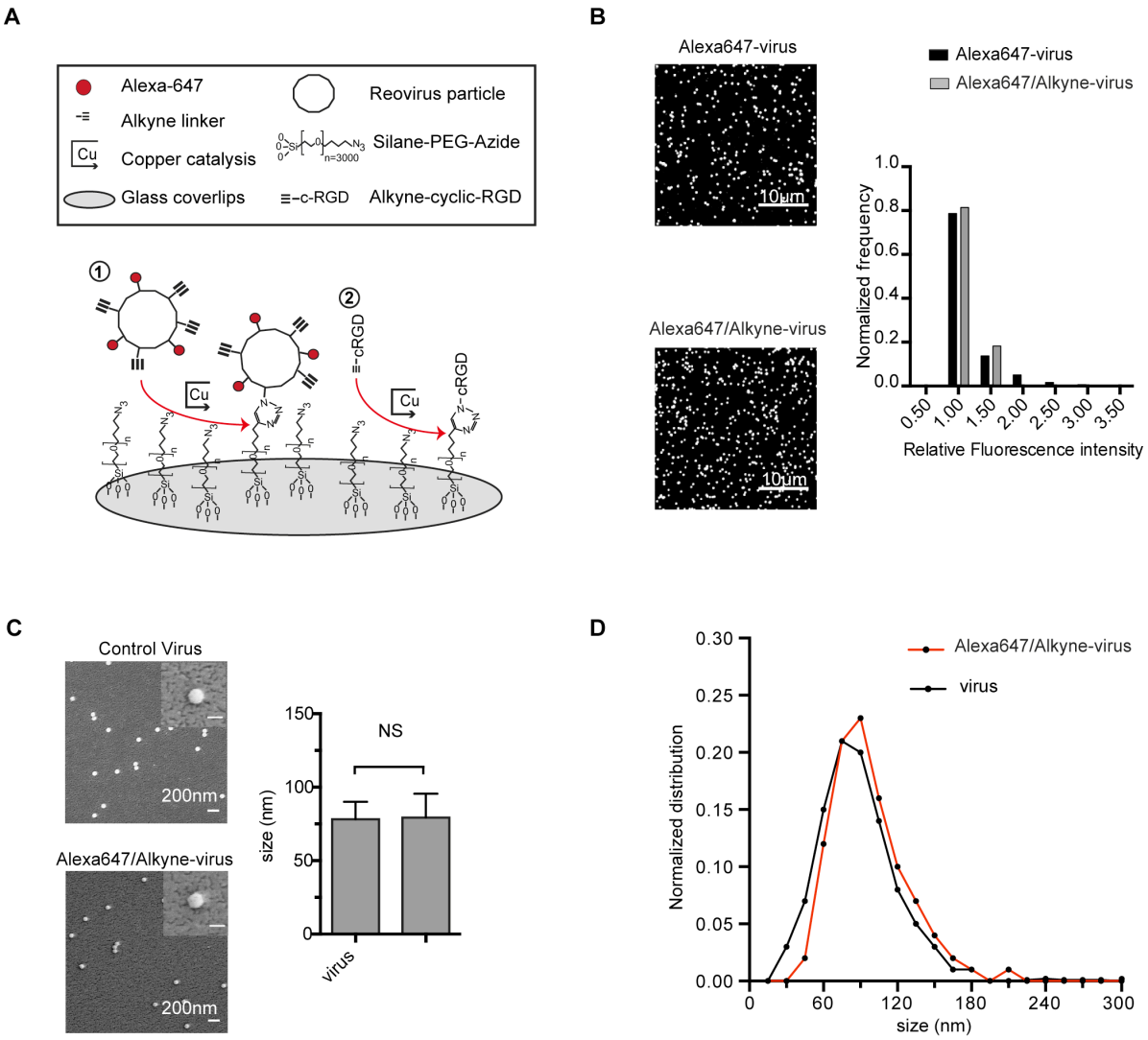

Figure 19. Chemical modification of reovirus particles. A) Schematic of reovirus immobilization onto glass surfaces. 1) Reovirus particles were fluorescently labeled with Alexa647 dye and coupled to an alkyne linker. Through CuAAC (Click chemistry), virus particles were covalently bound onto Si-PEG-N_3 coated coverslips. 2) To allow for proper cell adhesion on the surfaces, cyclic-RGDfK-alkyne peptides were clicked onto the same surface. B) (Left part) Reovirus particles were fluorescently labeled with Alexa647 dye and/or functionalized with an alkyne- linker and then deposited onto glass coverslips. The fluorescence intensities of particles for Alexa647-virus (n=11001) and Alexa647/Alkyne-virus (n=35027) were quantified using fluorescence microscopy. (Right part) The distribution of the normalized mean of fluorescence intensity (in arbitrary units) is shown in bins of 0.5. C) SEM imaging of non-modified and Alexa647/Alkyne-virus. Virus particles were deposited onto glass coverslips. Afterwards critical point drying of virus particles was performed and samples were sputter-coated with titanium and gold layers. (Left part) SEM images of non-modified virus and Alexa647/Alkyne-virus deposited on glass coverslips; Image magnification: 25000x. Inserts depict zoom-in of representative single virus particles, scale bar 80 nm. (Right part) The particle size of non-modified (n=1203) and Alexa647/Alkyne-virus (n=629) was measured as described in methods. Data are shown as mean value ± SD. p value <0.05 is considered significant (unpaired t-test). D) The size of non-modified virus particles (n=1004 particles) and Alexa647/Alkyne-virus particles (n=544 particles) was

obtained through dynamic light scattering measurement (in collaboration with Dr Pranav Shah, currently at Harvard Medical School, USA). The size distribution of the particles is shown. Adapted from Fratini et al., submitted.

Chemical modification of virus particles often results in the loss of virus infectivity. I therefore tested if virus infectivity was affected by conjugation of both the Alexa647 and the alkyne linker. BSC1 cells were infected with serial dilutions of control virus and Alexa647/alkyne-virus. One day after infection cells were fixed and immunostained against the reovirus μNS protein. An "In-Cell Western^{TM}" Assay (ICW) was used to assess infectivity as it automatically performs immunofluorescence quantification obtaining unbiased and detailed results. Fluorescence quantification of cell infected with control virus and Alexa647/alkyne-virus displayed the same values, confirming that virus infectivity was not affected by the labeling and alkyne linker conjugation (Figure 20 A). Furthermore, I controlled that virus replication was not affected by chemical modification. BSC1 cells were infected with same titer, as determined by the ICW, of control virus and Alexa647/alkyne virus. Cells were then lysed 3-4 days after infection to collect the newly formed virus particles. The cell debris was removed by centrifugation and the virus containing supernatant was serially diluted and used to infect a new round of BSC1 cells. One day after infection cells were fixed, immunostained against μNS and fluorescence quantification was performed by ICW. Data analysis revealed that virus progeny exhibits the same infectivity in control virus and Alexa647/Alkyne virus, demonstrating that virus replication was also not affected by chemical modification of virus capsids (Figure 20 B). All together these results confirmed that virus capsid modifications through labeling and addition of alkyne linker did not induce virus particle aggregation and did not affect virus infectivity and replication.

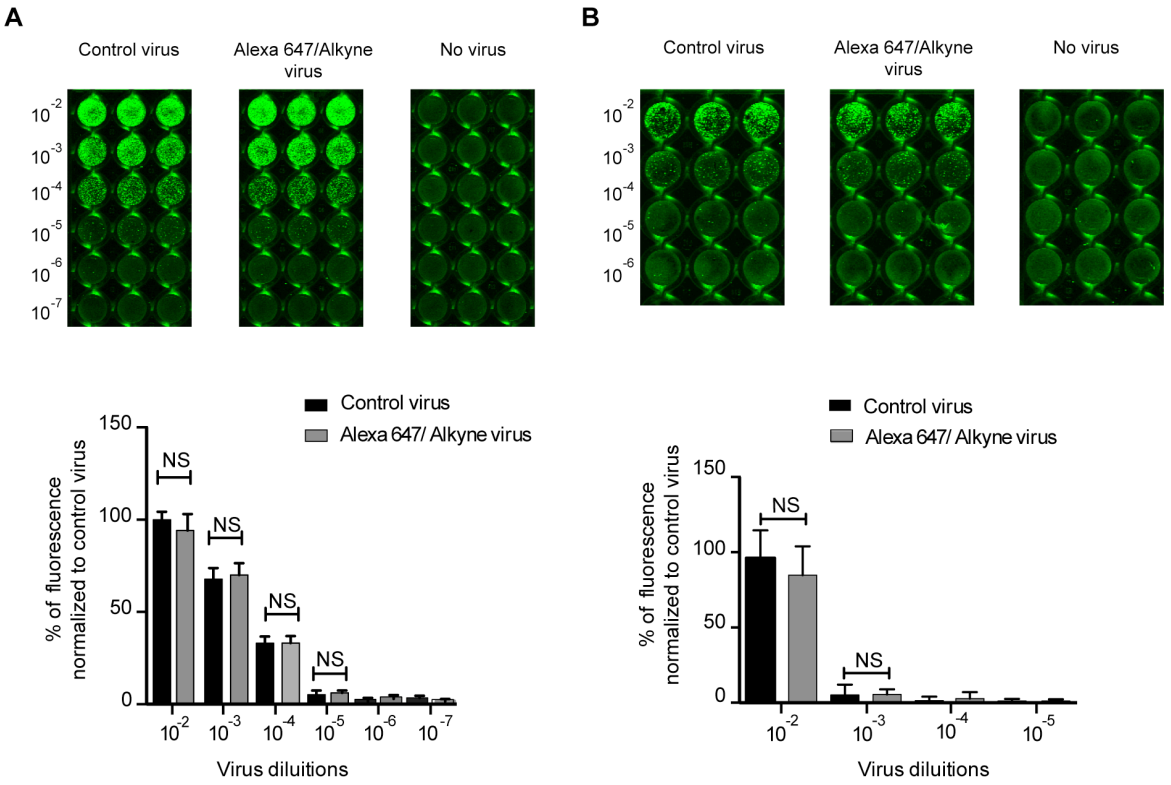

Figure 20. Chemical modification does not affect virus infectivity and replication. A) BSC-1 cell were infected with serial dilutions of non-modified virus and Alexa647/Alkyne-virus. Each dilution was performed in triplicate. 16-18 h post-infection, cells are were fixed and stained for reovirus infection using a reovirus anti- μNS antibody (green). Fluorescence measurement and quantification were performed using a LI-COR's Odyssey. (Lower panel) Normalized fluorescence intensity for each virus dilution. Data are shown as mean value ± SD from three independent experiments. p value < 0.05 is considered significant (unpaired t-test). B) BSC-1 cell infected using the same MOI of non-modified and Alexa647/Alkyne-virus. 72 hours post-infection, cells were lysed and de-novo virus production was addressed by in-cell western blot as described in A). Data are shown as mean value ± SD from three independent experiments. P value < 0.05 is considered significant (unpaired t-test). Adapted from Fratini et al., submitted.

2.1.4 Viruses are covalently linked to glass surfaces via click chemistry

As virus particles were efficiently modified by conjugation with fluorophores and alkyne functions, they now must be clicked onto azide-coated glass coverslips. Glass coverslips were modified by creating a self-assembled monolayer of silane-PEG(3000)-Azide (Si-PEG-N3) (see materials and methods) followed by addition of the Alexa647/alkyne-viruses by CuAAC click reaction (Figure 19 A, 1). To control the specificity of the covalent immobilization of Alexa647/alkyne-virus, the following samples were clicked onto Si-PEG-N3 surfaces: Alexa647-virus with copper and

Alexa647/alkyne-virus +/- copper. Samples were then imaged by fluorescence microscopy and the number of virus particles clicked onto the glass surface was measured and plotted. Efficient immobilization could be observed only with virus particles containing the alkyne linker and in the presence of copper (Figure 21 A). This demonstrated that the azide-alkyne bond between virus particles and glass surfaces was highly specific and strongly dependent on copper catalysis. The number of virus particles clicked onto the glass surface was adjusted to be compatible with live imaging (approximately 8.0 +/- 0.6 particles/ 10 μm^2).

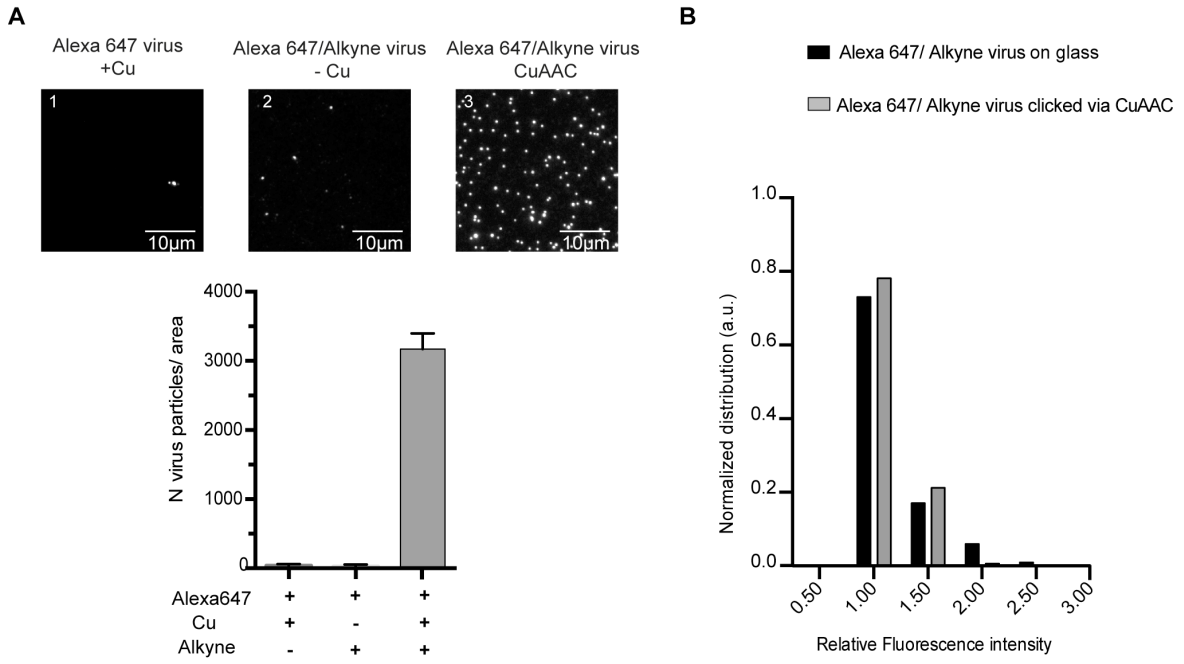

Figure 21. Validation of reovirus covalent immobilization onto glass surfaces. A) Alexa647-virus or Alexa647/Alkyne-virus were clicked on Si-PEG-N_3 coated glass coverslips in presence or absence of copper (Cu). The conjugation efficiency was estimated using fluorescence microscopy by counting the number of immobilized virus particles/area (3.9 x 10^4 μm^2). B) Alexa647/Alkyne-viruses were either deposited on glass or clicked on Si-PEG-N_3 coated coverslips. The fluorescence intensities of the labeled viral particles were measured and plotted as described in methods. Distribution of normalized fluorescence mean intensity (in arbitrary units) of particles was quantified for non-clicked (n=62204) and clicked particles (n=12965). Adapted from Fratini et al., submitted.

To ensure that virus immobilization through click chemistry was not inducing virus aggregation, I compared the fluorescence intensity distribution of Alexa647/alkyne-virus clicked onto glass surfaces virus with Alexa647/alkyne virus deposited on glass.

Fluorescence intensities showed similar distributions, ruling out the possibility that immobilization through CuAAC could induce virus aggregation (Figure 21 B).

Cell adhesion cannot occur on Si-PEG-N3 coverslips; the coating in fact creates a hydrophobic monolayer that prevents any kind of cell adhesion (Figure 22). Therefore, to favor cell attachment on modified glasses, the cRGDfK-alkyne peptide (cyclo[Arg-Gly-Asp-D-Phe-Lys]) was clicked after Alexa647/alkyne-virus had been immobilized[189] (Figure 19 A, 2). RGD is a small peptide that favors formation of cell adhesion patches, or focal adhesions, by interacting with integrin receptors[164]. I confirmed that cells seeded on only Si-PEG-N3 or on Si-PEG-N3 coated with only Alexa647/alkyne-virus could not adhere (Figure 22 A and B). Importantly, cells seeded on clicked cRGDfK only or on coverslips displaying both the cRGDfK peptide and clicked viruses showed no difference in seeding efficiency and focal adhesion formation, demonstrating that clicked viruses do not interfere with cell adhesion (Figure 22 A and B).

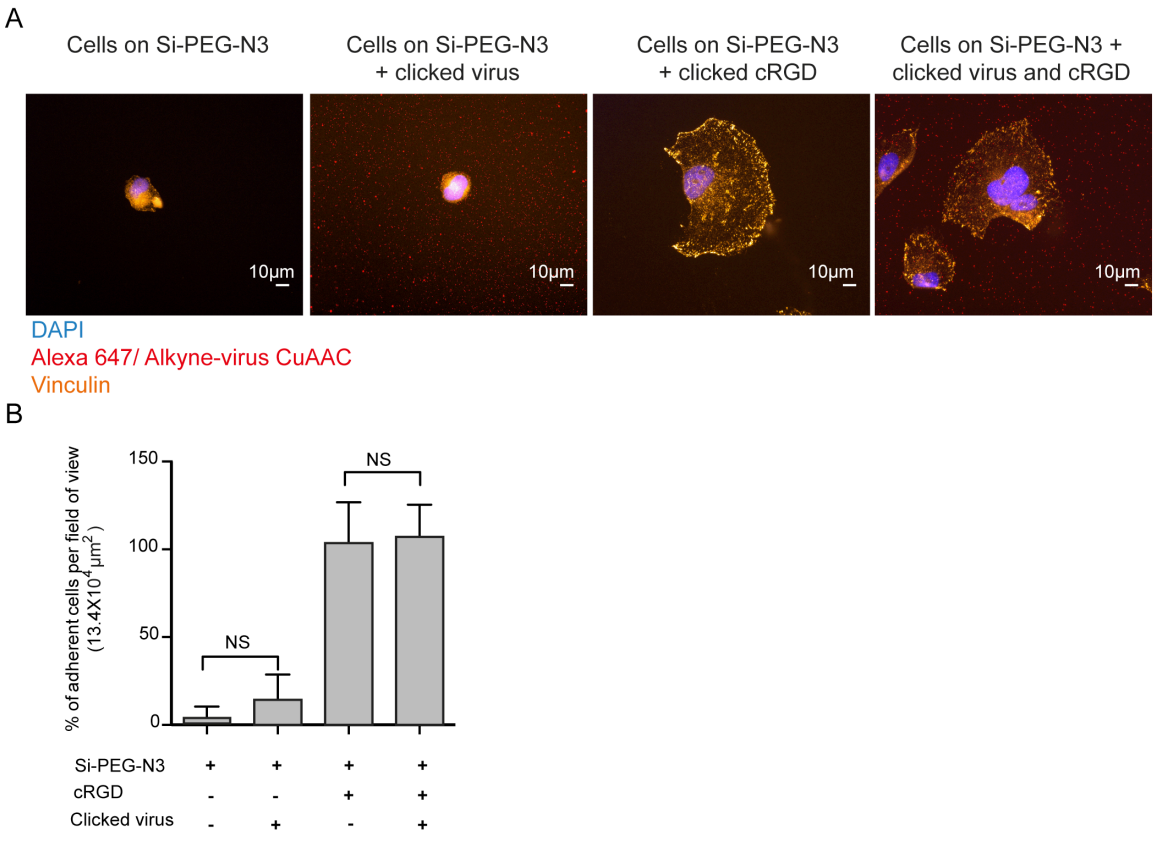

Figure 22. Clicked cRGDfK peptide is necessary for cells to adhere on Si-PEG-N_3 coverslips. A) U373 cells were seeded on Si-PEG-N_3 coverslips without or with cRGDfK or on Si-PEG-N_3

coverslips clicked with Alexa647/Alkyne-virus (red) without or with cRGDfK peptides. 6 hours post-seeding, cell adhesion was evaluated by indirect immunofluorescence using an anti-vinculin antibody (bright orange). B) The number of adherent cells per area in each sample was counted and normalized to the number of adherent cells on Si-PEG-N_3 with clicked cRGDfK. p value < 0.05 is considered significant (unpaired t-test). Adapted from Fratini et al., submitted.

Finally, I controlled if clicked viruses could be removed from modified glasses after seeding cells on top. BSC1 cells were seeded onto clicked-virus + clicked-RGD coated coverslips. As a positive control, BSC1 cells were infected with Alexa647/alkyne-virus pre-incubated with click chemistry reaction mix. One day post-seeding, cells were fixed and immunostained for the reovirus μNS protein. Interestingly, all virus particles remained attached to the coverslips and the cells remained uninfected (Figure 23 A and B). Importantly, this indicates that up to 24h after cell seeding no virus particle was observed within the cell cytoplasm. On the contrary, control cells infected with Alexa647/alkyne-virus pre-treated with click chemistry reaction mix exhibited the typical reovirus cytoplasmic factories resulting from reovirus infection (Figure 23 A).

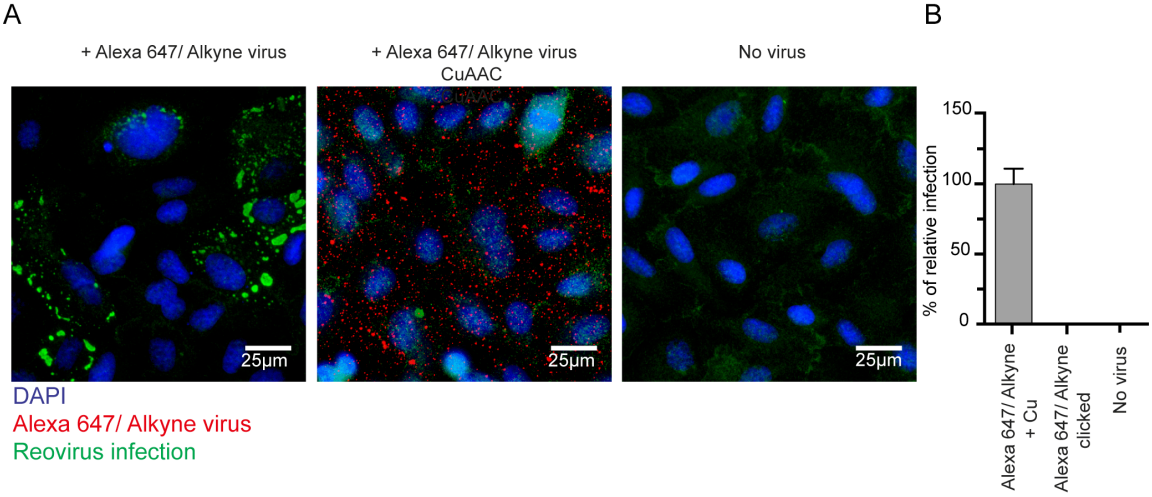

Figure 23. Clicked reovirus particles are not internalized by cells. A) (From left to right) BSC-1 cell were infected with $CuSO_4$ pre-incubated Alexa647/Alkyne-virus at MOI 1, seeded on clicked-virus coated coverslips, or were incubated with no virus. 16-18 hours post-infection, cells were fixed and stained for reovirus infection (green). The ratio of infected cells to total number of cells was normalized to cells infected with Alexa647/Alkyne-virus pre-incubated with $CuSO_4$. Data are shown as mean value ± standard deviation (SD) of three independent replicates. Adapted from Fratini et al., submitted.

In summary, click chemistry was a reliable method to stably and covalently immobilize fluorescence virus particles onto glass coverslips. This approach did not affect virus infectivity and/or virus replication, it is highly specific, and it highly depends on copper catalysis. Additionally, virus–coated surfaces were competent for cell adhesion through the clicking of Alkyne-RGD peptides.

2.2 Studying CME recruitment of above clicked-viruses

2.2.1 Clicked viruses co-localize with the Clathrin endocytic machinery

After controlling that Alexa647/alkyne-virus were still infectious and efficiently clicked onto modified glass surfaces, BSC1 and U373 cells expressing AP2-GFP were seeded on top of clicked-virus coated coverslips to address if the Clathrin machinery could interact with the immobilized virus particles (from now on, the term “clicked-virus coated coverslips” implies the presence of also clicked RGD to favor cell adhesion). Six hours post seeding, cells were fixed and imaged by fluorescence microscopy. As previously shown, cells perfectly adhered onto virus-coated coverslips and viruses remained attached to the surface. Interestingly, both cell lines displayed many co-localization spots between AP2-GFP and clicked-viruses (Figure 24, white arrows).

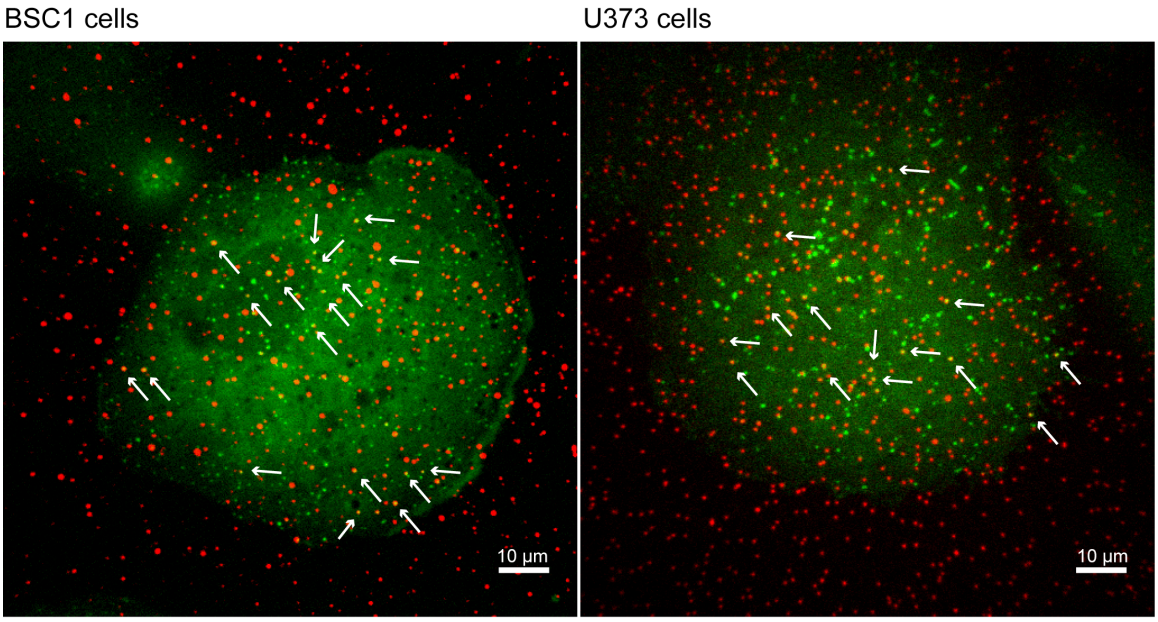

Figure 24. Clathrin machinery interacts with the clicked reovirus particles. BSC1 cells (left part) and U373 cells (right part) stably expressing AP2-GFP were seeded on top of clicked virus coated coverslips (red). 6 hours post-seeding cells were fixed and imaged by fluorescence microscopy. The white arrows indicate spots where the signal from AP2-GFP co-localizes with clicked virus particles.

To visualize how the interaction between AP2-GFP and the clicked virus takes place and to understand the dynamics of the AP2 signal above viruses, I performed live cell microscopy using a spinning disc confocal microscope (SDCLM). The AP2-GFP fluorescence from live imaging of Clathrin coated pits (CCPs) displays a constant and relatively slow growth that represents the nucleation and maturation phase. Afterwards, the signal reaches a peak that corresponds to the mature Clathrin coated vesicle (CCV) whose scission and release into the cell cytosol, defines a rapid loss of the fluorescence signal. This event takes place in about 1-2 mins[22,165]. Interestingly, by analyzing the intensity profile of AP2 it is possible to distinguish the different stages of CCPs[190].

U373 AP2-GFP cells were seeded onto clicked-virus coated coverslips and, 6 h post-seeding they were imaged by SDCLM. In most of the live imaging, movies were acquired for 10 mins with a time frame of 1 frame/ 3 seconds. Live-cell imaging confirmed the presence of many co-localization events between clicked-viruses and AP2-GFP. This result was further validated by performing live-cell imaging of BSC1 cells

stably expressing AP2-GFP seeded on clicked-virus (data not shown). 15 % of the virus particles located below the adherent area of U373 cells were co-localizing with the Clathrin machinery (Figure 25 A). This percentage of reovirus particles co-localizing with AP2-GFP is comparable with reovirus infection efficiency when particles are added into the cell culture media[22,165]. To analyze the dynamics of AP2 recruitment above clicked-virus, the fluorescence signal over time of AP2-GFP arising from clicked virus spots ("virus spots") was compared with the fluorescence signal coming from spots with no viruses ("empty pits"). Fluorescence intensities of empty pits exhibited a single intensity curve where fluorescence grows over time until reaching a peak and quickly disappears within a minute. This outcome represents the typical intensity profile of a CCP[22,116,190] (Figure 25 B, upper panel). On the contrary, the AP2-GFP fluorescence signal coming from virus spots displayed several recruitment cycles. The presence of multiple recruitment of AP2-GFP might represent the maturation of multiple CCPs above the clicked virus as an attempt from the cell to internalize the immobilized virus particles (Figure 25 B, lower panel). This result was completely unexpected; the aim of using a system were virus particles are immobilized onto glass surfaces was to "freeze" the early virus-cell interaction, but on the contrary, live-cell imaging reveled a highly dynamic behavior of the endocytic machinery above the clicked-virus particles.

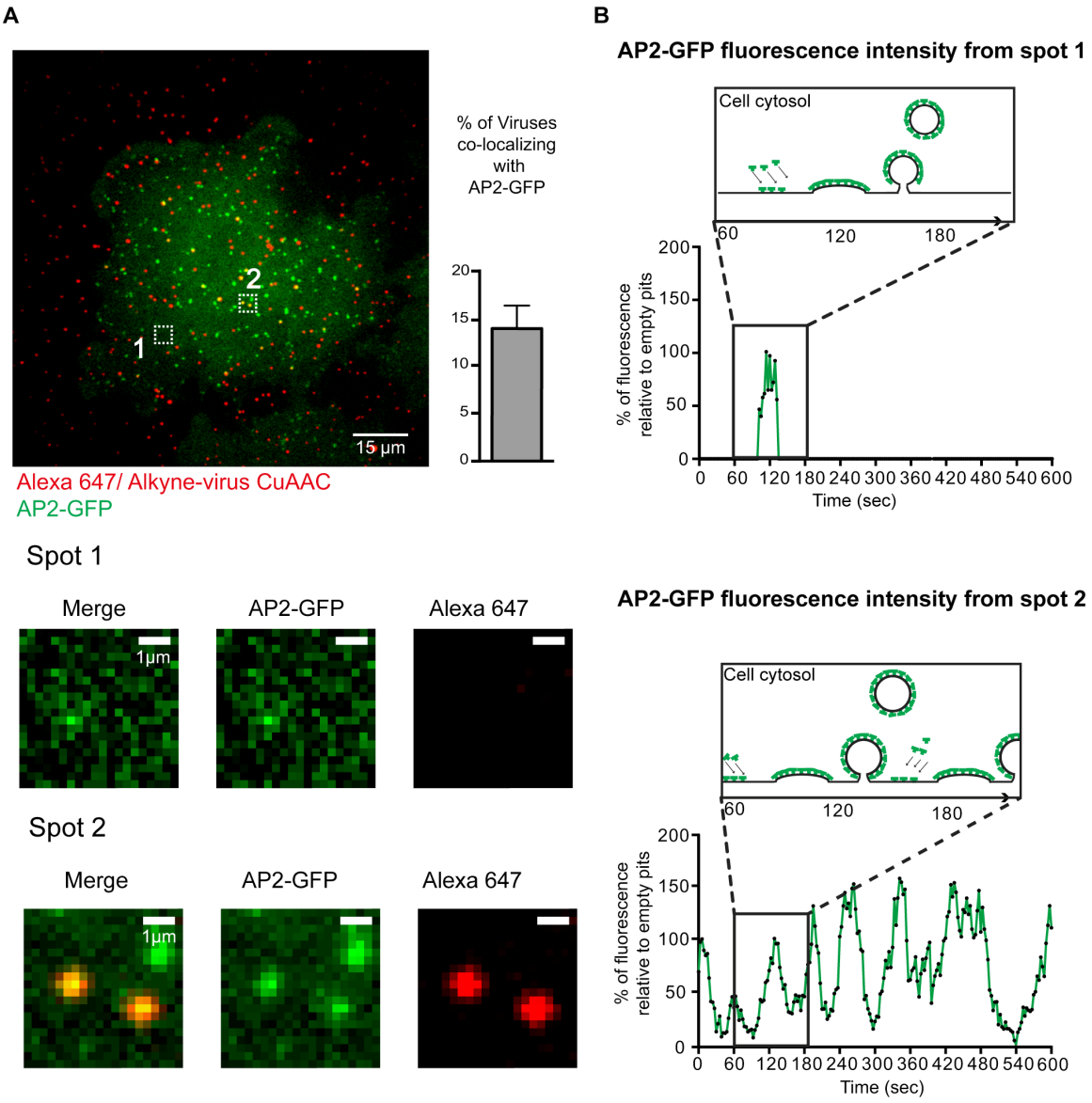

Figure 25. The endocytic Clathrin machinery is recruited on clicked reoviruses. A) (Upper part) Fluorescence live-cell imaging of U373 cells stably expressing AP2-GFP (green) seeded on clicked Alexa647/ Alkyne-virus (red) coated coverslips. Insert region 1 corresponds to a CCP without virus particle; insert region 2 is a representative example of virus particles co-localizing with the Clathrin machinery. The number of viral particles co-localizing with the Clathrin machinery was normalized to the total number of viruses located under each cell (mean and SD from three cells are shown). (Lower part) Zoom in of insert region 1 and 2; merged and single fluorescence channels are shown. B) (Upper panel) Kinetic intensity profiles and schematic representations of a representative CCP (green) (empty pit) and (lower panel) of CCP co-localizing with a single immobilized viral particle (red). The AP2-GFP fluorescence intensity for each time point was normalized to the average of the maximum AP2-GFP fluorescence intensity of empty pits in the same cell. Adapted from Fratini et al., submitted.

2.2.2 Clicked viruses specifically induce CME recurrent recruitment

To validate the recurrent recruitment observed above immobilized viruses and to further investigate how the induction of Clathrin machinery was mediated, it was essential to demonstrate that the recurrent recruitment was specifically induced the presence of the virus. To test this hypothesis, during live cell imaging I treated the cells with 1-butanol, which has been shown to induce a fast disassembly (on the order of a few seconds) of all CCPs from the cell membrane[55]. The presence of primary alcohols reduces the formation of PI(4-5)P2 at the cell membrane[191] and as a consequence AP2 cannot be recruited thereby rapidly disengaging CCPs. Removing 1-butanol from cells and replacing it with fresh media can easily reverse the mechanism. By treating cells with 1-butanol is therefore possible to induce the instant disassembly of all Clathrin coated structures from the cell membrane and synchronize the assembly of newly forming CCPs.

U373 cells stably expressing AP2-GFP were seeded onto clicked virus coated coverslips and live-cell imaging was performed for 10 min, at 1 frame/ 3 sec. Afterwards, 1-butanol was added into the cell media (2% final concentration which also maintains cell viability, data not shown). After confirming that CCPs had disappeared from the cell membrane, the imaging media was replaced with fresh media and as expected, new CCPs instantly formed back at the cell surface. Interestingly I could observe that the same virus particles that were recurrently co-localizing with AP2-GFP before 1-butanol treatment, started to co-localize again after 1-butanol washout (more than 80 % of the same virus particles co-localize with AP2-GFP before and after 1-butanol treatment) (Figure 26). Furthermore, for many clicked viruses co-localizing with AP2, the GFP signal did not completely disappear during 1-butanol treatment, but a weak fluorescence leftover was often visible. The observation the same virus particles were co-localizing before and after 1-butanol treatment could be explained by the presence of a “signal” (chemical or mechanical) that could be imprinted at the cell membrane by the virus particles and conserved over time. These results therefore strongly suggest that clicked viruses specifically induce the observed recurrent recruitment of the Clathrin machinery.

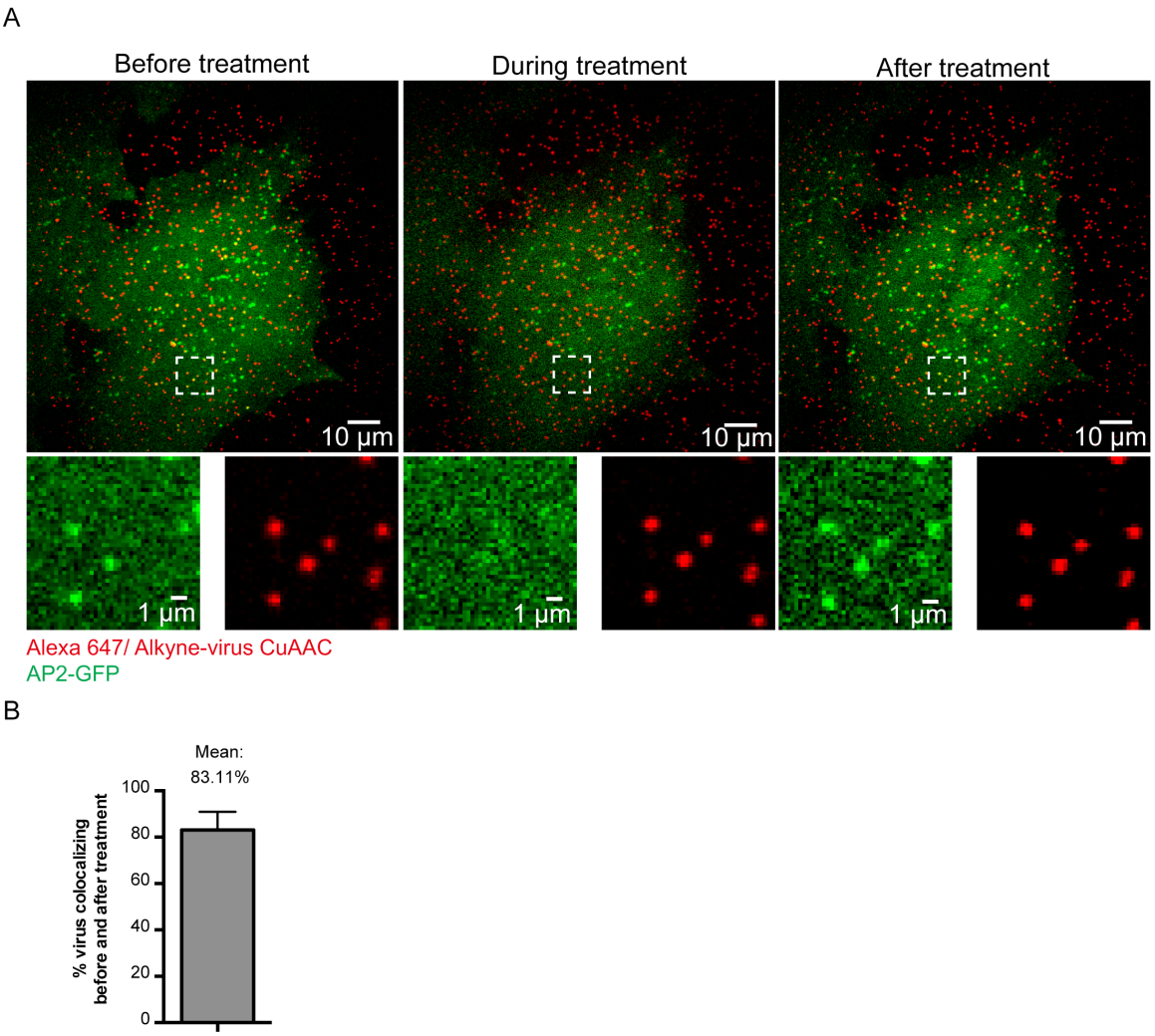

Figure 26. The recruitment of Clathrin machinery above virus particles is conserved. A) Live-cell imaging of U373 stably expressing AP2-GFP cells seeded on top of clicked reovirus coated coverslips (red); cells were imaged for 10 min (1 frame/3 sec), afterwards imaging media is supplemented with 2% 1- butanol for 2-3 seconds and immediately after the imaging media is replaced with fresh media. (From left to right) Cells before treatment, cells during 1-butanol treatment and cells after treatment. The inserts below show CCPs co-localizing with click virus particles before treatment, during treatment (where CCPs are instantly disengaged from cell membrane) and after treatment. B) Percentage of the same virus particles that co-localize with Clathrin machinery before and after treatment. The number of viral particles co-localizing with the Clathrin machinery was normalized to the total number of viruses located under each cell (mean and SD from three cells are shown).

2.2.3 Development of statistical approach to automatically analyze data

To address if the recurrent recruitment of AP2-GFP above the immobilized viruses was statistically significant, the number of AP2 cyclic events above virus particles needed to be compared with the events at the cell spots not co-localizing with viruses.

Considering that live-cell imaging involves the tracking of thousands of CCPs, and that getting data in triplicates generates more than 100 virus co-localizing spots, I developed, in close collaboration with Dr Panagiotis Kastritis (EMBL, Heidelberg) an automatic system to analyze the dynamics of CCPs at the cell surface. Briefly, through this method, Gaussian curves with fixed width were fitted into each peak of AP2 fluorescence; in this way, it was possible to characterize and quantify the dynamics of Clathrin machinery recruitment (see materials and methods) (Figure 27 A - D).

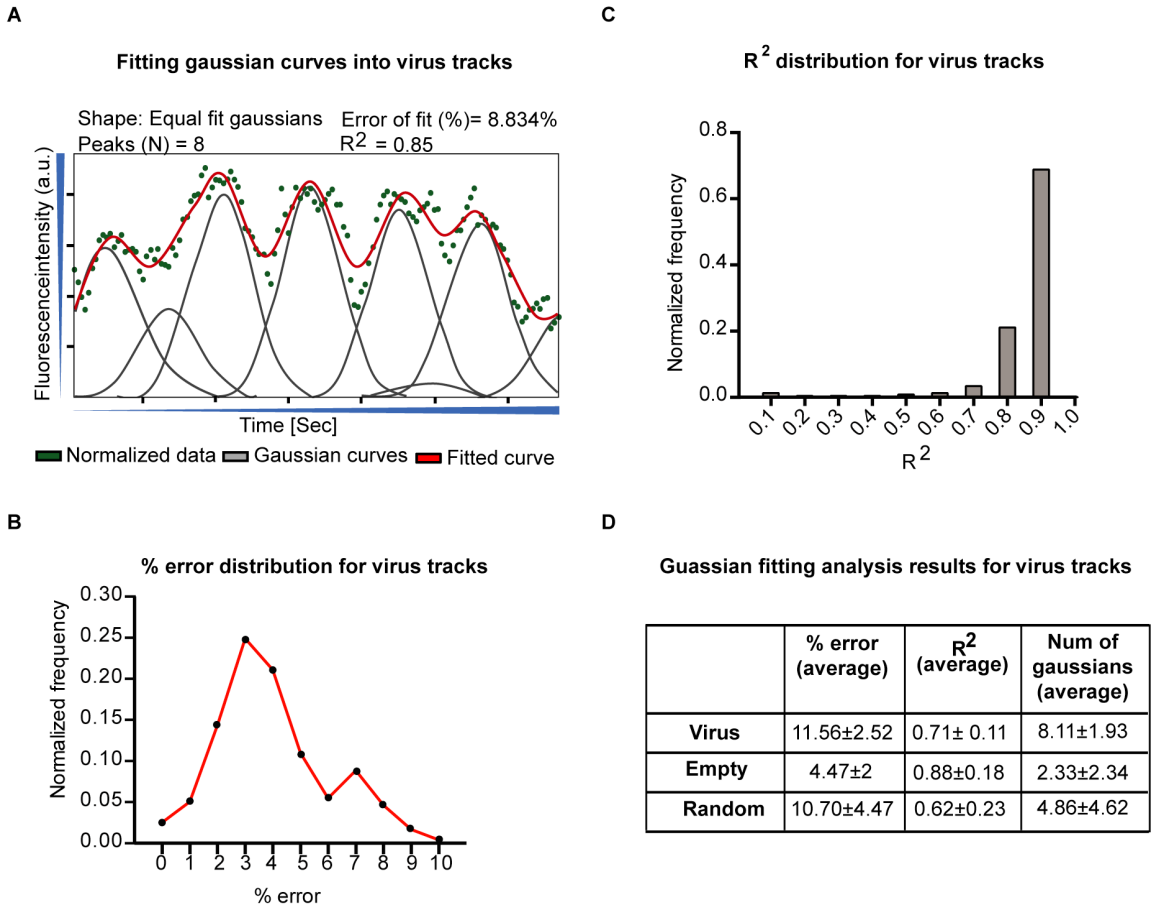

	% error (average)	R^2 (average)	Num of gaussians (average)
Virus	11.56±2.52	0.71± 0.11	8.11±1.93
Empty	4.47±2	0.88±0.18	2.33±2.34
Random	10.70±4.47	0.62±0.23	4.86±4.62

Figure 27. Establishment of a Gaussian fitting approach to quantify the dynamics of CME recruitment. A) Example of the Mathlab workflow used to fit Gaussians curves (grey) into acquired normalized fluorescence data (green). Fitted curve is shown in red. B) and C) Percentage error and R^2 distribution of the fitted Gaussian curves from 87 virus particles. D) Percentage error, R^2 and number of Gaussian curves fitted from all virus data set analyzed. Gaussian fitting analysis and results were performed in collaboration with Dr. Panagiotis Kastritis, EMBL, Heidelberg. Adapted from Fratini et al., submitted.

Gaussian functions were fitted into fluorescence curves from CCPs co-localizing with virus ("virus spots"), CCPs not co-localizing with virus ("empty pits") and spots randomly collected from the cell ("random spots"). From the data analysis, it was possible to obtain the number of AP2 recruitments onto a specific spot at the cell membrane, the rate of peak occurrence and the width of peaks. Gaussian fitting analysis of U373 AP2-GFP cells, revealed that AP2 was recruited above virus particles 8.1 ± 1.9 times every 10 min while empty pits and random spots revealed a significantly lower number of events corresponding to 2.3 ± 2.3 events every 10 min and 4.7 ± 4.6 events every 10 min, respectively (Figure 28 A). These data further demonstrate that the recurrent recruitment of the Clathrin machinery is specifically induced by the presence of the virus. Measurements of the rate of peak occurrence onto clicked virus (time distance between two peaks of AP2) corresponded to 74.8 ± 37.8 secs (Figure 28 B) and the width of peaks (time duration of peaks, on average) was 58.96 ± 21.5 secs (Figure 28 C), which corresponded to the average lifetime of CCPs reported in literature[22,116,190]. In conclusion, the use of the Gaussian fitting method further validated that virus particles specifically induce the recurrent recruitment of the Clathrin machinery and that this mechanism exhibits a specific, regular time structure. Moreover, these results, together with results from the 1-butanol experiment (Figure 26), suggest that the signal (chemical or physical) generated by the immobilized particles is not removed and is responsible for the observed recurrence.

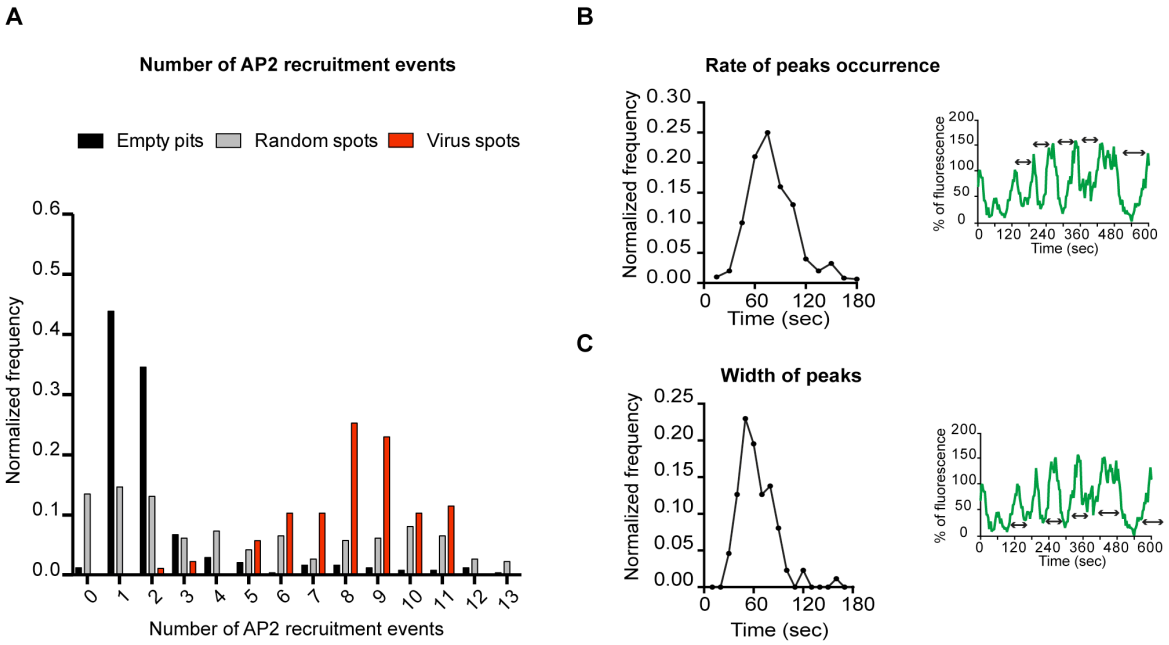

Figure 28. The endocytic Clathrin machinery is specifically recruited on clicked reoviruses and it exhibits a defined mechanism. A) Normalized number of AP2 recruitment on virus particles (87 spots), Random spots (271 spots) and empty pits (271 spots). The x-axis shows the number of CCP recruitment over 10 min. Data collected from three cells. B) Normalized frequency of the rate of peak occurrence onto clicked virus (time distance between peaks of AP2; illustration in the insert). C) Normalized distribution of the lifetimes of CCPs onto clicked viruses (time duration of each peak, illustration in the insert). Data generated from 87 virus particles. Adapted from Fratini et al., submitted.

2.2.4 Dynamin and Clathrin are recruited above immobilized virus particles

After confirming that the recurrent recruitment of Clathrin machinery was specifically induced by the virus particles, it was necessary to control that the AP2-GFP fluorescence signal coming from above the immobilized viruses corresponded to the presence of properly assembled CCPs and was not resulting from protein overexpression. To test this, gene edited SK-MEL-2 cell expressing Dynamin-GFP and Clathrin-Tomato (SK-MEL-2 hCLTA^{en}/DNM2^{en}) were used. Gene edited cells have been created by the integration of the GFP and Tomato genes directly at the Dynamin and Clathrin cell genome locus, respectively, in order to study such proteins at their physiological level. Dynamin is a GTPase protein which is recruited to mature CCPs and favors their release from the plasma membrane[35,60,83]. Recruitment of Dynamin occurs immediately before AP2 and Clathrin reach the peak of fluorescence intensity; release of the CCV by

Dynamin is followed by a rapid loss of fluorescence intensity. SK-MEL-2 hCLTA^{en}/DNM2^{en} were seeded upon virus-coated coverslips and imaged 6 h post-seeding (10 min, 1 frame/3 sec). As previously shown with U373 AP2-GFP cell lines, I could confirm the presence of virus particles recurrently recruiting Clathrin machinery. The Clathrin-Tomato signal above co-localizing virus particles, displayed the same dynamics as the AP2–GFP. Interestingly, I could also observe that dynamin was recruited at every Clathrin cycle (Figure 29).

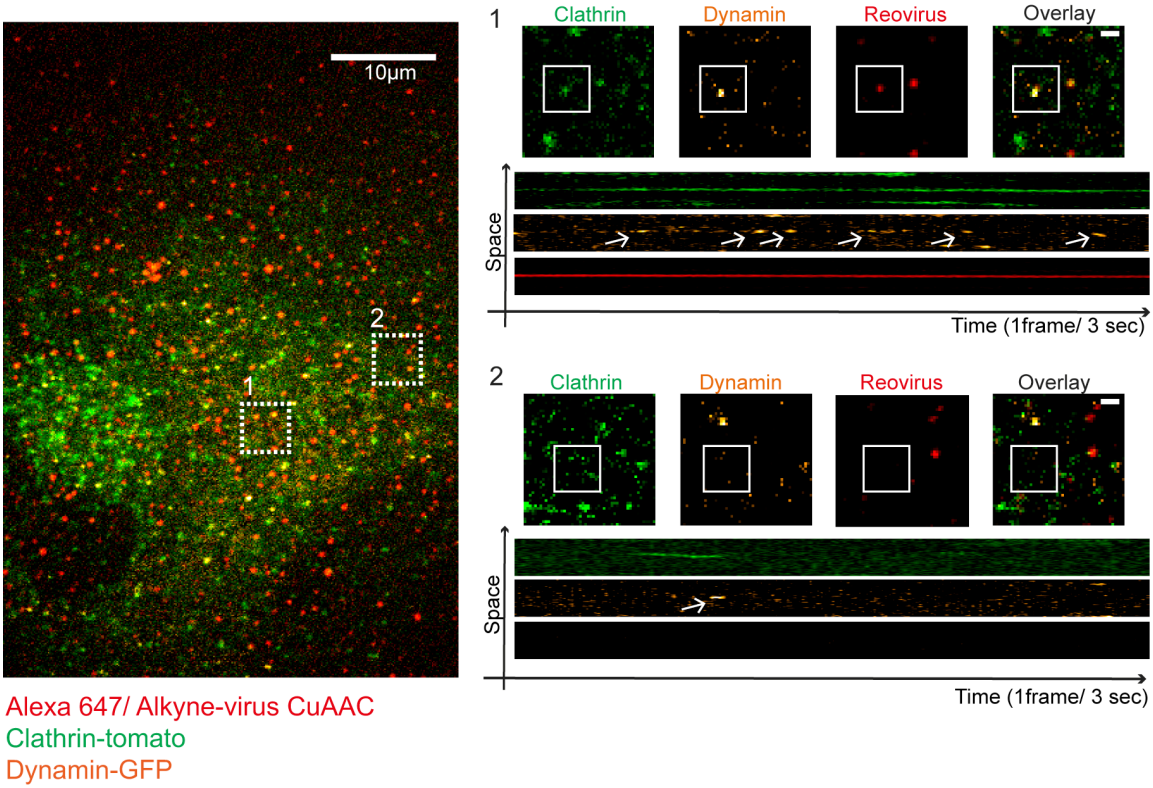

Figure 29. Dynamin is recurrently recruited at the end of each recurrent endocytic events. Fluorescence live cell imaging of the genome edited SK-MEL-2 cells expressing Clathrin light chain A fused to RFP (CLC-RFP) and dynamin fused to GFP (Dyn-GFP), seeded on clicked-viruses coated coverslips. Inset region 1 is a representative example of virus particles co-localizing with the Clathrin machinery; (lower part) kymograph showing Clathrin and dynamin recruitment on virus particle over time. Inset region 2 corresponds to a CCP with no virus particle (empty pit); (lower part) kymograph shows Clathrin and dynamin recruitment on empty pit over time. Frame rate of data acquisition of 3 sec for 10 min. Scale bar in the insets: 1 µm. Adapted from Fratini et al., submitted.

This result, confirmed that the fluorescence dynamics observed on U373 AP2-GFP cells are not resulting from protein overexpression but they can be reproduced in different cell lines, with different markers (Clathrin and Dynamin) expressed at their physiological level. More importantly, this experiment strongly suggests that virus particles induce the recruitment of Clathrin machinery and favor maturation of CCPs and release of CCVs. This hypothesis can be further corroborated by the fact that each peak of Clathrin/ AP2 recruitment onto virus spots has a lifetime comparable to the average lifetime of terminal CCPs (Figure 28 C)

2.3 Investigating chemical VS mechanical induction of CME

2.3.1 Role of receptors in inducing CME recruitment

The previous results show a model where immobilized virus particles induce recurrent recruitment of the Clathrin machinery. This recruitment is specific and leads to the production and Dynamin-based release of CCVs. However, is well known that virus entry is mediated by receptor binding[123]. For some viruses it has been shown that virus interaction with certain receptors induces cellular signaling activation that in turn favors virus entry through endocytosis[123,130]. While some viruses can hijack pre-formed CCPs[134,192], some other can induce *de novo* formation of CCPs[23]. Reovirus binding is described to induce *de novo* formation of CCPs[22,165]; nevertheless, a clear evidence of signaling activation followed by Clathrin recruitment is missing. Studying virus-induced receptor signaling represents a challenging field, especially because of the transient nature of virus cell-interaction. I therefore used my new system to investigate whether receptor/virus binding was responsible for the recurrent recruitment of CME.

2.3.2 CME recurrent recruitment is independent from JAM-A receptors

Reovirus binding with cell receptors has been thoroughly characterized. The virus capsid subunit σ1 interacts with SA exposed at the plasma membrane[149]; afterwards the JAM-A receptor is engaged by the same capsid subunit[146]. Together, the binding of SA and JAM-A, induces a strong adhesion of the virus particles at the cell membrane. Afterwards the λ2 capsid subunit recruits the integrin beta 1 receptor and the virus is internalized by receptor-mediated endocytosis[148]. Treating cells with anti-integrin beta 1

antibody affects reovirus infection (around 50% reduction), while blocking JAM-A binding induce a strong inhibition of reovirus internalization[146,148]. Most of the receptor binding assays have been performed in HeLa cells; therefore I adapted my system to seed HeLa cells above clicked virus coated coverslips. To validate that cell treatment with anti-JAM-A or anti-integrin beta 1 was affecting reovirus infection, Hela cells were pretreated with blocking antibody for 1h at room temperature. Subsequently cells were washed and incubated 30 min in ice with virus dilutions to allow viruses to bind the cell surface but inhibit internalization. Finally, cells were washed and incubated overnight at 37^{o}C. The following day, cells were fixed and immunostained for μNS. Unfortunately in our hands treating cells with anti-integrin beta 1 antibody did not block reovirus infection (data not shown). However, pre-incubation with anti-JAM-A antibody induced a strong reduction of infection (Figure 30 A). Therefore, JAM-A was used in future studies to determine CME activation upon reovirus binding.

Hela cells were transfected with Clathrin light chain (CLC) tomato. Suspension of HeLa-CLC tomato cells were incubated 1h at room temperature with anti-JAM-A antibody. Afterwards cells were seeded onto virus-coated coverslips, and 6 hours post-seeding HeLa-CLC cells were imaged by SDCLM (Figure 30 B). The virus-coated coverslips were glued on the bottom of a multi wells imaging plate; in this way, cells treated and not-treated with antibody solution could be seeded onto the same coverslips. Live imaging was performed for 5 min with a frame rate of 1 frame/ 3secs. Interestingly, compared to control cells, I could measure a slight reduction in the number of virus particles co-localizing with Clathrin machinery in samples treated with anti-JAM-A antibody (52.9 ± 12.2 % co-localization in control cells and 31.6 ± 10.1 % of co-localization for anti-JAM-A antibody treated cells) (Figure 30 C, upper panel). Nevertheless, by analyzing the number of recruitment events of the Clathrin machinery above virus particles (using the pre-established Gaussian fitting method), I observed the same dynamics in control cells and cells pretreated with anti-JAM-A antibody (5.1 ± 1.2 recruitment events in 5 min movie duration; JAM-A antibody treated cells, 5.5 ± 1.1 recruitment events in 5 min movie duration, Figure 30 D-E).

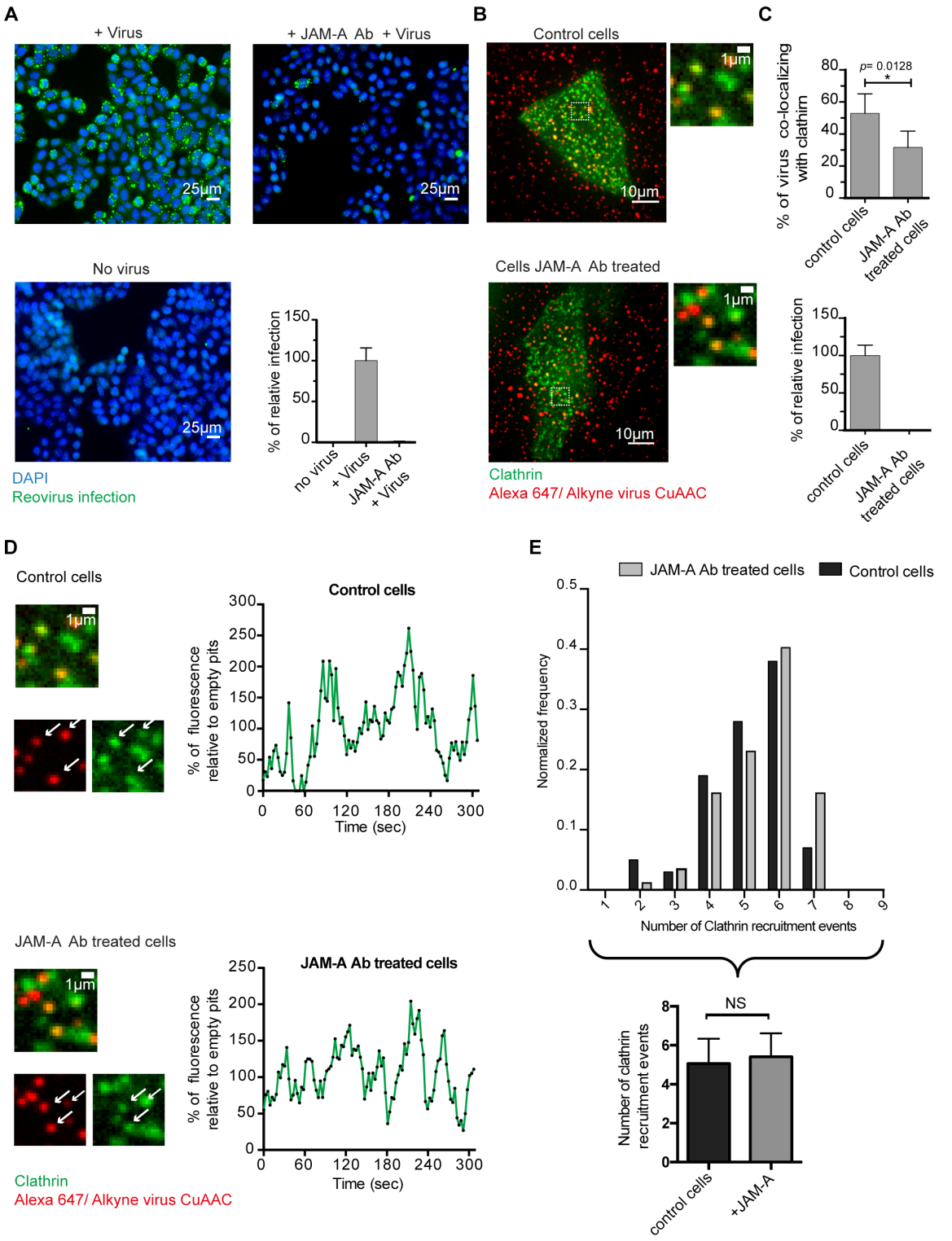

Figure 30. CCP recruitment on virus particles is JAM-A independent. A) Hela cells were pre-incubated with PBS (control) or PBS + JAM-A antibody (10 mg/ml) and subsequently infected with reovirus at MOI=1. Virus infection was monitored by indirect immunofluorescence

using an anti-μNS antibody (green). Infectivity was measured by counting the percentage of infected cells; data were normalized to cells infected by reovirus in absence of JAM-A neutralizing antibody. Data are shown as mean value ± SD. B) Hela cells expressing CLC-tomato (in green) were pre-incubated for 1 hour at RT with PBS or PBS + JAM-A. Cells were seeded onto clicked Alexa647/Alkyne virus (in red) coated coverslips and live-cell imaging was performed. C) (Upper panel) The number of viral particles co-localizing with the Clathrin machinery was normalized to the total number of viruses located under each cell. Data are shown as mean value ± SD from five cells per conditions. p value < 0.05 was considered significant (unpaired t-test). (Lower panel) Relative number of infected cells in control and in samples treated with JAM-A neutralizing antibody after infection post-live imaging. D) Kinetic intensity profiles of a representative CCP (green) co-localizing with a single immobilized viral particle (in red) in control cells (upper panel) and in cells treated with JAM-A neutralizing antibody (lower panel) (frame rate of data acquisition of 1 frame/3 sec for 10 min). E) (Upper panel) Normalized frequency of Clathrin recruitment to virus particles in control cells (black columns) (95 virus spots) and in cells treated with JAM-A neutralizing antibody (grey columns) (87 virus spots). (Lower panel) Number of Clathrin recruitments on virus particles in control cells and in cells treated with JAM-A neutralizing antibody, obtained from upper panel. Five cells per condition were analyzed. Adapted from Fratini et al., submitted.

Finally, to control that treatment with the neutralizing antibody was indeed inhibiting virus–receptor interaction during live data acquisition, immediately after imaging control cells and cells pretreated with anti-JAM-A antibody were infected with same concentration of virus. As shown in Figure 30 C (lower panel), cell pretreated with neutralizing antibody, which displayed the same recurrent recruitment above clicked viruses, could not be infected. On the contrary, control cells could efficiently favor virus entry and infection (Figure 30 C, lower panel). This result validates that during live-cell imaging, treatment with anti JAM-A antibody was efficiently blocking reovirus–JAM-A receptor interaction. In conclusion, these results demonstrate that the recurrent recruitment above clicked viruses is JAM-A receptor independent.

2.3.3 Immobilization of beads of specific size induces Clathrin machinery recruitment.

As I have ruled out the JAM-A receptor –virus interaction as the signal for the recurrent recruitment, I next addressed if the physical presence of the virus itself could be the signal. The induction of a cellular pathway through mechanical, rather than chemical, stimuli is called “mechanical induction”. In this case, the mechanical stimuli would consist of the imposed external membrane curvature induced by the presence of the virus.
It was previously shown that seeding cells onto coverslips containing nanocones structures favors the recruitment of specific curvature inducing/stabilizing proteins, such as

Amphiphysin, at the curved cell membrane[120]. Similarly, curvature imposed at the cell surface by nanopillars with a diameter < 200 nm induce recruitment of the Clathrin machinery[121]. Therefore, protein recruitment and more specifically Clathrin machinery recruitment can be mediated by imposed external curvature (mechanical induction). However, the role of small nanoparticles, such as virus, in favoring mechanical induction of CME, and how the recruitment takes place at the single particle level has not been investigated.

To address if a specific curvature induced by the presence of the virus could favor CME recruitment, the chemical signaling that might be induced by the virus onto the cell membrane was uncoupled from the mechanical properties of the virus particle itself. To do this, latex beads of similar size of virus particles (100 nm) were immobilized onto modified glass surfaces to mimic the mechanical properties of virus particles. In parallel, to investigate the role of size in inducing CME, beads of 20, 300 and 1000 nm diameter were immobilized. Amino modified latex beads were used to couple the beads with Alexa647-NHS and alkyne-NHS linker, as previously shown for virus. Afterwards Alexa647/Alkyne-beads were clicked onto Si-PEG-N3 coated coverslips. SEM imaging of clicked beads and subsequent size measurements demonstrated that chemical modification was not affecting beads size (Figure 31). Additionally, fluorescence imaging showed that beads were equally distributed among the glass surface (data not shown). Beads of the smallest size, 20 nm, often exhibited a high degree of aggregation; several attempts to reduce such effect were applied without substantial improvement (sonication, increasing concentration of alkyne linker) (data not shown); however live-cell imaging was performed using coverslips where 20 nm clicked beads exhibited the lowest aggregation rate. No or few aggregation was observed on other size of beads; imaging of 100 nm beads was focused on diffraction-limited objects, while single beads were identified in the case of 300 and 1000 nm beads.

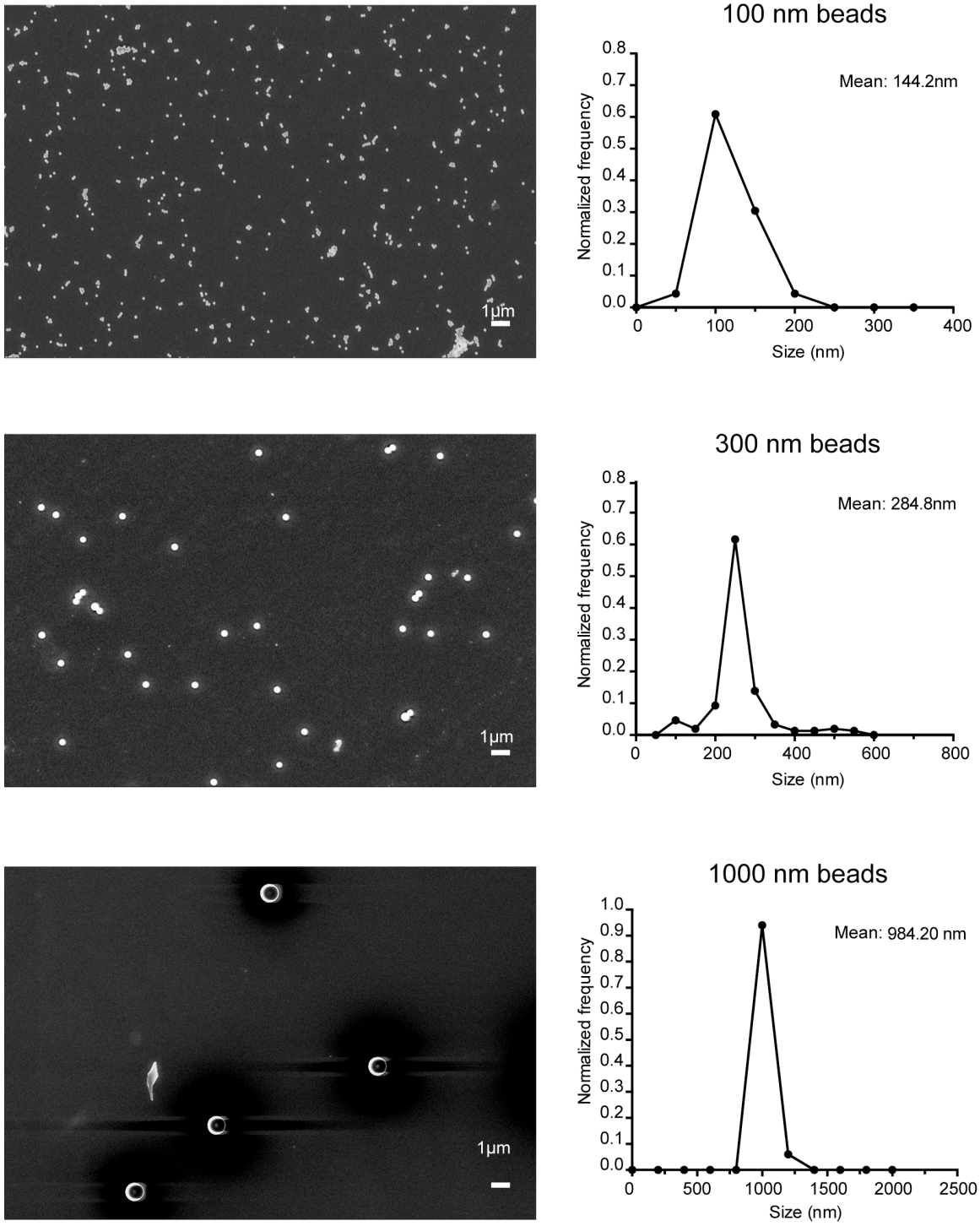

Figure 31. SEM imaging of coverslips coated with clicked polystyrene beads. 100, 300 and 1000 nm beads were fluorescently labeled with Alexa647 dye and functionalized with an alkyne linker; beads were then clicked on Si-PEG-N_3 coverslips. Coverslips were sputter-coated with carbon and imaged by SEM. Single beads were identified and their diameter was measured as described in methods. The size distribution of 100, 300 and 1,000 nm beads is shown. A total of 984 (100 nm), 322 (300 nm) and 140 (1000 nm) beads were counted. Images magnification: 4000x. Adapted from Fratini et al., submitted.

U373 AP2-GFP cells were seeded on top of beads-coated coverslips and live cell imaging was performed. Clathrin machinery was found to co-localize with 100 and 300 nm beads (50-60% co-localization), while no or few co-localization events were observed with 20 and 1000 nm beads (Figure 32 A and B). These results confirmed the data present in literature which asserts that beads having size <500 nm and > 50 nm diameter are mainly internalized by CME. Interestingly above 100 and 300 nm beads I could observe the recurrent recruitment of the Clathrin machinery as previously shown onto virus particles (Figure 32 A). In particular, 300 nm beads exhibited 5.6 ± 1.2 recruitment events every 10 min, while 100 nm beads exhibited on average 7.5 ± 1.5 events every 10 min (Figure 32 C and D); in both cases the timing was lower compared to virus particles (8.1 ± 1.9 events every 10 min, Figure 28 A). Detailed measurements of the dynamics of recruitment revealed that AP2 was recruited every 117.38 ± 38.46 secs for 300 nm beads and every 83.25 ± 29.49 secs for the 100 nm (Figure 33 A) (for the virus particles it was 74.8 ± 37.8 secs, Figure 28 B and 33 A).

These results suggest that beads of 100 and 300 nm diameter can specifically induce Clathrin machinery recruitment. As beads to not have a receptor it is tempting to speculate that the curvature induced by the beads is the signal favoring CME activation.

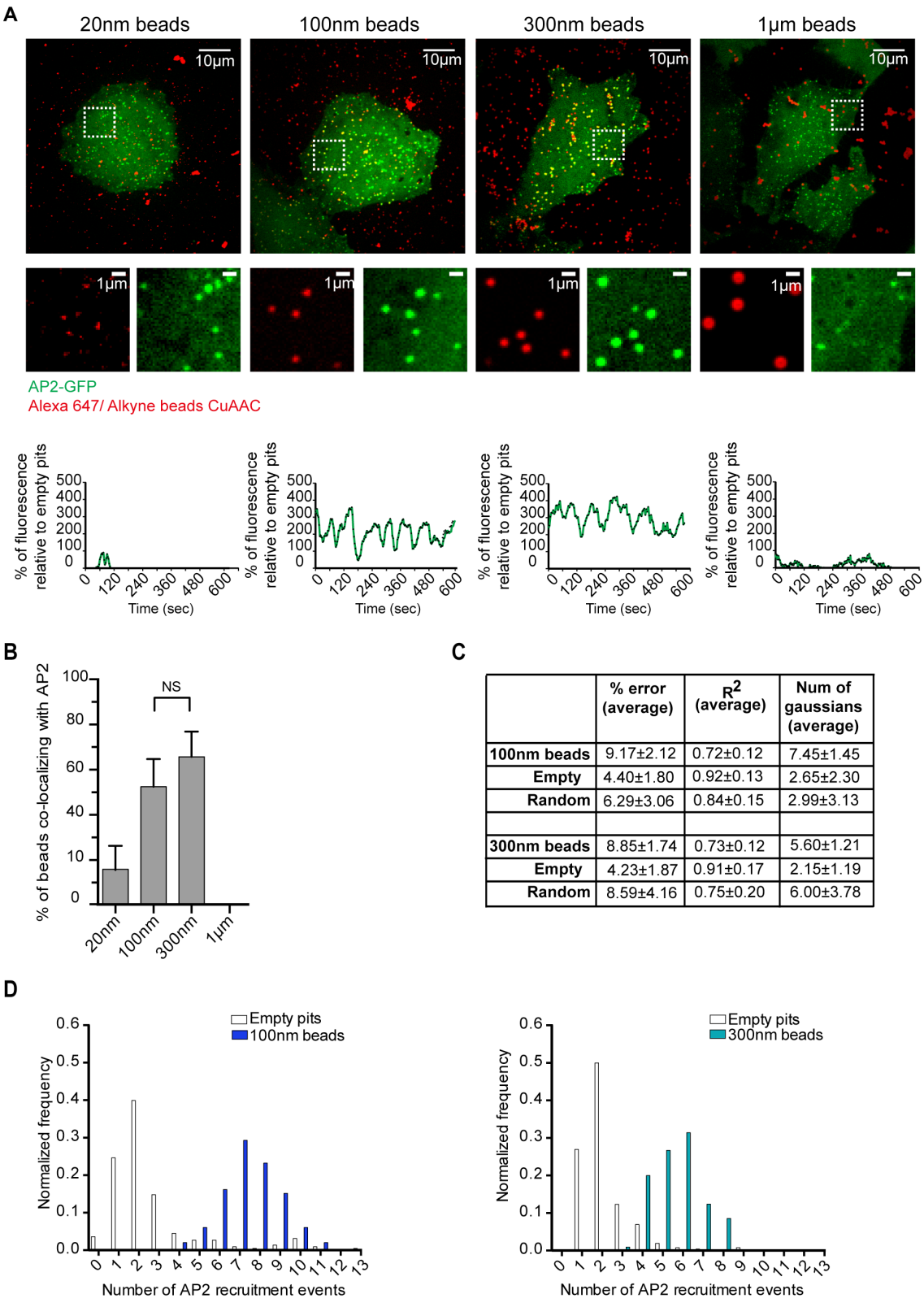

	% error (average)	R^2 (average)	Num of gaussians (average)
100nm beads	9.17±2.12	0.72±0.12	7.45±1.45
Empty	4.40±1.80	0.92±0.13	2.65±2.30
Random	6.29±3.06	0.84±0.15	2.99±3.13
300nm beads	8.85±1.74	0.73±0.12	5.60±1.21
Empty	4.23±1.87	0.91±0.17	2.15±1.19
Random	8.59±4.16	0.75±0.20	6.00±3.78

Figure 32. Recruitment of CCP to nanoparticles depends on their sizes. A) Fluorescence live-cell imaging of U373 cells stably expressing AP2-GFP (green) seeded on 20, 100, 300 and 1000

nm clicked beads (red). Inserts are representative examples of beads and AP2 in each sample; (lower part) kinetic intensity profiles of representative CCPs co-localizing with single immobilized beads. The AP2-GFP fluorescence intensity for each time point was normalized to the average of the maximum AP2-GFP fluorescence intensity of empty pits in the same cell. B) Percentage of beads co-localizing with AP2-GFP. The number of beads co-localizing with the Clathrin machinery was normalized to the total number of beads located under each cell (mean and SD from four cells are shown; p value < 0.05 is considered significant, unpaired t-test). C) Percentage error, R^2 and number of Gaussian curves fitted from all 100 and 300 nm beads data set analyzed. D) Normalized frequency of AP2 recruitment on 100 and 300 nm beads (n=99 and n=105 respectively) and empty pits (n=333 and n=329 respectively). The x-axis shows the number of AP2 recruitment per 10 min. Data collected from three cells per condition. Adapted from Fratini et al., submitted.

2.3.4 CCVs size and commitment are defined at early cargo – cell interaction

The size of a CCP it is correlated with its lifetime[19,22,116]: therefore a large CCP requires more time for assembly. By analyzing the assembly time of CCPs above beads and virus, the measurements obtained through Gaussian fitting revealed that the assembly of the Clathrin coat takes on average 59.0 ± 21.5 secs on virus particles, 88.5 ± 22.0 secs for 100 nm beads and 106.7 ± 25.7 secs for 300 nm beads (Figure 33 B). Therefore these results suggest that the size of CCPs is dependent on the size of the immobilized nanostructures, although the clicked virus/ beads are not internalized.

Besides lifetime, also quantification of fluorescence intensity of CCPs provides information regarding the size of Clathrin structures. By using Correlative Light and Electron Microscopy *(*CLEM) it was demonstrated by us and other groups, that fluorescence intensity highly correlates with the size of Clathrin structures[21,116]. In particular, the plateau (Max) value of each CCP track, gives reliable information regarding the size of the CCV just before it is released into cell cytosol. To investigate the size of the Clathrin coated structures growing on top immobilized nanostructures, I therefore measured the Max value of each AP2 fluorescence intensity track coming from virus spots and beads spots. Fluorescence intensity was normalized against the Max fluorescence of empty pits (pits not co-localizing with virus/ beads). Results obtained from analyzing multiple cells revealed that Clathrin structures growing on top 100 and 300 nm beads, were 3.2 ± 1.3 and 5.5 ± 1.1 times larger than empty pits, respectively (Figure 33 C). Structures growing on top of virus particles were 1.7 ± 0.7 times larger (Figure 33 C). Interestingly, I noticed the presence of a protein leftover during each AP2 recruitment

above the same immobilized nanostructure, referred as “min” in Figure 33 C. This residual amount of Clathrin coat structure was proportional with the size of the beads/virus (Figure 33 C).

The presence of Clathrin/adaptor leftover after pinching of CCVs was already described at the Clathrin “hotspots”; nevertheless its function is not clear. It is possible that the presence of the protein leftover at each CCP cycle might help the recruitment of further adaptor proteins/Clathrin molecules favoring the recurrent generation of CCVs and therefore helping the formation of hotspots.

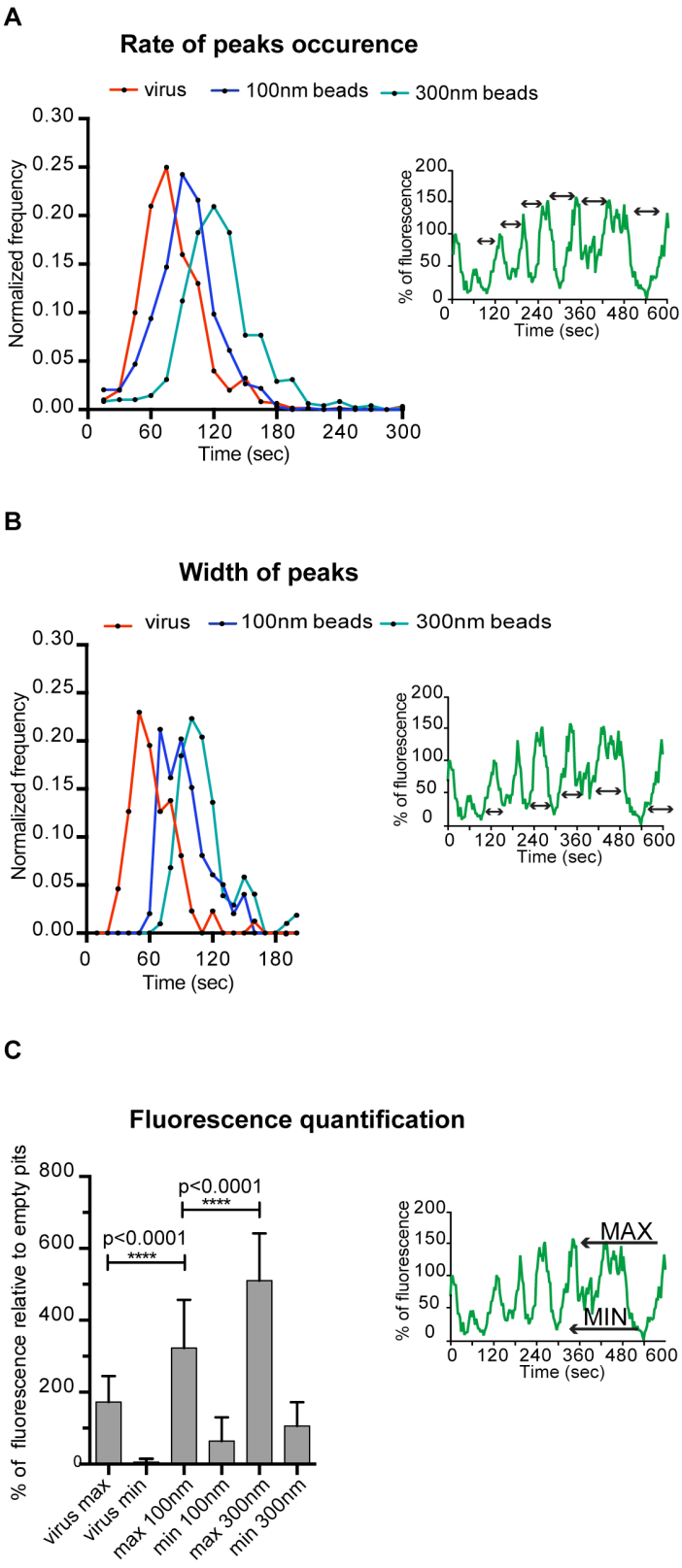

Figure 33. Dynamics and quantification of AP2 recurrent recruitment on beads and reoviruses. A) Normalized distribution of the rate of peak occurrence (time distance between

peaks of AP2; illustration in the insert). Data were generated from 87 virus particles, 99 and 105 beads of 100 and 300 nm, respectively. B) Normalized distribution of coated pits lifetime (time duration of each peak, illustration in the insert). Data were generated from 87 virus particles, 99 and 105 beads of 100 and 300 nm, respectively. C) Fluorescence intensity quantification from live-cell imaging of U373 expressing AP2-GFP (green) seeded on clicked-viruses or clicked-beads. The AP2-GFP fluorescence intensity for each time point was normalized to the average of the maximum AP2-GFP fluorescence intensity of empty pits into the same cell. The Max fluorescence intensity from viruses and beads represents the average of the maximum values of AP2 recruited on each particle. The Min fluorescence intensity represents the residual amount of AP2 left behind after completion of each AP2 recurrent recruitment (illustration in inset). Data are shown as the mean value ± SD. Data collected from 3 cells per condition. P value < 0.05 is considered significant (unpaired t-test). Adapted from Fratini et al., submitted.

To further assess if the Clathrin structure growing on top of the immobilized beads corresponded to a properly folded CCPs and CCVs, the recruitment of other Clathrin-related proteins was also investigated: FCHO1, a F-BAR protein recruited at nascent CCPs[49,134], Epsin, an early curvature protein which is believed to promote maturation[62] and Amphyphysin, an NBAR protein recruited at the latest stages favoring vesicle scission[108]. U373 cells stably expressing AP2-GFP were transiently transfected with either FCHO1-mcherry, or Epsin-mcherry or Amphyphysin–mcherry. One day post-transfection cells were seeded on top of 100 nm coated coverslips and 6 h post-seeding live-cell imaging was performed. By analyzing the fluorescence signal of AP2-GFP and m-cherry FCHO1/ Epsin/ Amphyphysin, it was possible to observe that all proteins, together with AP2, were recurrently recruited above the immobilized beads (Figure 34 A and B). Interestingly the amount of AP2 over the beads was always two times higher compared to FCHO1, Epsin and Amphyphysin (Figure 34 A). Importantly, by analyzing the correlation between the fluorescence signals from the different proteins I could show that the fluorescence signals between AP2 and FCHO1 and between AP2 and Epsin were positively correlated (Figure 34 B and C). FCHO1 and Epsin are known to be recruited early to nascent CCPs and their amount grows over time together with AP2 during the maturation stages. Surprisingly, detailed analysis revealed that while AP2 and Epsin fluorescence signals reach their minimum and maximum at the same time frames (correlation efficient = 0.8), fluorescence signal from FCHO1 is slightly shifted compared to AP2 (correlation efficient = 0.4) (Figure 34 B and C). The fluorescence signal from AP2 and Amphiphysin was instead anti-correlated. Recruitment of Amphiphysin takes place at the final stage of CCPs maturation, favoring vesicle constriction and scission; an

increase of Amphiphysin fluorescence defines therefore a decline of AP2-GFP fluorescence and consequently the two signals were anti-correlated (correlation coefficient = - 0.4) (Figure 34 B and C). These results are compatible with the presence of genuine CCPs that mature into CCVs, above the clicked beads

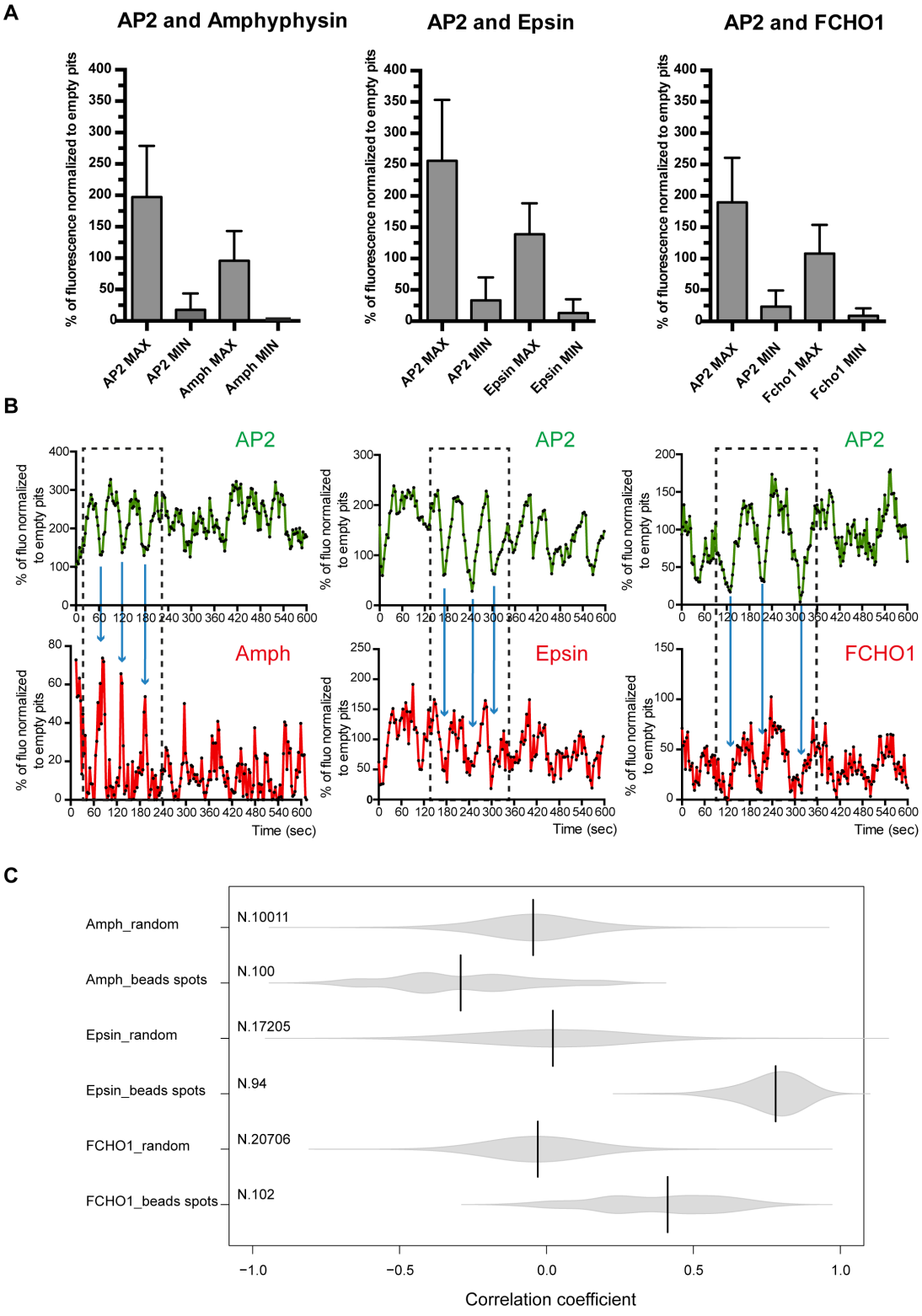

Figure 34. Amphiphysin, Epsin and FCHO1 are recruited above 100 nm immobilized beads. A) Fluorescence intensity quantification from live-cell imaging of U373 stably expressing AP2-

GFP (green) and transiently transfected with either Amphiphysin-cherry, Epsin-cherry or FCHO1-cherry, and seeded on 100 nm clicked-beads. The fluorescence intensity of each protein for each time point was normalized to the average of the maximum fluorescence intensity of the same protein from empty pits of the same cell. The Max fluorescence intensity represents the average of the maximum values of AP2 and either Amphiphysin or Epsin or FCHO1 recruited on each bead. The Min fluorescence intensity represents the residual amount of AP2 and either Amphiphysin or Epsin or FCHO1 left behind after completion of each CME recurrent recruitment. Data are shown as the mean value ± SD. p value < 0.05 is considered significant (unpaired t-test). Data collected from three cells from each condition. B) Kinetic intensity profiles of representative CCPs co-localizing with single immobilized beads. The fluorescence intensity of each protein (AP2, Amphiphysin, Epsin and FCHO1) for each time point was normalized to the average of the maximum fluorescence intensity of the same protein from empty pits in the same cell. The dashed inset and blue arrows highlight the relation between the intensity profiles of AP2 and Amphiphysin, Epsin or FCHO1 C) Correlation analysis between AP2 tracks and Amphiphysin/ Epsin/ FCHO1 tracks. The Pearson correlation coefficient between the intensity profile signal from AP2 and the corresponding Amphiphysin/ Epsin/ FCHO1 signal from each bead spots is calculated and plotted as already described by Kastritis et al., 2017[193]. Results are compared with Pearson correlation coefficient from intensity profile signals of AP2 and Amphiphysin/ Epsin/ FCHO1 from different beads spots (randomized spots). The number of tracks analyzed (N) for each condition is shown in the plot. Data collected from three cells from each condition.

To further confirm these results, stimulated emission depletion (STED) super-resolution microscopy was performed. U373 AP2 cells were seeded above 100 and 300 nm beads, and were subsequently fixed and analyzed by STED microscopy. Interestingly I could observe the presence of AP2 “ring” structures surrounding the beads, which have been already described for the presence of mature CCPs[116,194,195] (Figure 35).

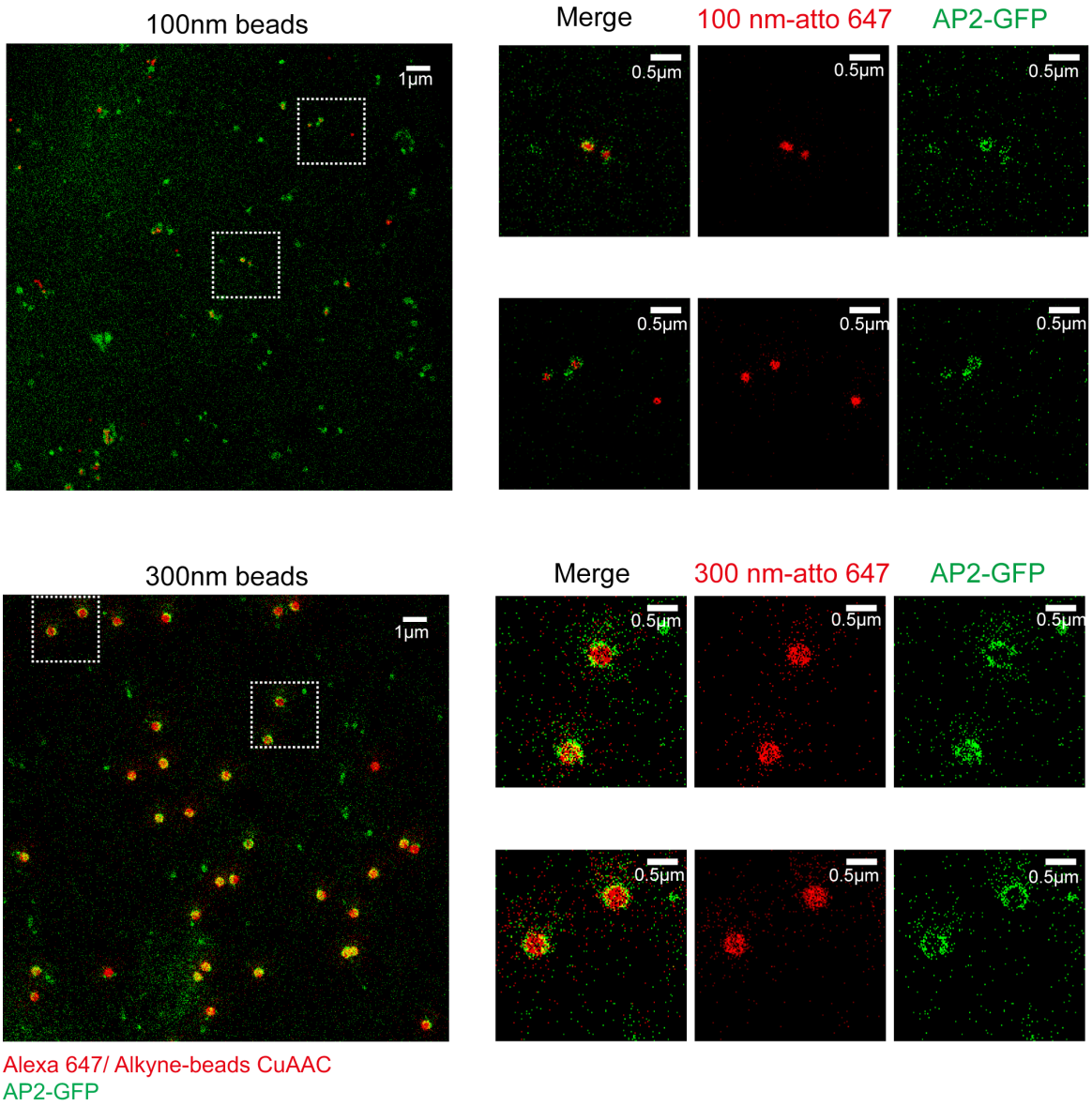

Figure 35. STED imaging of U373 AP2-GFP cells seeded on clicked beads. Cells were seeded on coverslips coated with 100 nm (upper part) and 300 nm (lower part) clicked-beads and fixed with paraformaldehyde 6 hours post-seeding. Samples were then mounted and imaged using STED microscopy. Image analysis reveals the presence of AP2 "ring structures" around clicked beads. Imaging was performed in collaboration with Dr. Zhongxiang Jiang, Leica Microsystems GmbH, Mannheim, Germany. Green: AP2. Red: Alexa647/Alkyne clicked beads. Adapted from Fratini et al., submitted.

Finally, to visualize the presence of CCPs and possibly of CCVs growing on top of the immobilized nanostructures, transmission electron microscopy (TEM) was performed. To inspect CCPs at the basal membrane of the cells, U373 cells seeded on top of beads

were sectioned perpendicularly to the glass surface. By imaging samples with no beads I could identify Clathrin-coated structures at the cell membrane (Figure 36 A); interestingly, by imaging cells seeded onto beads I could observe CCPs growing on top of the 100 and 300 nm beads. Moreover, by looking at the serial section, it was possible to identify above the beads, all stages of Clathrin machinery maturation, from early recruitment to maturation of CCPs and constriction of vesicle (Figure 36 B).

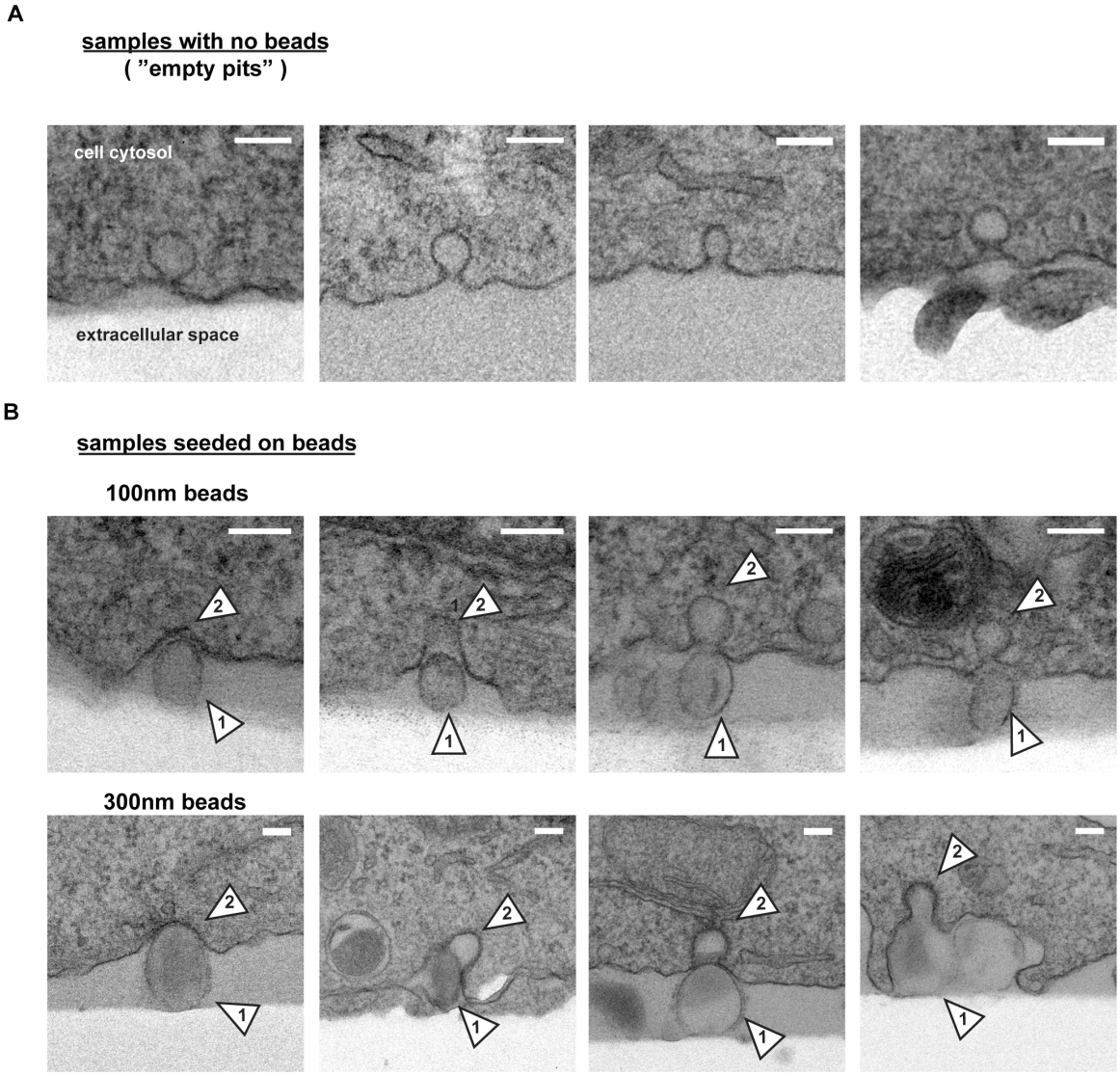

Figure 36. The size of nanoparticles imprints the final size of CCVs. A) TEM images of CCPs from ultra-thin sections of U373 cells seeded on glass coverslips with no beads. Cells were seeded upon glass coverslips; 6 hours post-seeding, cells were fixed and processed for TEM imaging (scale bar 100 nm). B) TEM images from ultra-thin sections of U373 cells seeded upon bead coated coverslips (100 nm beads (upper), 300 nm beads (lower). Cells were seeded upon

clicked-beads coated coverslips; 6 hours post-seeding cells were fixed and processed for TEM imaging. Sequence of pictures shows different stages of Clathrin coated pit assembly upon immobilized beads (scale bar 100 nm). 1) Clicked beads 2) CCP growing on top of beads. Sample processing and imaging was performed in collaboration with Dr. Charlotta Funaja (Electron Microscopy Core Facility (EMCF) Heidelberg University). Adapted from Fratini et al., submitted.

By combining fluorescence microscopy quantification, super resolution microscopy and electron microscopy I could confirm the presence of CCPs growing into CCVs on top of 100 and 300 nm beads. Moreover it was found that the size of the CCV growing on top of the nanostructures is directly correlated with the size of the beads, although these are not internalized. The early interaction between nanostructures and cells can therefore induce the recruitment of the Clathrin machinery and imprint the size of the future CCVs independently for beads/virus internalization. It is tempting to speculate that the specific curvature imposed at the cell membrane by reovirus, 100 and 300 nm beads might act as a mechanical signal for the recruitment of curvature proteins and in turn Clathrin. In this model, the CCP starts to be assembled on top of the nanostructures and afterwards, since the virus/beads are immobilized at the glass surface, the growing CCP disengages from the cargo and it continues growing accordingly to the initial curvature imprinted at the cell membrane. These conclusions suggest the presence of a CCPs early commitment that is induced by the early cargo-cell interaction but it is independent from cargo internalization.

2.3.5 Transferrin coated 20-nm beads and AAV2 induce CME recruitment

After confirming that recruitment of the Clathrin machinery strongly depends on the size of the nanostructures, and that immobilized reovirus, 100 and 300 nm beads can specifically induce CME recruitment without involvement of any receptor, I addressed again the role of receptors in the internalization of small molecules. I had previously shown that 20 nm beads cannot induce recruitment of Clathrin machinery (Figure 32), suggesting that 20 nm diameter objects might induce a curvature at the cell membrane that does not favor Clathrin machinery activation. To address if internalization of such structures by CME could be induced by receptor signaling, 20 nm beads were coated with transferrin and then immobilized onto modified glass surfaces. Transferrin (Tf) is a small

protein of 80 kDa that is internalized by CME through the binding with its receptor, the transferrin receptor (TfR). Previous studies demonstrated that induction of TfR clustering induces CCPs nucleation and maturation, but the mechanism behind has not been clarified yet[52]. Therefore 20 nm beads were coated with Alexa647-tranferrin and clicked onto Si-PEG-N3 coverslips. Afterwards BSC1 AP2-GFP cells were seeded on top and live-cell imaging was performed. Surprisingly, I could observe that compared to beads without any coating, 20 nm transferrin-coated beads co-localized with the Clathrin machinery (Figure 37). This observation might result from TfR clustering mediated by transferrin-coated beads that may provide/stabilize a specific curvature at the cell membrane that in turn recruits Clathrin. Currently in fact, TfR is considered to be constitutively internalized by the Clathrin machinery, meaning that no specific signaling appears to be involved in activating the endocytic machinery.

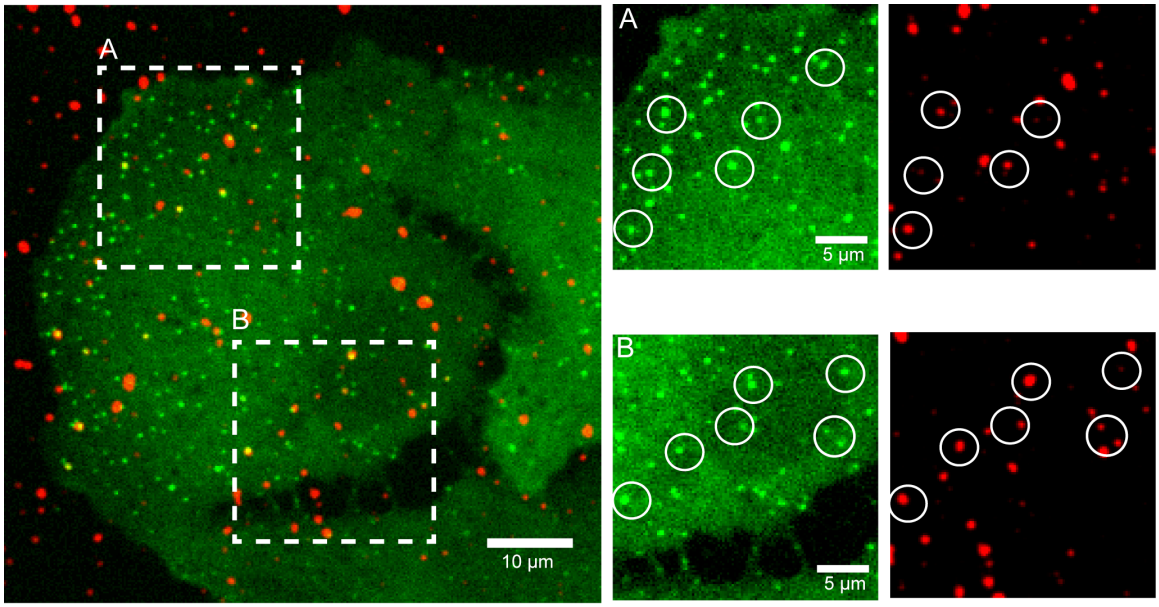

Figure 37. Beads of 20 nm diameters induce CME recruitment when coated with transferrin. 20 nm beads are coated with transferrin-647 (20 nm-Tf 647) and clicked onto azide-modified glass coverslips. (Left part) U373 cells stably expressing AP2-GFP are seeded on top and 6 hours post-seeding live-cell imaging is performed. Insert region A and B are representative areas where 20 nm-Tf 647 co-localize with the Clathrin machinery (Right part) Zoom in of fluorescent channels from insert region A and B. White circles highlight the co-localization spots between 20 nm-Tf 647 and AP2-GFP.

To further validate the role of receptor in inducing CME but using an alternative virus, I immobilized onto glass surfaces the 20 nm Adeno-associated virus (AAV)[196]. AAVs are small icosahedral viruses containing a single-stranded DNA genome and are known enter cells through CME[197]. Although they can infect humans and other primates, they are not associated with any disease; importantly, they are widely used in the field of gene therapy[198]. The most investigated AAV serotype is the AAV2, which attaches the cell surface using the heparan sulfate proteoglycan[199]. Recently through a genome wide screening approach an AAV receptor (AAVR) was characterized, which consist of a trans-membrane protein exposing five immunoglobulin-like (Ig-like) domains[200]. Interestingly, this receptor appeared to be involved in the internalization of all AAV serotype[200].

To address if AAV particles could induce CME recruitment, despite displaying a size that is below the critical diameter for favoring mechanical induction of CME, AAV2 viruses were labeled and conjugated with an alkyne linker and clicked onto Si-PEG-N3 surfaces. Afterwards, U373 AP2-GFP cells were seeded on top and live-cell imaging was performed. Surprisingly, a great percentage of AAV particles (30%, Figure 38) co-localized with AP2-GFP inducing the previously recurrent recruitment of Clathrin machinery.

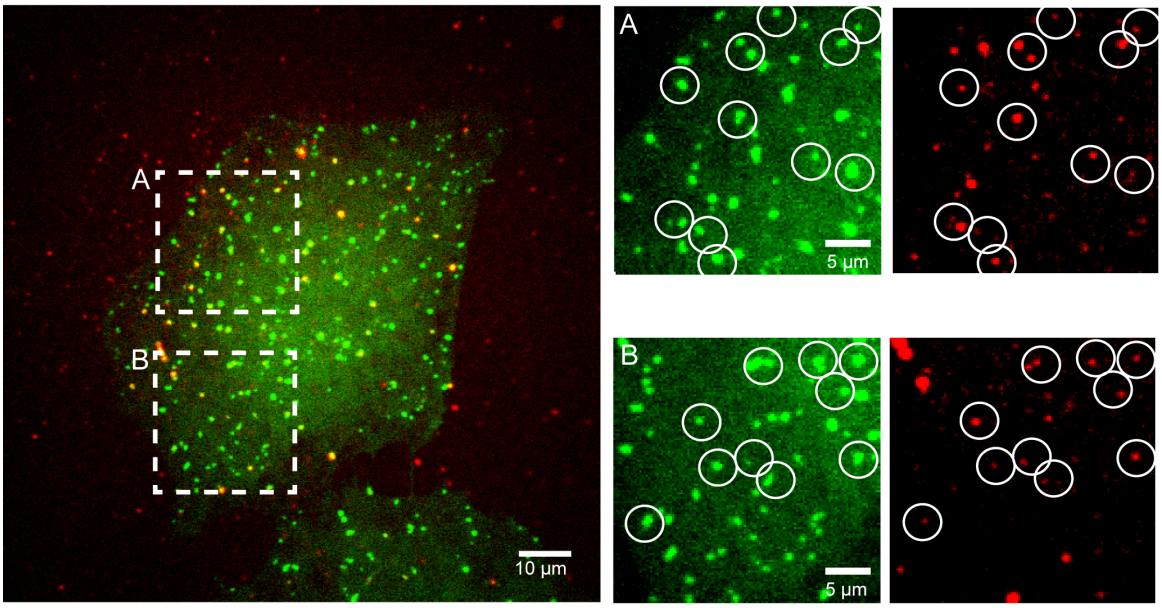

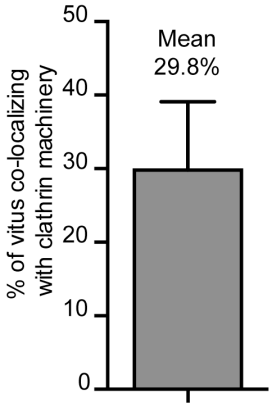

Figure 38. The endocytic Clathrin machinery is recruited on the clicked 20 nm diameter AAV2 viruses. AAV2 particles are labeled with Alexa647 and conjugated with an alkyne linker. Virus particles are afterwards clicked onto azide modified coverslips, U373 cells stably expressing AP2-GFP are seeded on top and (Left part) 6 hours post-seeding live-cell imaging was performed. Insert region A and B are representative areas where Alexa647/ Alkyne-AAV2 co-localize with the Clathrin machinery. (Right part) Zoom in of fluorescent channels from insert region A and B. White circles highlight the co-localization spots between Alexa647/ Alkyne-AAV2 and AP2-GFP.

These results suggest that the presence of a strong signaling and/ or induction of receptor clustering might favor Clathrin machinery recruitment on those cargos whose size is too small to support mechanical induction.

3 Discussion

The text from the discussion part has been adapted from Fratini et al., submitted, which corresponds to the manuscript resulting from my PhD research project.

In this thesis I presented a new method to study the early stages of virus infection. The initial interaction between virus and cells represents a multistep process whose dynamics and structure are difficult to characterize. In particular, how the endocytic machinery is activated upon virus binding represents a challenging topic to address. The limits of understanding this process are imposed by the fact that some viruses diffuse extremely fast at the cell surface[130], their internalization takes place in the range of 1-2 minutes[22,165] and it is spatially and temporally arduous to predict. CME is one of the major pathways used by viruses for their internalization. CME was discovered more than 40 years ago and since then thousands of scientific investigations reconstructed each single step of the process and characterized many proteins participating in this pathway[201]. Nevertheless, how the Clathrin machinery is recruited upon virus binding and which proteins play a role in initializing the process it is still a matter of debate[7,56].

3.1 A new method to study virus - cell interaction

Due to the strong limitations in studying early steps of virus infection using canonical assays, where "free" virus particles are released into cell culture media, the first milestone of this work was to establish a new method to dissect and analyze the early factors associated with early virus-cell interaction. The design of this new approach was to covalently immobilize virus particles onto glass surfaces and subsequently seed cells on top of these particles. According to this method, cells can interact with virus particles but they cannot internalize them, therefore avoiding infection. Covalent immobilization of viruses was achieved through click chemistry. Virus particles were modified by the addition of fluorophores, to allow the tracking of virus positions during live-cell imaging, and an alkyne linker, used to "click" the particles onto azide-modified glass surfaces. Chemical modification of virus capsids represents an innovative research field that it is starting to raise the interest of many investigators[202–206]. Kwak and colleagues, previously

described an new method to immobilize fd phage on glass surfaces[205]. In this study, virus particles were genetically engineered to have an aldehyde functional group on their capsid that can be employed for immobilization on amine-coated glass coverslips. Although this method offers site-directed virus modification and ultimately would allow for controlled orientation of the virus particle upon immobilization, it imposes genetic modifications, which are not always applicable for all viruses. Moreover, the method I chose for my work is less invasive and it exhibits a faster experimental set up. In this thesis I showed that reovirus capsid modification preserves virus infectivity and replication (Figure 20 A and B). Moreover, immobilized virus particles can still interact with Clathrin machinery (Figure 24 and 25). Additionally, this method can be easily applied to different virus species; in this thesis both reovirus and AAV2 virus were successfully modified and clicked onto azide–coated coverslips.

Interestingly, the Clathrin machinery was found to co-localize with virus particles (15% co-localization, Figure 25 A); this result was confirmed using several markers for CME (AP2, Clathrin, dynamin) and also in gene edited cell lines, where the proteins of interest were expressed at their physiological level (Figure 29). To analyze the dynamics of the recruitment of Clathrin machinery above the virus particles live-cell imaging was performed. By looking at the fluorescence intensity profile of AP2 and in particular at the recruitment of dynamin, it was possible to speculate that CCPs recurrently nucleates and mature above the clicked virus (Figure 25 and 29). Even though the goal of having immobilized virus particles was to “freeze” the interaction between cell surface and the Clathrin machinery, this result suggested that the early Clathrin machinery interaction with immobilized cargos exhibits a highly dynamic behavior. The recurrent recruitment of the Clathrin machinery was demonstrated to be specific at the virus spots both experimentally, by chemically removing and synchronize CCPs formation at the cell surface (Figure 26), and statistically, by establishing a Gaussian fitting approach to automatically analyze the data from multiple cells (Figure 27 and 28). Therefore, immobilized virus particles specifically interact with the cell surface, demonstrating that this new method can be used to investigate early steps of virus infection and endocytic machinery activation.

3.2 Role of mechanical induction in favoring CME recruitment

Reovirus enters cells through receptor-mediated endocytosis[22,148,207,208]. It was shown that in HeLa cells the virus particles land and attach to the cell surface through the interaction with SA and the JAM-A receptors; afterwards the integrin beta1 receptor is engaged and viruses are internalized. While blocking integrin beta 1 receptor reduces 30-50 % of the virus infection[148], blocking JAM-A receptors instead completely abrogates reovirus entry and infection in HeLa cells[146]. To confirm the role of JAM-A receptor, HeLa cells were pretreated with anti-JAM-A antibody and infected with reovirus particles. As previously shown[146,148], blocking JAM-A receptor induced a strong reduction of reovirus infectivity in HeLa cell (Figure 30 A). Therefore, to address if the recurrent recruitment of Clathrin machinery was mediated by reovirus receptors, HeLa cells were pretreated with blocking antibody against JAM-A receptor, seeded on top of clicked viruses and live imaging was performed (Figure 30 B). Interestingly the Clathrin machinery was still recurrently recruited above the immobilized virus particles (Figure 30 D and E). This result indicates that the CME induction and maturation mechanism is independent from receptor JAM-A receptor binding. Nevertheless, it is not possible to absolutely exclude the presence of a non-identified reovirus receptor involved in inducing a specific signaling that in turn activates Clathrin machinery.

Therefore, to further address how the recruitment of CME is activated, whether this recruitment could be mechanically induced, and if receptors play a role, I immobilized latex beads with a similar size as virus particles. Such beads have been described to be internalized by cells in the absence of specific interaction with cellular receptors[209], and therefore represent an ideal negative control. Moreover, as further controls, beads smaller and larger than viruses were immobilized as well; in total, 20, 100, 300 and 1000 nm beads were immobilized onto glass surface. Latex beads were immobilized using the same strategy established for virus particles. Cells were seeded on top of clicked beads and live-cell imaging was performed. Interestingly nanoparticles of 100 and 300 nm diameter could induce recurrent recruitment of Clathrin machinery, while 20 and 1000 nm could not. These results confirm that CME recruitment can be induced by the mechanical presence of a cargo with a specific size, independently from receptor signaling (mechanical induction). It is temping to hypothesize that a specific size

of the cargo might mechanically induce a specific curvature at the cell membrane that is recognized by specific curvature proteins (e.g. BAR proteins). Recruitment of such proteins could in turn favor recruitment of Clathrin. Nanoparticles whose size is too small (e.g. 20 nm) or too big (e.g. 1000 nm) may induce a curvature that can not be "sensed" by the Clathrin machinery. Interestingly, by analyzing the recruitment of Epsin and FCHO1 above 100 nm clicked beads, it was observed that while Epsin and AP2 signals almost perfectly correlate (average correlation coefficient = 0.8) (Figure 34 B and C) the signals from FCHO1 and AP2 are slightly shifted (which results in a average correlation coefficient = 0.4) (Figure 34 B and C). It is possible to notice that when the fluorescence signal from AP2 reaches its minimum, FCHO1 fluorescence signal is already almost half way to reach its maximum (Figure 34 B, right panel). It is exciting to speculate a potential role of FCHO1 in stabilizing a specific curvature of the membrane above the immobilized beads and in inducing CME recurrent recruitment. Further studies will be able to address the role of curvature proteins in supporting mechanical induction of CME.

In the last years more and more work has been performed to understand how mechanical stimuli can induce and/or affect Clathrin machinery induction and maturation[120–122,190,210]. For instance, it was shown that increased tension at the cell membrane can induce several responses from the Clathrin pathway; the energy barrier to bend the membrane increases[211], CCPs lifetime becomes longer[69,190], membrane curvature is delayed[116] and there is a greater recruitment and polymerization of actin[69,210]. In particular, it was shown how certain proteins can "sense" the increased tension at the cell membrane favoring actin recruitment to overcome the energetic barrier of membrane bending during CCPs maturation[70]. Additionally, using nanocones or nanopillar of 100-200 nm diameter, which invaginate the cell membrane, it was shown that these invaginations can favor CME recruitment, demonstrating how mechanical stimuli play a major role in favoring certain cellular pathways[120,121]. Moreover, while nanocones and nanopillar exhibit a dense distribution at the glass surface, concentration of clicked virus/beads can be easily tuned in order to get a density compatible with single molecule analysis.

It is important to consider that such mechanical induction is not only the result of an artificial system, but it can be faced by cells in their natural environment. It was shown

that curvature induced by seeding cells onto 3D structures of collagen fibers, induce recruitment of CCPs[122] (Figure 39 A). Formation of CCPs above collagen fibers releases the tension at the adherent side of the cells favoring cell migration[122].

The recruitment of CME mediated by the mechanical presence of virus particle at the cell membrane is a topic that so far was not investigated; nevertheless, it is reasonable to believe that in their natural 3D environment viruses might exert an external "push" at the cell surface. Some viruses can spread from one cell to the other creating cell-cell contact areas for virus transmission which are called "virus synapses", because of their functional similarity with neuronal synapses[212,213]. HIV virus in particular forms a virus synapse in the contact area between dendritic cells (DT) and T-lymphocytes (T-cell) that help the spread of infection (Figure 39 B)[212,213]. Once released from the DT infected cells, virus particles diffusion is limited in the narrow space (100-300 nm) of the virus synapse favoring the infection of the adjacent T-cell. Since HIV infection is inhibited by blocking CME[214] and since HIV particles have a diameter of 100 nm, it is extremely tempting to claim that virus particles released from DT cells might exert a direct push on the membrane of the T-cell at the virus synapse favoring, together with receptor binding, its direct internalization. Importantly, this aspect might not only be associated with viral synapse, but it can be broadly related with virus infection when considering virus release and spread in the context of tissues, where cells displays tight interactions within each other.

One more interesting example on how a specific curvature may mechanically induce recruitment of CME in virus internalization is the entry of the vesicular stomatitis virus (VSV). The VSV has typical bullet shape that displays one flat and one curved end. Although the unusual size (120 nm long and 85 nm wide in diameter) VSV is internalized by CME and it was observed that it induces Clathrin-dependent uptake *via* its curved end. TEM analysis of the endocytic structures revealed that the Clathrin coat does not fully assemble around the VSV particles but only caps the tip of the virus by following the curvature radius of the curved end[23,68]. The last stages of VSV entry are mediated by a strong recruitment of actin[23] (Figure 39 C). It is tempting to speculate that the initial curvature induced by the curved end of the virus could mechanically induce CME recruitment; the nascent CCP will grow accordingly to the initial curvature imposed by

the virus and afterwards, since the VSV displays a length that overcome the size limit of CCVs, a substantial recruitment of actin cooperates to favor vesicle completion.

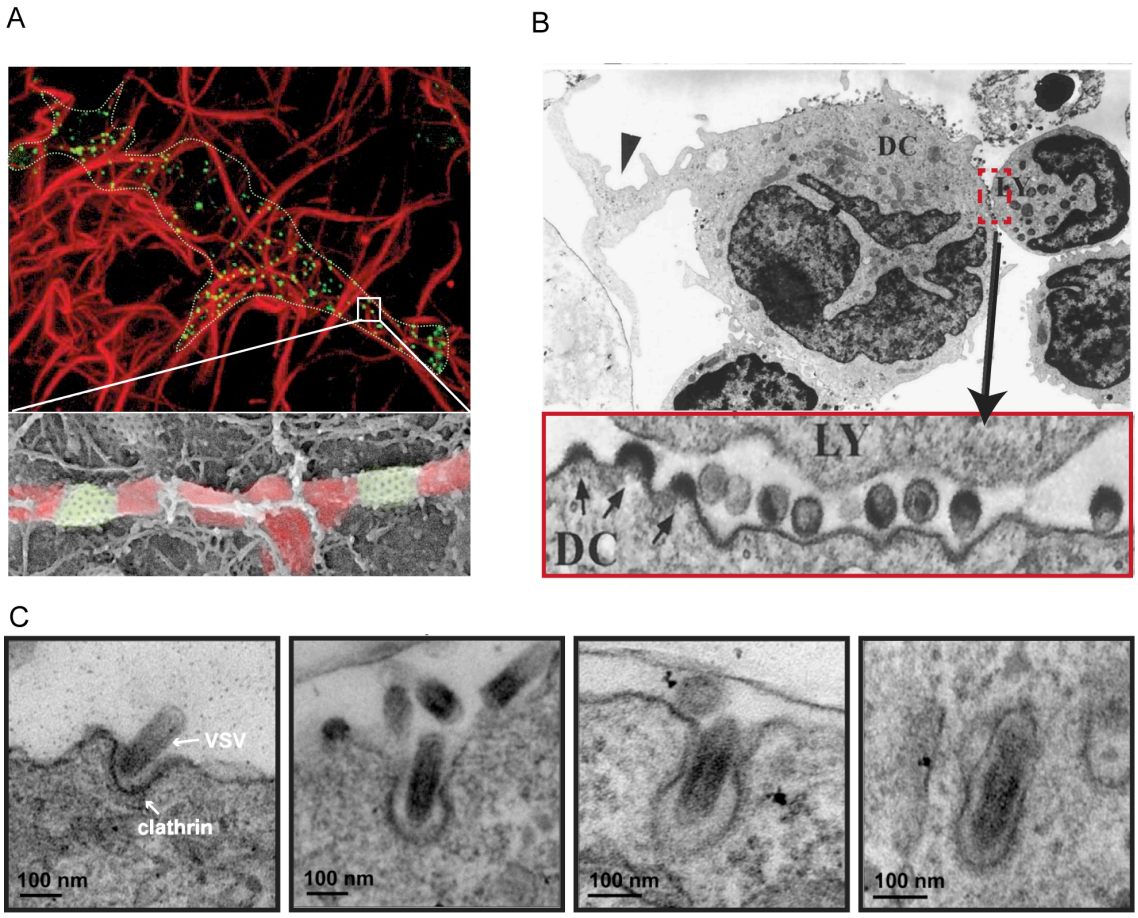

Figure 39. Mechanical bending of cell membrane can affect cellular processes. Representative examples of how membrane passive deformation imposed by external objects can/ may favor cellular processes. A) Curvature imposed at the cell membrane by collagen fibers induces Clathrin recruitment. Inset region, CLEM imaging showing a collagen fiber (red) and Clathrin cages on top (green). Adapted from Elkhatib et al., 2017. B) Virus synapse. HIV particles can facilitate their spread from dendritic cells (DC) to T cells (LY) exploiting specific cell-cell contact areas, generating a virus-synapse (zoom in, red insert). Image adapted from Hladik et al., 1999. C) Vesicular stomatitis virus (VSV) entry. Electron microscopy pictures of sequential stages of VSV entry. The VSV virus displays a bullet shape, having a curved and a flat edge; its entry is mediated by CME and it starts with the interaction of the virus-curved edge (85 nm in diameter) with the cell membrane. Adapted from Cureton et al., 2010.

All these investigations underline an important role of mechanical induction in activating/favoring certain cellular pathways, in particular CME, and the importance of investigating virus infection trying to resemble as close as possible the real environment of the viruses and cells.

3.3 Role of receptors in inducing CME recruitment

By immobilizing beads and virus onto surfaces it was demonstrated that a specific size of a cargo can favor CME recruitment independently from receptor activation. Blocking the reovirus JAM-A receptor in HeLa cells does not affect the recurrent recruitment of the Clathrin machinery above clicked viruses (Figure 30 D and E). Beads of 100 and 300 nm diameter can induce CME, 20 and 1000 nm do not. This result underlines an important function played by the mechanical induction during virus entry; nevertheless, the role of receptor binding and probably receptor signaling upon virus attachment definitely can not be excluded. To further address the role of receptors in CME activation and in CME recruitment above virus binding, 20 nm particles were coated with transferrin (Tf) (~5nm in diameter). This protein, after binding its own receptor (TfR), is specifically internalized by CME[215]. Interestingly, by seeding cells on 20 nm beads coated with transferrin (20 nm-Tf) I could observe co-localization with the Clathrin machinery (Figure 37). Although the TfR is constitutively internalized by CME[43], meaning that its internalization does not require cargo engagement, it was shown that induction of clustering of TfR favors CCPs nucleation[52] and maturation[22]. Therefore, while 20 nm "naked" beads do not mechanically induce CME recruitment, coating such beads with Tf might induce TfR clustering and in turn CCPs nucleation. It is possible to speculate two ways through which clustering of TfR might favor CME recruitment. In the first place, the clustering of TfR could be involved in activating a specific cellular signaling which in turn recruits Clathrin. The second way relies on the fact that TfR is a trans-membrane protein, and therefore, clustering of TfR can induce membrane bending by generating local asymmetry at the lipid bilayer. The generation of a curved membrane may in turn stabilize the maturation of CCPs[22]. Finally, it is not possible to exclude that both mechanisms might act synergistically in inducing CME recruitment upon 20 nm-Tf beads binding

To confirm the role of receptors I immobilized also AAV2 particles, which are 20 nm in diameter and are internalized by CME. By seeding cells on top of clicked AAV2 I could observe that a high fraction of the virus particles were co-localizing with Clathrin machinery and inducing its recurrent recruitment (Figure 38). In particular, 30% of the AAV2 clicked viruses were found to co-localize with AP2-GFP (Figure 38), a percentage

which is two times higher than the one for reovirus (15 %, Figure 25 A) in the same cells. Since the size of the AAV2, compared to reovirus, is too small to support mechanical induction of CME, this result suggests the presence of a strong receptor signaling/clustering that might be involved in inducing CME recruitment. Unfortunately, AAV2 receptors have not been clarified yet, although many candidates have been proposed in different cell lines[199,200,216,217].

3.4 Early cargo-cell interactions define CCP nucleation and commitment

The observation that dynamin was recruited at the end of each endocytic event taking place on top of clicked viruses, strongly suggested the potential release of CCVs (Figure 29). Interestingly, the lifetime of CCPs growing on top of clicked virus was similar to the lifetime of canonical, terminal, CCPs (around 1 minute duration) (Figure 28 C). To confirm the presence of assembled CCPs and CCVs above clicked cargos, the recruitment of FCHO1, Epsin and Amphiphysin was also investigated. Such proteins are either recruited at early CCPs (FCHO1), or are involved in maturation (Epsin) or in pinching of CCVs (Amphiphysin). By performing live-cell imaging it was found that all these proteins are recruited together with AP2 to the beads (Figure 34, A and B); Amphiphysin, in particular, is recruited towards the end of each AP2 recruitment cycle and its fluorescence signal anti-correlates with AP2 fluorescence signal (Figure 34 B and C). These results strongly suggest the presence of CCPs above immobilized beads that mature into CCVs that are recurrently released. To further confirm this finding, STED and SEM imaging were performed. While from STED imaging it was possible to observe the typical “ring structures” of genuine CCPs on top of clicked-beads (Figure 35), through TEM it was possible to identify CCPs and CCVs directly on top of clicked beads (Figure 36).

The potential release of CCVs from immobilized beads/viruses represents an important point of interest since the role of cargo in CME is still a matter of debate. While initial investigations excluded any role of the cargo in CME initiation, further studies highlight how certain cargos can favor CCPs nucleation and maturation into CCVs[48,52]. Observing that CCVs are potentially released from immobilized beads/viruses suggests a role of cargo in inducing CME initiation and maturation independently from

its internalization. This raises interesting hypothesis on the presence of an early CCP commitment that is "activated" by the early cargo-cell interaction and that favors CCP maturation into CCVs independently from cargo internalization.

Therefore, together with previous results, while Clathrin recruitment is dependent on the size of the cargo, the final commitment into CCVs is independent from cargo internalization. These conclusions underline how mechanical stimuli and not only chemical signaling can affect both early and late stages of CME.

3.5 Size of CCVs is imprinted at early cargo-cell interaction

Using live-cell imaging I could observe that the dynamics of Clathrin recruitment and the size of the Clathrin structures were correlated with the size of the immobilized viruses and beads. The width of peaks (the time to complete a cycle of AP2 GFP recruitment) and the rate of peak occurrence (time between two cycles of AP2 GFP recruitment) of AP2-GFP recruitment increase accordingly with the diameter of the immobilized nanoparticles (i.e. virus (85 nm) to 100 and 300 nm beads) (Figure 28 B and C; Figure 33 A and B). Moreover, through CLEM analysis of CCPs, it was shown that the total amount of fluorescence signal of Clathrin structures directly correlates with their size[21,116]. Fluorescence quantification analysis of AP2-GFP revealed that CCPs growing on the top of viruses are almost two times larger than empty pits, while for 100 and 300 nm beads, CCPs are three times and fives times larger than on empty pits, respectively (Figure 33 C). By quantifying the fluorescence signal from AP2-GFP, FCHO1-mcherry, Epsin-mcherry and Amphiphysin-mcherry at immobilized 100 nm beads, it was observed that the amount of AP2 is always almost two times higher than the other proteins (Figure 34 A). This might be explained by the fact that such proteins, compared to AP2, do not completely enclose the nascent Clathrin structure above the immobilized beads; Amphiphysin, in particular, is recruited at the neck of the nascent vesicle. The presence of genuine CCPs and CCVs on top of beads was afterwards further confirmed through STED microscopy and TEM, where it is possible to visualized different stages of CCPs maturation above the immobilized cargos (Figure 35 and 36).

These results strongly suggest that not only CCP maturation, but also that the size of the Clathrin vesicle is imprinted at the early cargo-cell interaction independently from

cargo internalization (Figure 40). Why and how the initial curvature imposed by both nanoparticles and virus particles dictates the final size of CCVs remains unclear. A possible way to explain this result can be found in the different interactions among the Clathrin triskelia. As mentioned in the introduction, each Clathrin triskelion can interact with other triskelia generating polygonal shapes of pentagon and hexagon[18,19,20]. If a Clathrin lattice is formed by only hexagons it has a flat structure, the addition of pentagons generates curvature into a flat lattice; the ratio among pentagons and hexagons defines spherical cages of different sizes. The smallest Clathrin cage contains 12 pentagons and 4 hexagons[18]. It was also shown that CCPs nucleate and start to grow as flat arrays; curvature is acquired at late stages of maturation[21,116,117]. Re-arrangements of Clathrin triskelia from hexagon to pentagon and curvature generation are favored by an extremely high and fast triskelia turnover (every 2 sec)[21]. Compared to CCPs that nucleate as flat arrays, the presence of immobilized cargo (virus/beads) might push the cell membrane generating a certain curvature and such specific curvature will be able to accommodate a specific hexagon-pentagon combination. In other terms, it might be that a specific curvature imposed at the cell membrane could limit the high flexibility of triskelia interaction generating a specific pentagon/hexagon ratio. During CCPs maturation, since the beads/virus are immobilized, the coat will disengage from the cargo keeping the initial, imposed, curvature.

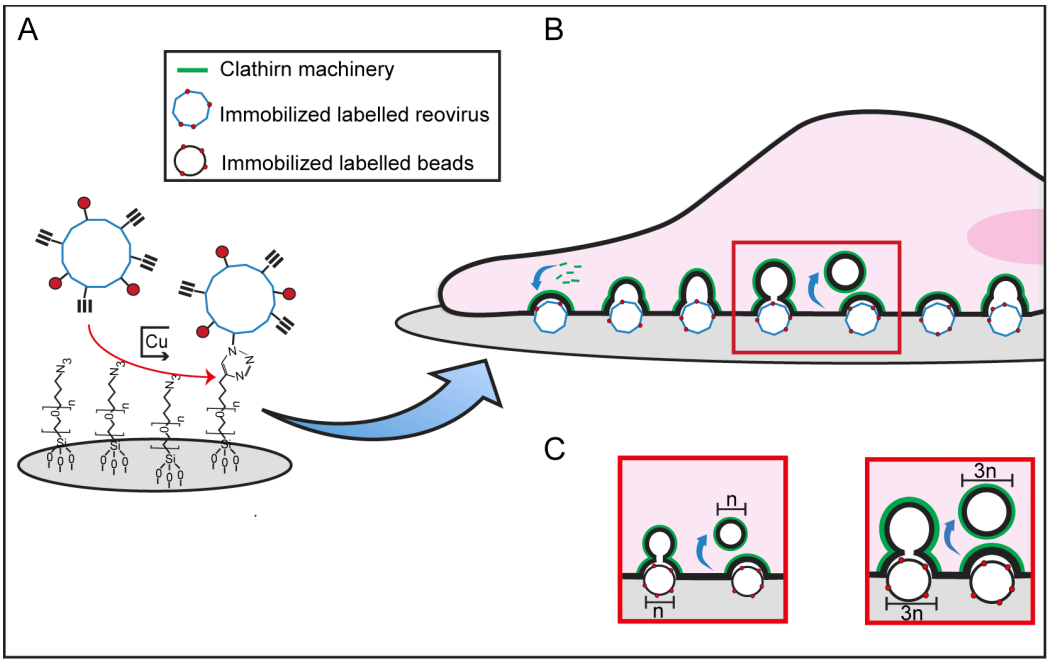

Figure 40. Proposed model. (A and B) Click chemistry can be used to immobilized cargo onto glass surfaces allowing their interaction with cell surface to be studied. B) The curvature imposed by the presence of the clicked reovirus induce CME recurrent recruitment; CCVs are recurrently released on top of virus suggesting that commitment of CCPs into CCVs is independent from cargo internalization. C) The diameter of the cargo defines the size of CCV independently from cargo internalization. Immobilization of 100 and 300 nm beads induce CME recruitment and CCVs release; fluorescence quantification, fluorescence kinetics analysis and TEM imaging suggest that the size of the vesicle is correlated with the size of the cargo, independently from its internalization. Adapted from Fratini et al., submitted.

Interestingly, every recruitment of the Clathrin machinery above virus/beads is characterized by the presence of a protein leftover after each AP2 peak (Figure 33 C); the amount of leftover correlates with the size of the virus/beads (Figure 33 C). The presence of this leftover, probably caused by the fact that the cargo is not internalized, might preserve the specific pentagon/hexagon ratio at the nascent CCPs therefore favoring AP2 recruitment cycles which are extremely regular (Figure 33 A and B) and release of vesicles which have all the same size. The same conclusion is supported also by observing that by removing all CCPs at the cell membrane through 1-butanol treatment, many virus particles that were co-localizing with the Clathrin machinery displayed some AP2-fluorescence leftover that could not be removed by the treatment. These results suggest the presence of a strong interaction and probably a remarkable rigidity among Clathrin triskelia upon the immobilized cargos. This observation could support the

hypothesis that the initial curvature of the coat imposed by external push can be conserved during CCPs maturation and vesicle formation.

The repetitive recruitment of Clathrin machinery at the same spot is referred in the field as a "hot spot"[22,38,92]. Although it is not yet clear how they are generated, it is believed that they represent endocytic platforms at the plasma membrane for receptor/cargo recycling and/or or clustering[92]. Contrary to the particle/beads endocytic sites, which have a very regular frequency of Clathrin recruitment, the previously reported "hot spots" display a broad distribution of the lag time between each endocytic event nucleation[92]. This difference of Clathrin recruitment frequency might be explained by the fact that in the observed "hot spots" no specificity of cargo molecules was imposed and each "hot spots" might contain different cargo. On the contrary, the "hot spots" observed on immobilized particles are specific to a unique cargo (i.e. virus particle). As such, it is possible that the observed dynamics of "hot spots" is dependent on cargo. Importantly, the observed regular recruitment of the endocytic machinery suggests that the signal (chemical or physical) generated by the immobilized particles is not removed and is responsible for the observed recurrence.

3.6 Early events at virus - cell interaction

All these results together, suggest how both chemical (receptor-mediated) and mechanical (size-mediated) induction play an important role in virus entry and CME recruitment. Importantly they demonstrate the presence of a balance between these two mechanisms that can be tuned by virus particles in order to be internalized. A specific size of virus particles, between 80-300 nm diameter can favor CME recruitment independently from receptor engagement. Small particles of 20 nm diameter, such as AAV2 or 20 nm-Tf beads, are too small to induce mechanical recruitment of Clathrin machinery; nevertheless, induction of either receptor clustering, and/ or potentially receptor signaling, can favor CME recruitment.

Importantly, it was shown how early events of virus-cell interaction can affect late stages of Clathrin endocytic machinery, such as CCPs commitment and vesicle size. All these aspects could have not been investigated with canonical cell biology techniques. How a specific size can favor CME recruitment, and which proteins play a role in such

mechanism it is still unknown. Additionally, although it is apparent that cell receptors play a major role in virus attachment and entry, detailed information on how many viruses induce receptor clustering and endocytosis activation are still missing. Generally, the role of receptors in activating CME after virus binding is a difficult topic to address; virus attachment and entry are events that take place extremely fast and are spatially unpredictable. In this thesis I showed how immobilization of virus particles onto glass surfaces represents a new tool to investigate transient phenomena such as virus binding and early events of CME. The establishment of this new approach can be easily and broadly applied in the field of virology and endocytosis to unveil new details on how viruses manage to infect our cells and how the endocytic machinery is regulated.

4 Materials and methods

4.1 Materials

Table 1. Primary antibodies

Primary antibody	Source	Species	Application
Anti-Human Vinculin	Sigma	Monoclonal mouse	IF : 1:600
Anti-Reovirus μNS	Boulant Lab	Monoclonal Guinea pig	IF: 1:5000
Anti -Human JAM-A	Santa Cruz biotech	Monoclonal mouse	Blocking experiments: 10 μg/ml

Table 2. Secondary antibodies

Secondary antibody	Source	Species	Application
Anti-mouse IgG (H+L) Alexa Fluor 568	Invitrogen	polyclonal goat	IF: 1:1000
Anti-guinea pig IgG (H+L) Alexa Fluor 568	Invitrogen	polyclonal	IF: 1:1000
Anti-Guinea pig IgG (H+L) IRDye 800CW	LICOR	polyclonal Donkey	LICOR assay 1:10000

Table 3. Plasmids

Plasmid	Application	Prokaryotic Resistance	Eukaryotic Resistance
Sigma2-eGFP (AP2-GFP)	CMV-driven mammalian expression of fusion protein	KAN	G418
Tdtomato-CLCa (Clathrin light chain)	CMV-driven mammalian expression of fusion protein	KAN	G418
Epsin-mcherry	CMV-driven mammalian expression of fusion protein	KAN	G418
FCHO1-mcherry	CMV-driven mammalian expression of fusion protein	KAN	G418
Amphiphysin-mcherry	CMV-driven mammalian expression of fusion protein	KAN	G418

Table 3. Fluorescence reagents, chemical linkers, peptides and beads

Reagent	Source
Alexa Fluor647 carboxylic acid, succinimidyl ester	Invitrogen
Atto647 carboxylic acid, succinimidyl ester	Sigma
Transferrin-Alexa 647	Life Technologies
Draq5	eBiosciences
ProLong Gold Antifade +/- 4,6-diamidino-2-phenylindole mounting medium	Molecular Probes
Alkyne NHS linker	custom made from Iris –Biotech
Silane-PEG_{3000}-azide	Rapp Polymere
Alkyne RGD	BioTrend
20 nm Aliphatic Amine Latex Beads, 2% w/v	Thermo fisher
100 nm Aliphatic Amine Latex Beads, 2% w/v	Thermo fisher
300 nm Aliphatic Amine Latex Beads, 2% w/v	Thermo fisher
1000 nm Aliphatic Amine Latex Beads, 2% w/v	Thermo fisher

Table 4. Chemicals

Chemicals	Source
Sulfuric acid 96 %:	Sigma
Hydrogen peroxide (H2O2) 30 %:	Sigma
Toluene	Sigma
Triethylamine 99.5 %	Sigma
Tris HCl	Roth
$CuSO_4$	Grussing GmbH
L-ascorbic acid	Sigma
1-butanol	Sigma
Methanol	Fisher Chemicals
Freon 1,1,2-trichloro-1,2,2-trifluoroethane	Sigma
Cesium Chloride	Sigma
Ethyl acetate	Sigma
1-butanol	Sigma
Triton x100	Sigma
Tween 20	MP Biomedicals
Lipofectamine 3000	Invitrogen

BSA	New Englan Biolabs
PFA	Sigma
Glutaraldehyde	Sigma

Table 5. Buffers

Buffer	**Composition/ Source**
PBS	Sigma
HO buffer	10 mM Tris, pH7.5, 250 mM NaCl, 10 mM 2-mercaptoethanol
Virus Buffer	150 mM NaCL, 10 mM MgCl2, and 10 mM Tris-HCl, pH 7.5
EDAC	Sigma
MES	Sigma

Table 6. Cells and Media

Cells/ Media	**Source**
Bsc1- African green monkey kidney epithelial cells	ATCC
U373- Human glioblastoma astrocytoma	Tom Kirchhausen, Harvard medical School, Boston, USA
HeLa-Human cervical carcinoma	ATCC
Lcells- Mouse subcutaneous connective tissue	ATCC
SK-MEL-2 hCLTA^{en}/DNM2^{en} (gene edited cell line) Human malignant melanoma	David G. Drubin, Department of Molecular and Cell Biology, University of California, USA
0.05 % Trypsin-EDTA	Gibco
0.25 % Trypsin-EDTA	Gibco
DMEM	Gibco
DMEM without phenol red	Gibco
DMEM/F12	Gibco
Joklik MEM	Sigma-Aldrich
Opti-MEM	Gibco
L-Glutamine	Gibco
Neonatal calf serum	Gibco
Fetal bovine serum	Biochrom, GmbH
Penicillin	Gibco
Streptomycin	Gibco
Geneticin (G418	Gibco

4.2 Methods

The methods part has been taken or adapted from Fratini et al., (submitted), which corresponds to the manuscript resulting from my PhD research project.

4.2.1 Virus production and purification

Reovirus T3D strain was produced as previously described[144] by infecting suspension of L-cells with a T3D stock originally obtained from B. N. Fields. L cells were grown into a spinner flask of 1.5 liter at 35°C, until reaching a concentration of 2 x 10^6/ ml. Afterwards cells were infected with reovirus particles at MOI 5. After 3-4 days post infection, cells were centrifuged and re-suspended into single gradients of 2 x 10^8 cells each, in HO buffer. L-cells gradients are then stored at -80 °C. To proceed with virus purification, gradients of L cells were thawed at room temperature. Afterwards, virus particles were first pre-purified from L-cell by sonication and freon extraction; virus particles were then purified through ultracentrifugation on Cesium Chloride (CsCl) gradient and stored in virus buffer as previously described[144] .

AAV2 virus stocks were kindly provided by Dr. Martin Muller (DKFZ, Heidelberg).

4.2.2 Electrostatic immobilization of virus particles.

100 µl of reovirus particles (~10^{13} particles/ml stock) were mixed with 0.4 µl of Alexa647 NHS Ester (8 mM starting concentration) for 1 h at room temperature. To remove the unbound fluorophores, virus particles were then purified by gel filtration (7K molecular weight cutoff, Invitrogen*).* To electrostatically immobilize reovirus particles upon glass surfaces, glass coverslips are placed into 6-well plate and incubated with dilutions of PBS and different virus concentration. Samples were then incubated at 4°C over night. The day after, coverslips are washed two times in PBS and cells are seeded on top.

4.2.3 Virus and Latex Beads chemical modification

100 µl of virus particles (~10^{13} particles/ml stock) were mixed with 0.4 µl of Alexa647 NHS Ester (8 mM starting concentration) and 0.4 µl of Alkyne-NHS linker

(8.3 mM starting concentration) for 1 h at room temperature. To remove the unbound linker/fluorophores, virus particles were then purified by gel filtration (7K molecular weight cutoff, Invitrogen*)*.

Reovirus particles quantification by light scattering was performed using the Nanosight machine NS300 (Malvern). DLS is an optical technique that measures the scattering of light within a sample containing suspension of nanoparticles; by analyzing the fluctuation of light scattering it is possible to derive physical properties of the sample, such as the nanoparticles size. A total of 1,004 non-modified reovirus particles and 544 Alexa647/Alkyne-reovirus particles were counted.

Chemical modification of beads was performed similarly to virus particles except for the following modifications: for 20 nm beads: final concentrations of 20 mM and 41.5 mM for Alexa647 NHS Ester and Alkyne-NHS linker were used, respectively. For 100 nm beads: final concentrations of 0.08 mM and 20.75 mM for Alexa647 NHS Ester and Alkyne-NHS linker were used, respectively. For 300 nm beads: final concentrations of 0.5 mM and 83 mM for Alexa647 NHS Ester and Alkyne-NHS linker were used, respectively. For 1000 nm beads: final concentrations of 0.64 mM and 124.5 mM for Alexa647-NHS Ester and Alkyne-NHS linker were used, respectively. For STED imaging beads were labeled with Atto647 NHS Ester (0.08 mM final concentrations).

4.2.4 Preparation of transferrin-coupled beads

100 µL of 20 nm beads (~10^{13} beads/ml) were mixed with 0.4 µl of Alkyne-NHS linker (8.3 mM starting concentration) for 1 h at room temperature. To remove the unbound linker, virus particles were then purified by gel filtration (7K molecular weight cutoff, Invitrogen*)*. Afterwards, purified Alkyne-beads, were incubated with 250 µg/mL of human Transferrin-Alexa Fluor 647 (TF-647) in the presence of 100 mg/mL EDAC (dissolved in 25 mM MES buffer) to catalyze the amide bond formation. Samples were incubated for 3-4 hours with shaking, the TF-647-Alkyne-beads were purified by centrifugation (20 min at 10,000 g). The supernatant was removed and the pellet re-suspended in 100 µL PBS.

4.2.5 Silane-PEG-Azide coating of glass coverslips

Pegylation of glass coverslips was performed as previously described[189]. Briefly, 24 mm glass coverslips (high precision glass coverslips No. 1.5H, Marienfeld Lauda-Königshofen, Germany) were cleaned for 1 h in freshly prepared piranha solution (3:1 H_2SO_4 / H_2O_2), washed three times with deionized water, and dried in a stream of nitrogen. Surfaces were then immersed into a 0.125 mM solution of Silane-PEG(3000)-Azide in dry toluene; dry triethylamine was added to a final concentration of 25 µM. The reaction mix was then heated at 80°C overnight under nitrogen atmosphere. Finally, glass coverslips were sonicated for 5 min in ethyl-acetate and 5 min in methanol, and dried under a nitrogen stream.

4.2.6 Click reaction

Click reaction between azide coated glass coverslips and alkyne functions on virus particles was performed as previously described[189]. Briefly, azide-coated glass coverslips were placed upside down for 1.5 h at RT on a 100 µl drop of freshly prepared reaction mixture consisting of: 100 mM L-ascorbic acid, 100 mM Tris HCl (pH 9.5), 1 mM $CuSO_4$,, 10^{10} Alexa647/ Alkyne virus particles (reovirus or AAV2), H_2O (ultrapure water). Samples were then washed three times with PBS and re-incubated for a second click reaction to covalently bind the cRGDfK peptides on glass coverslips. 0.05 mM Alkyne-cRGDfK were clicked for 30 min at RT. Glass coverslips were then washed three times and stored in PBS at 4°C. The same procedure was applied to click latex beads on azide-coated coverslips. Depending on the size, the following number of beads particles are added into the mix: 10^{12}, 10^{11} 10^{10} and 10^{8} for 20 (naked or coated with transferrin), 100, 300 and 1000 nm beads respectively.

4.2.7 Cell culture and cell lines

BSC1 cells, HeLa cells and U373 were kept in DMEM (Gibco) Media containing 10% fetal bovine serum, 1 % v/v of penicillin and streptomycin at 37°C and 5% CO_2. To obtain U373 cells stably expressing AP2-GFP, cells were transfected with a plasmid encoding the sigma 2 subunit of AP2 fused to GFP and subjected to G418 selection (2

μg/ml). Genome edited SK-MEL-2 hCLTA^{en}/ were maintained in DMEM/F12 Media containing 10% fetal bovine serum, 1% v/v of penicillin and streptomycin at 37°C and 5% CO_2. Suspensions of L-cells for virus production were maintained in Joklik MEM medium supplemented with 1% L-Glutamine, 2% fetal bovine serum 2% Neonatal calf serum and 1% v/v of penicillin and streptomycin at 35 °C.

4.2.8 Transfection and selection

Cell transfection was performed with Lipofectamine^{TM} 3000 following manufacturer's protocol. Cells were seeded the day before into a 6 well plate to reach the 80-90% of confluence the day of transfection. 2 μg of DNA (for AP2-GFP) or 0.5 μg of DNA (for Clathrin light chain-tomato, Epsin-mcherry, FCHO1-mcherry and Amphiphysin-mcherry) were mixed in a tube together with 125 μl of Opti-MEM and 5 μl of P3000 reagent; 4 μl of Lipofectamine 3000 was diluted into a second tube with 125 μl of Opti-MEM. The two tubes were then mixed together, incubated 10 min at RT and the solution was added onto the cells. Cells were incubated with transfection solution for 8-10 h; the media was then replaced with fresh media. For transient transfection, cells were imaged the day after transfection; for stable cells lines, cells were kept under selection starting from two days after transfection.

4.2.9 Infectivity studies and indirect immunofluorescence

To measure Alexa647/Alkyne virus infectivity we employed the "In-Cell Western^{TM}" Assay (ICW) from LI-COR technology, which exploits laser-based scanning of near infrared to perform immunofluorescence quantification. Briefly, BSC1 cells were seeded one day before the experiment into a 96 well plate to reach 80-90% of confluence the day of infection. The day after cells were infected with serial dilutions (from 10^{-2} to 10^{-7}) of control virus (virus with no modifications) and Alexa647/Alkyne virus; each dilution is made in triplicate. Negative samples (cells not infected) were as well included in the assay. 16-18 h post-infection cells were fixed with 2% paraformaldehyde for 15 min at RT. Cells were then permeabilized two times with 0.1% TritonX, and blocked with 1% BSA for 30 min. Samples were then incubated with primary antibodies against reovirus μNS diluted in 1% bovine serum albumin in PBS at RT for 1 h. Coverslips were washed three times with PBS and incubated with the secondary antibody (IR dye 800

anti-mouse for reovirus μNS protein, and Draq5 to stain cells DNA) for 1 h at RT. Finally, coverslips were washed three times in PBS. Afterwards the plate was scanned using an Odyssey infrared imaging system and quantitative values from 700 nm and 800 nm excitation channels were exported.First, fluorescence values from the 700 nm channel (Draq5) were analyzed to confirm that cell density was the same throughout the 96 wells (data not shown). To normalize fluorescence values from the 800 nm excitation channel (reovirus μNS protein), first, fluorescence intensity in negative samples was measured; the average value + three times standard deviation was considered as the lowest threshold to determine virus infectivity (0%); the average intensity values from the highest dilution of cell infected with control virus (virus with no modifications) was considered as 100% infection.

To test Alexa647/Alkyne virus replication efficiency, BSC1 cells were seeded the day before the experiment into a 24 well plate to reach 80-90% of confluence the day of infection. The day after, cells were infected with same titer of control virus and Alexa647/Alkyne virus. 3-4 days after infection, cells were disrupted by repeated cycles of freezing and thawing. Samples are centrifuged (2500 rpm form 10-15 min) and the supernatant containing newly produced virus particles is used to infecte BSC1 cells previously seeded into a 96 well plate. To test the infectivity we performed an ICW assay from LI-COR technology as described above.

For indirect immunofluorescence assay, BSC1 cells were seeded the day before the experiment onto a 12 mm diameter glass coverslips (Marienfeld, Lauda-Königshofen, Germany) to reach 70-80 % of confluence the day of infection. Virus solutions were then added onto the cells; cells were incubated for 16-18 h and then fixed with 2% paraformaldehyde, 15 min at RT. To test Alexa647/ alkyne virus infectivity in the presence of copper, virus solutions were incubated 1 h at RT with 1 mM $CuSO_4$; afterwards the virus was purified by gel filtration (7K molecular weight cutoff, Invitrogen) and added to cell cultures. Fixed samples were washed three times in PBS and permeabilized with 0.05% Triton-X100 for 15 min at RT. Cells were blocked with 1% bovine serum albumin in PBS for 30 min at RT. Samples were then incubated with primary antibodies diluted in 1% bovine serum albumin in PBS at RT for 1 h. Coverslips were washed three times with PBS and incubated with the secondary antibody for 1 h at

RT. Finally, coverslips were washed three times in PBS, rinsed in water and mounted in ProLong Gold Antifade mounting medium supplemented with 4,6-diamidino-2-phenylindole. Slides were then imaged by epifluorescence using a Nikon Eclipse Ti-S (Nikon) microscope (20X and 40 magnification).

For JAM-A experiments, HeLa cells were seeded onto a 12 mm diameter glass coverslips one day before the experiment to reach 70-80 % of confluence the day of infection. Cells were then incubated 1 h at RT with 10 µg/ml JAM-A antibody solution in PBS; cells were then washed and incubated 30 min on ice with virus solutions in PBS. Finally, cells were washed again in PBS and incubated 16-18 h in normal growth medium before being fixed in 2% PFA. Indirect immunofluorescence assay was performed as described above.

4.2.10 Live-cell microscopy

To perform live-cell microscopy we used a spinning disc confocal microscope[22,23,50,68,190,218]. Cells were seeded on 24 mm diameter coverslips coated with clicked virus or beads and cRGDfK and live-cell microscopy was performed 6 h after seeding using cell media without phenol red. Live-cell imaging was performed with an inverted spinning-disk confocal microscope (PerkinElmer) using oil immersion objectives (60x, 1.42 numerical aperture, Apo TIRF, Nikon or 100x, 1.4 numerical aperture, Plan Apo VC, Nikon) and a CMOS camera (Hamamatsu Orca Flash 4). Cells, objectives and microscope stage were kept at 37°C and 5% CO2 through the presence of an environment-control chamber. Cells were imaged for 5 or 10 min with a frame interval of 3 sec/frame.

To perform 1-butanol treatment, U373-AP2 GFP cells were seeded on coverslips coated with clicked reovirus and live-cell microscopy was performed 6 hours after seeding. Before treatment cells were imaged for 10 min with a frame rate of 1 frame/3 secs. Afterwards imaging media was supplemented with 2% 1-butanol for 2-3 seconds; immediately after imaging media is removed by using a syringe and new imaging media is added. Live-cell microscopy is afterwards performed on the same cell for a further 10 minutes at the same frame rate.

To perform live-cell imaging of HeLa cells in the presence of JAM-A antibody, a suspension of HeLa cells was first incubated for 1 h with an anti-JAM-A antibody (final concentration 10 μg/ml); afterwards, cells were seeded onto a virus coated coverslip previously glued to the bottom of a multi-well chamber. In this way, control cells and cells treated with anti-JAM-A antibody were seeded onto the same virus coated coverslip and imaged in parallel. Cells were imaged 6 h after seeding; JAM-A antibody was added into the sample every 1.5 h (final concentration 10 μg/ml). After imaging, the same concentration of virus was added into cells treated with anti-JAM-A antibody and control cells; cells were incubated 30 min on ice with virus solutions in PBS. Finally, cells were washed again in PBS and incubated 16-18 h in normal growth medium before being immunostained for reovirus infectivity (protocol as described above).

4.2.11 SEM Sample preparation and imaging

Coverslips coated with clicked viruses were fixed in 2% paraformaldehyde in PBS for 15 min at RT; afterwards critical point drying of virus particles was performed using a CPD 030 Critical point dryer (Bal-Tec). Samples were finally sputter-coated with a titanium-gold layer using a Leica ACE600 machine. Coverslips presenting clicked beads were fixed in 2% paraformaldehyde for 15 min at RT; samples were directly sputter-coated with a carbon layer using a Leica EM ACE200. Samples were imaged with a ZEISS SEM Leo1530.

4.2.12 TEM sample preparation and imaging

TEM imaging was performed at the EM Core Facility at Heidelberg University in collaboration with Dr. Charlotta Funaja. Cells growing on coverslips coated with 100 and 300 nm beads, were fixed in 2.5% glutaraldehyde in 50 mM cacodylate buffer pH 7.2 supplied with 2% sucrose, 50 mM KCl, 2.6 mM $MgCl_2$, 2.6 mM $CaCl_2$, for 30 min at RT and at 4˚C overnight. Afterwards samples were further fixed in 1% osmium in cacodylate buffer, washed in water, and incubated in 0.5% uranylacetate in water for 30 min. Dehydration was performed in 10 min steps in an ethanol gradient followed by Spurr resin embedding and polymerization at 60˚C. The blocks were cut in 70 nm thin serial-sections using a Leica UC6 ultramicrotome (Leica Microsystems Vienna) and collected on pioloform coated slot grids. The post-stained sections were imaged on a JEOL JEM-

1400 electron microscope (JEOL, Tokyo) operating at 80 kV and equipped with a 4K TemCam F416 (Tietz Video and Image Processing Systems GmBH, Gautig).

4.2.13 STED sample preparation and imaging

STED microscopy was performed at the Leica Microsystems GmbH, Mannheim, in collaboration with Dr. Zhongxiang Jiang. U373 AP2-GFP cells were seeded on coverslips containing 100 or 300 nm clicked-beads (labeled with Atto647N). Cells were fixed 6 h post seeding and mounted using a ProLong Gold Antifade mounting medium (Molecular Probes). STED imaging was performed using the Leica TCS SP8 STED 3X system (Leica Microsystems GmbH, Mannheim, Germany) with a 100x, 1.4 numerical aperture STED White objective. Gated STED signal of AP2-GFP was generated with 488 nm excitation from a white light laser (WLL) and 592 nm depletion. Atto647N was excited with 633 nm from the WLL and depleted with 775 nm pulsed laser.

4.2.14 Image analysis and quantification

In order to count the number of virus particles on modified/un-modified glass surfaces and to measure virus fluorescence distribution, the pixel classification and object classification workflow in Ilastik (http://ilastik.org) was used. To measure fluorescence intensity distribution of Alexa647 virus deposited on glass, a total of 12,306 Alexa647 viruses were counted and mean intensity were measured. To measure fluorescence intensity distribution of Alexa647/Alkyne-virus clicked or deposited on glass, a total of 62,204 Alexa647/Alkyne-virus deposited on glass and 12,965 Alexa647/Alkyne-virus clicked on azide coated coverslips were counted and the mean intensities were measured. Fluorescence intensity values were normalized to the average intensity from each group and plotted in bins of 0.5 relative fluorescence units; the percentage of total particles falling within each bin is shown on the y-axis. The same procedure was adopted to measure fluorescence intensity distribution of Alexa647-virus and Alexa647/Alkyne-virus deposited on glass. A total of 11,001 Alexa647-virus and 35,027 Alexa647/Alkyne-virus deposited on glass were counted and mean intensities were measured; data are normalized and plotted as described above.

In order to measure the size of virus particles and polystyrene beads from the images obtained with SEM, the pixel classification and object classification workflow in Ilastik (http://ilastik.org) was used. A total of 655 of non-modified virus particles and 629 Alexa647/Alkyne-virus particles were counted.

CME events were tracked using Fiji (https://fiji.sc/). For the analysis of AP2-GFP signal and/or FCHO1-mcherry, Epsin-mcherry and Amphiphysin-mcherry on virus/beads spots, spots of interest were manually listed into a ROI manager and fluorescence intensity over time was automatically measured. To track GFP/mcherry protein signal over time from empty pits (pits not co-localizing with virus/beads spots) the TrackMate plugin from Fiji was used. Data were normalized to the average highest fluorescence intensity of empty pits in each cell. After normalization, quantification analysis was performed. I extracted for each virus/beads track, the value with highest fluorescence intensity (MAX-fluo) and the value with the lowest intensity (MIN-fluo). The abovementioned measurements were calculated for every experiment for three cells per condition (virus, 100 and 300 nm beads).The correlation analysis between the AP2-GFP signal and the corresponding FCHO1-mcherry, Epsin-mcherry or Amphiphysin-mcherry signal coming from the same bead spot, was performed by automatically measuring the correlation coefficient between each GFP and mcherry track, as previously described[193].

4.2.15 Fitting of Gaussian profiles into fluorescence signals

The normalized AP2-GFP fluorescence signal from virus/beads spots, empty pits and random spots served as input to the interactive peak fitter (IPF version 8.4) program in Matlab (MathWorks, USA) under command line mode (peakfit.m)[219] (https://terpconnect.umd.edu/~toh/spectrum/InteractivePeakFitter.htm). Random spots were collected by unsupervised selection of pixels within each cell imaged with live-cell microscopy. The number of empty pits and random spots was set to be approximately three times higher than the virus/beads spots for further analysis. Because each fluorescence signal from virus/bead spots was composed to up to 12 maxima within the time window of acquisition, 1-13 Gaussian functions were fitted to each track. Gaussian functions with fixed width significantly outperformed other functions (e.g. Lorenzian; Gaussian with variable width) in fitting as reported by goodness-of-fit measures (r^2,

percentage error of fit of the fitted curve composed of Gaussian functions) (data not shown). Therefore, the fluorescence signal was de-convolved with Gaussian models of fixed width. The exact number of Gaussian functions explaining each profile was chosen based on goodness-of-fit measures (Figure 27 B and C). To avoid overfitting of the Gaussian functions, visual inspection of the fits was performed to finally select the number of Gaussians (number of events). Because Gaussian profiles fitted also to the background signal, a cut-off (average of MIN-fluo of virus/beads per cell + standard deviation) of fluorescence intensity was chosen to remove those events. Then, I defined three measures for modeling the fluorescence signal: (a) Number of recruitment events of Clathrin machinery that is described by counting the number of Gaussian profiles fitted per virus/bead track and statistically compared to empty and random spots. (b) Rate of peak occurrence (time between two cycles of AP2 GFP recruitment) that is described by the time window in sec between two concurrent maxima of Gaussian functions fitted to the fluorescence signal. (c) Lifetime of pits (time of a complete cycle of AP2 GFP recruitment) that is described by the fixed width of the Gaussian functions fitted per track. The abovementioned measures were calculated per track and their distributions are then plotted in a comparative manner.

5 References

1. Doherty, G. J. & McMahon, H. T. Mechanisms of Endocytosis. *Annu. Rev. Biochem.* **78,** 857–902 (2009).
2. A., F. S. & Sergio, G. Phagocytosis: receptors, signal integration, and the cytoskeleton. *Immunol. Rev.* **262,** 193–215 (2014).
3. Gordon, S. Phagocytosis: An Immunobiologic Process. *Immunity* **44,** 463–475 (2016).
4. Mercer, J. & Helenius, A. Gulping rather than sipping: macropinocytosis as a way of virus entry. *Curr. Opin. Microbiol.* **15,** 490–499 (2012).
5. Marques, P. E., Grinstein, S. & Freeman, S. A. SnapShot:Macropinocytosis. *Cell* **169,** 766–766.e1 (2017).
6. McMahon, H. T. & Boucrot, E. Molecular mechanism and physiological functions of clathrin-mediated endocytosis. *Nat. Rev. Mol. Cell Biol.* **12,** 517 (2011).
7. Kaksonen, M. & Roux, A. Mechanisms of clathrin-mediated endocytosis. *Nat. Rev. Mol. Cell Biol.* **19,** 313 (2018).
8. Parton, R. G. & del Pozo, M. A. Caveolae as plasma membrane sensors, protectors and organizers. *Nat. Rev. Mol. Cell Biol.* **14,** 98 (2013).
9. Cheng, J. P. X. & Nichols, B. J. Caveolae: One Function or Many? *Trends Cell Biol.* **26,** 177–189 (2016).
10. Sandvig, K., Kavaliauskiene, S. & Skotland, T. Clathrin-independent endocytosis: an increasing degree of complexity. *Histochem. Cell Biol.* **0,** 1–12 (2018).
11. Wideman, J. G., Leung, K. F., Field, M. C. & Dacks, J. B. The Cell Biology of the Endocytic System from an Evolutionary Perspective. *Cold Spring Harb. Perspect. Biol.* **6,** a016998 (2014).
12. Roth, T. & Porter, K. Yolk Protein Uptake in the Oocyte of the Mosquito Aedes Aegypti. L. *J. Cell Biol.* **20,** 313–332 (1964).
13. Kanaseki, T. & Kadota, K. The 'vesicle in a basket'. A morphological study of the coated vesicle isolated from the nerve endings of the guinea pig brain, with special reference to the mechanism of membrane movements. *J. Cell Biol.* **42,** 202–220 (1969).

14. Pearse, B. M. F. Coated vesicles from pig brain: Purification and biochemical characterization. *J. Mol. Biol.* **97,** 93–98 (1975).
15. Heuser, J. Three-dimensional visualization of coated vesicle formation in fibroblasts . *J. Cell Biol.* **84,** 560–583 (1980).
16. Ungewickell, E. & Branton, D. Assembly units of clathrin coats. *Nature* **289,** 420–422 (1981).
17. Kirchhausen, T. & Harrison, S. C. Protein organization in clathrin trimers. *Cell* **23,** 755–761 (1981).
18. Fotin, A. *et al.* Molecular model for a complete clathrin lattice from electron cryomicroscopy. *Nature* **432,** 573–579 (2004).
19. Kirchhausen, T. Imaging endocytic clathrin structures in living cells. *Trends Cell Biol.* **19,** 596–605 (2009).
20. Kirchhausen, T., Owen, D. & Harrison, S. C. Molecular structure, function, and dynamics of clathrin-mediated membrane traffic. *Cold Spring Harb. Perspect. Biol.* **6,** a016725 (2014).
21. Avinoam, O., Schorb, M., Beese, C. J., Briggs, J. A. G. & Kaksonen, M. Endocytic sites mature by continuous bending and remodeling of the clathrin coat. *Science* **348,** 1369–72 (2015).
22. Ehrlich, M. *et al.* Endocytosis by random initiation and stabilization of clathrin-coated pits. *Cell* **118,** 591–605 (2004).
23. Cureton, D. K., Massol, R. H., Saffarian, S., Kirchhausen, T. L. & Whelan, S. P. J. Vesicular Stomatitis Virus Enters Cells through Vesicles Incompletely Coated with Clathrin That Depend upon Actin for Internalization. *PLoS Pathog.* **5,** (2009).
24. Huang, F., Khvorova, A., Marshall, W. & Sorkin, A. Analysis of clathrin-mediated endocytosis of epidermal growth factor receptor by RNA interference. *J. Biol. Chem.* **279,** 16657–16661 (2004).
25. Poupon, V. *et al.* Clathrin light chains function in mannose phosphate receptor trafficking via regulation of actin assembly. *Proc. Natl. Acad. Sci. U. S. A.* **105,** 168–173 (2008).
26. Lu, R., Drubin, D. G. & Sun, Y. Clathrin-mediated endocytosis in budding yeast at a glance. *J. Cell Sci.* **129,** 1531–1536 (2016).

27. Robinson, M. S. 100-kD coated vesicle proteins: molecular heterogeneity and intracellular distribution studied with monoclonal antibodies. *J. Cell Biol.* **104,** 887–895 (1987).

28. Collins, B. M., McCoy, A. J., Kent, H. M., Evans, P. R. & Owen, D. J. Molecular architecture and functional model of the endocytic AP2 complex. *Cell* **109,** 523–535 (2002).

29. Gaidarov, I. & Keen, J. H. Phosphoinositide-AP-2 interactions required for targeting to plasma membrane clathrin-coated pits. *J. Cell Biol.* **146,** 755–764 (1999).

30. Honing, S. *et al.* Phosphatidylinositol-(4,5)-bisphosphate regulates sorting signal recognition by the clathrin-associated adaptor complex AP2. *Mol. Cell* **18,** 519–531 (2005).

31. Ohno, H., Fournier, M. C., Poy, G. & Bonifacino, J. S. Structural determinants of interaction of tyrosine-based sorting signals with the adaptor medium chains. *J. Biol. Chem.* **271,** 29009–29015 (1996).

32. Owen, D. J. & Evans, P. R. A structural explanation for the recognition of tyrosine-based endocytotic signals. *Science* **282,** 1327–1332 (1998).

33. Kelly, B. T. *et al.* A structural explanation for the binding of endocytic dileucine motifs by the AP2 complex. *Nature* **456,** 976–979 (2008).

34. Mattera, R., Boehm, M., Chaudhuri, R., Prabhu, Y. & Bonifacino, J. S. Conservation and diversification of dileucine signal recognition by adaptor protein (AP) complex variants. *J. Biol. Chem.* **286,** 2022–2030 (2011).

35. Ferguson, S. M. & De Camilli, P. Dynamin, a membrane-remodelling GTPase. *Nat. Rev. Mol. Cell Biol.* **13,** 75–88 (2012).

36. Maldonado-Baez, L. & Wendland, B. Endocytic adaptors: recruiters, coordinators and regulators. *Trends Cell Biol.* **16,** 505–513 (2006).

37. Jackson, L. P. *et al.* A large-scale conformational change couples membrane recruitment to cargo binding in the AP2 clathrin adaptor complex. *Cell* **141,** 1220–1229 (2010).

38. Gaidarov, I., Santini, F., Warren, R. A. & Keen, J. H. Spatial control of coated-pit dynamics in living cells. *Nat Cell Biol* **1,** 1–7 (1999).

39. Shih, W., Gallusser, A. & Kirchhausen, T. A clathrin-binding site in the hinge of the beta 2 chain of mammalian AP-2 complexes. *J. Biol. Chem.* **270,** 31083–31090 (1995).

40. Traub, L. M., Downs, M. A., Westrich, J. L. & Fremont, D. H. Crystal structure of the alpha appendage of AP-2 reveals a recruitment platform for clathrin-coat assembly. *Proc. Natl. Acad. Sci. U. S. A.* **96,** 8907–8912 (1999).

41. Roos, J. & Kelly, R. B. Dap160, a neural-specific Eps15 homology and multiple SH3 domain-containing protein that interacts with Drosophila dynamin. *J. Biol. Chem.* **273,** 19108–19119 (1998).

42. Schledzewski, K., Brinkmann, H. & Mendel, R. R. Phylogenetic analysis of components of the eukaryotic vesicle transport system reveals a common origin of adaptor protein complexes 1, 2, and 3 and the F subcomplex of the coatomer COPI. *J. Mol. Evol.* **48,** 770–778 (1999).

43. Motley, A., Bright, N. A., Seaman, M. N. J. & Robinson, M. S. Clathrin-mediated endocytosis in AP-2-depleted cells. *J. Cell Biol.* **162,** 909–918 (2003).

44. Conner, S. D. & Schmid, S. L. Differential requirements for AP-2 in clathrin-mediated endocytosis. *J. Cell Biol.* **162,** 773–779 (2003).

45. Henne, W. M. *et al.* FCHo proteins are nucleators of clathrin-mediated endocytosis. *Science* **328,** 1281–1284 (2010).

46. Henne, W. M. *et al.* Article Structure and Analysis of FCHo2 F-BAR Domain : A Dimerizing and Membrane Recruitment Module that Effects Membrane Curvature. 1–14 (2007). doi:10.1016/j.str.2007.05.002

47. Cocucci, E., Aguet, F., Boulant, S. & Kirchhausen, T. The first five seconds in the life of a clathrin-coated pit. *Cell* **150,** 495–507 (2012).

48. Kadlecova, Z. *et al.* Regulation of clathrin-mediated endocytosis by hierarchical allosteric activation of AP2. *J. Cell Biol.* **216,** 167 LP-179 (2017).

49. Ma, L. *et al.* Transient Fcho1/2Eps15/RAP-2 Nanoclusters Prime the AP-2 Clathrin Adaptor for Cargo Binding. *Dev. Cell* **37,** 428–443 (2016).

50. Boucrot, E., Saffarian, S., Zhang, R. & Kirchhausen, T. Roles of AP-2 in clathrin-mediated endocytosis. *PLoS One* **5,** e10597 (2010).

51. Loerke, D. *et al.* Cargo and Dynamin Regulate Clathrin-Coated Pit Maturation. **7,**

(2009).

52. Liu, A. P., Aguet, F., Danuser, G. & Schmid, S. L. Local clustering of transferrin receptors promotes clathrin-coated pit initiation. *J. Cell Biol.* **191,** 1381–1393 (2010).
53. Hopkins, C. R., Miller, K. & Beardmore, J. M. Receptor-mediated endocytosis of transferrin and epidermal growth factor receptors: a comparison of constitutive and ligand-induced uptake. *J. Cell Sci. Suppl.* **3,** 173–186 (1985).
54. Posor, Y., Eichhorn-Grünig, M. & Haucke, V. Phosphoinositides in endocytosis. *Biochim. Biophys. Acta - Mol. Cell Biol. Lipids* **1851,** 794–804 (2015).
55. Boucrot, E., Saffarian, S., Massol, R., Kirchhausen, T. & Ehrlich, M. Role of lipids and actin in the formation of clathrin-coated pits. *Exp. Cell Res.* **312,** 4036–4048 (2006).
56. Godlee, C. & Kaksonen, M. From uncertain beginnings: Initiation mechanisms of clathrin-mediated endocytosis. *J. Cell Biol.* **203,** 717–725 (2013).
57. Varnai, P., Thyagarajan, B., Rohacs, T. & Balla, T. Rapidly inducible changes in phosphatidylinositol 4,5-bisphosphate levels influence multiple regulatory functions of the lipid in intact living cells. *J. Cell Biol.* **175,** 377–382 (2006).
58. Heo, W. Do *et al.* PI(3,4,5)P3 and PI(4,5)P2 lipids target proteins with polybasic clusters to the plasma membrane. *Science* **314,** 1458–1461 (2006).
59. Schifferer, M., Feng, S., Stein, F., Tischer, C. & Schultz, C. Reversible chemical dimerizer-induced recovery of PIP2 levels moves clathrin to the plasma membrane. *Bioorg. Med. Chem.* **23,** 2862–2867 (2015).
60. Taylor, M. J., Perrais, D. & Merrifield, C. J. A high precision survey of the molecular dynamics of mammalian clathrin-mediated endocytosis. *PLoS Biol.* **9,** (2011).
61. Merrifield, C. J., Perrais, D. & Zenisek, D. Coupling between clathrin-coated-pit invagination, cortactin recruitment, and membrane scission observed in live cells. *Cell* **121,** 593–606 (2005).
62. Messa, M. *et al.* Epsin deficiency impairs endocytosis by stalling the actin-dependent invagination of endocytic clathrin-coated pits. *Elife* **3,** e03311 (2014).
63. Ford, M. G. J. *et al.* Curvature of clathrin-coated pits driven by epsin. *Nature* **419,**

361–366 (2002).

64. Peter, B. J. *et al.* BAR domains as sensors of membrane curvature: the amphiphysin BAR structure. *Science* **303,** 495–499 (2004).
65. Franquelim, H. G., Khmelinskaia, A., Sobczak, J.-P., Dietz, H. & Schwille, P. Membrane sculpting by curved DNA origami scaffolds. *Nat. Commun.* **9,** 811 (2018).
66. Farsad, K. *et al.* Generation of high curvature membranes mediated by direct endophilin bilayer interactions. *J. Cell Biol.* **155,** 193–200 (2001).
67. Farsad, K. & De Camilli, P. Mechanisms of membrane deformation. *Curr. Opin. Cell Biol.* **15,** 372–381 (2003).
68. Cureton, D. K., Massol, R. H., Whelan, S. P. J. & Kirchhausen, T. The length of vesicular stomatitis virus particles dictates a need for actin assembly during clathrin-dependent endocytosis. *PLoS Pathog.* **6,** e1001127 (2010).
69. Boulant, S., Kural, C., Zeeh, J.-C., Ubelmann, F. & Kirchhausen, T. Actin dynamics counteract membrane tension during clathrin-mediated endocytosis. *Nat. Cell Biol.* **13,** 1124–1131 (2011).
70. Daste, F. *et al.* Control of actin polymerization via the coincidence of phosphoinositides and high membrane curvature. *J. Cell Biol.* **216,** 3745–3765 (2017).
71. Wakeham, D. E., Chen, C. Y., Greene, B., Hwang, P. K. & Brodsky, F. M. Clathrin self-assembly involves coordinated weak interactions favorable for cellular regulation. *EMBO J.* **22,** 4980–4990 (2003).
72. Legendre-Guillemin, V. *et al.* Huntingtin interacting protein 1 (HIP1) regulates clathrin assembly through direct binding to the regulatory region of the clathrin light chain. *J. Biol. Chem.* **280,** 6101–6108 (2005).
73. Itoh, T., Koshiba, S., Kigawa, T. & Kikuchi, A. Role of the ENTH Domain in Phosphatidylinositol- 4 , 5-Bisphosphate Binding and Endocytosis. **291,** 1047–1052 (2001).
74. Schuske, K. R. *et al.* Endophilin is required for synaptic vesicle endocytosis by localizing synaptojanin. *Neuron* **40,** 749–762 (2003).
75. Verstreken, P. *et al.* Synaptojanin is recruited by endophilin to promote synaptic

vesicle uncoating. *Neuron* **40,** 733–748 (2003).

76. Perera, R. M., Zoncu, R., Lucast, L., De Camilli, P. & Toomre, D. Two synaptojanin 1 isoforms are recruited to clathrin-coated pits at different stages. *Proc. Natl. Acad. Sci. U. S. A.* **103,** 19332–19337 (2006).
77. Posor, Y. *et al.* Spatiotemporal control of endocytosis by phosphatidylinositol-3,4-bisphosphate. *Nature* **499,** 233–7 (2013).
78. Schoneberg, J. *et al.* Lipid-mediated PX-BAR domain recruitment couples local membrane constriction to endocytic vesicle fission. *Nat. Commun.* **8,** 15873 (2017).
79. Shpetner, H. S. & Vallee, R. B. Identification of dynamin, a novel mechanochemical enzyme that mediates interactions between microtubules. *Cell* **59,** 421–432 (1989).
80. Zhang, P. & Hinshaw, J. E. Three-dimensional reconstruction of dynamin in the constricted state. *Nat. Cell Biol.* **3,** 922–926 (2001).
81. Chen, C. D. *et al.* Molecular determinants of resistance to antiandrogen therapy. *Nat. Med.* **10,** 33–39 (2004).
82. Mears, J. A., Ray, P. & Hinshaw, J. E. A corkscrew model for dynamin constriction. *Structure* **15,** 1190–1202 (2007).
83. Antonny, B. *et al.* Membrane fission by dynamin : what we know and what we need to know. **35,** 2270–2284 (2016).
84. Kozlovsky, Y. & Kozlov, M. M. Membrane Fission: Model for Intermediate Structures. *Biophys. J.* **85,** 85–96 (2003).
85. Boucrot, E. *et al.* Membrane fission is promoted by insertion of amphipathic helices and is restricted by crescent BAR domains. *Cell* **149,** 124–136 (2012).
86. Sousa, R. & Lafer, E. M. The role of molecular chaperones in clathrin mediated vesicular trafficking. *Front. Mol. Biosci.* **2,** 26 (2015).
87. Zoncu, R. *et al.* A phosphoinositide switch controls the maturation and signaling properties of APPL endosomes. *Cell* **136,** 1110–1121 (2009).
88. Cremona, O. *et al.* Essential role of phosphoinositide metabolism in synaptic vesicle recycling. *Cell* **99,** 179–188 (1999).
89. Erdmann, K. S. *et al.* A role of the Lowe syndrome protein OCRL in early steps of

the endocytic pathway. *Dev. Cell* **13,** 377–390 (2007).

90. Keyel, P. A., Watkins, S. C. & Traub, L. M. Endocytic adaptor molecules reveal an endosomal population of clathrin by total internal reflection fluorescence microscopy. *J. Biol. Chem.* **279,** 13190–13204 (2004).
91. Saffarian, S., Cocucci, E. & Kirchhausen, T. Distinct dynamics of endocytic clathrin-coated pits and coated plaques. *PLoS Biol.* **7,** e1000191 (2009).
92. Nunez, D. *et al.* Hotspots Organize Clathrin-Mediated Endocytosis by Efficient Recruitment and Retention of Nucleating Resources. *Traffic* **12,** 1868–1878 (2011).
93. McMahon, H. T. & Gallop, J. L. Membrane curvature and mechanisms of dynamic cell membrane remodelling. *Nature* **438,** 590–596 (2005).
94. Kirchhausen, T. Bending membranes. *Nat. Cell Biol.* **14,** 906–908 (2012).
95. McMahon, H. T. & Boucrot, E. Membrane curvature at a glance. *J. Cell Sci.* **128,** 1065–1070 (2015).
96. Suetsugu, S., Kurisu, S. & Takenawa, T. Dynamic shaping of cellular membranes by phospholipids and membrane-deforming proteins. 1219–1248 (2014). doi:10.1152/physrev.00040.2013
97. Takei, K., Slepnev, V. I., Haucke, V. & Camilli, P. De. Functional partnership between amphiphysin and dynamin in clathrin- mediated endocytosis. **180,** 33–39 (1999).
98. Faini, M., Beck, R., Wieland, F. T. & Briggs, J. A. G. Vesicle coats: structure, function, and general principles of assembly. *Trends Cell Biol.* **23,** 279–288 (2013).
99. Dannhauser, P. N. & Ungewickell, E. J. Reconstitution of clathrin-coated bud and vesicle formation with minimal components. *Nat. Cell Biol.* **14,** 634–639f (2012).
100. Shimada, A. *et al.* Curved EFC/F-BAR-domain dimers are joined end to end into a filament for membrane invagination in endocytosis. *Cell* **129,** 761–772 (2007).
101. Frost, A. *et al.* Structural basis of membrane invagination by F-BAR domains. *Cell* **132,** 807–817 (2008).
102. David, C., Solimena, M. & De Camilli, P. Autoimmunity in stiff-Man syndrome with breast cancer is targeted to the C-terminal region of human amphiphysin, a

protein similar to the yeast proteins, Rvs167 and Rvs161. *FEBS Lett.* **351,** 73–79 (1994).

103. Bauer, F., Urdaci, M., Aigle, M. & Crouzet, M. Alteration of a yeast SH3 protein leads to conditional viability with defects in cytoskeletal and budding patterns. *Mol. Cell. Biol.* **13,** 5070–5084 (1993).
104. Takei, K. Generation of coated intermediates of clathrin-mediated endocytosis on protein-free liposomes. *Cell* **94,** 131–141 (1998).
105. Mim, C. *et al.* Structural basis of membrane bending by the N-BAR protein endophilin. *Cell* **149,** 137–145 (2012).
106. Voeltz, G. K., Prinz, W. A., Shibata, Y., Rist, J. M. & Rapoport, T. A. A class of membrane proteins shaping the tubular endoplasmic reticulum. *Cell* **124,** 573–586 (2006).
107. Simunovic, M., Voth, G. A., Callan-Jones, A. & Bassereau, P. When Physics Takes Over: BAR Proteins and Membrane Curvature. *Trends Cell Biol.* **25,** 780–792 (2015).
108. Meinecke, M. *et al.* Cooperative recruitment of dynamin and BIN/amphiphysin/Rvs (BAR) domain-containing proteins leads to GTP-dependent membrane scission. *J. Biol. Chem.* **288,** 6651–6661 (2013).
109. Chen, H. *et al.* Epsin is an EH-domain-binding protein implicated in clathrin-mediated endocytosis. *Nature* **394,** 793–797 (1998).
110. Wendland, B., Steece, K. E. & Emr, S. D. Yeast epsins contain an essential N-terminal ENTH domain, bind clathrin and are required for endocytosis. *EMBO J.* **18,** 4383–4393 (1999).
111. Kay, B. K., Yamabhai, M., Wendland, B. & Emr, S. D. Identification of a novel domain shared by putative components of the endocytic and cytoskeletal machinery. *Protein Sci.* **8,** 435–438 (1999).
112. Itoh, T. & Camilli, P. De. BAR , F-BAR (EFC) and ENTH / ANTH domains in the regulation of membrane – cytosol interfaces and membrane curvature. **1761,** 897–912 (2006).
113. Kirchhausen, T. Coated pits and coated vesicles - sorting it all out. *Curr. Opin. Struct. Biol.* **3,** 182–188 (1993).

114. Nossal, R. Energetics of clathrin basket assembly. *Traffic* **2,** 138–147 (2001).
115. Ferguson, M. L. *et al.* Clathrin triskelia show evidence of molecular flexibility. *Biophys. J.* **95,** 1945–1955 (2008).
116. Bucher, D. *et al.* Clathrin-adaptor ratio and membrane tension regulate the flat-to-curved transition of the clathrin coat during endocytosis. *Nat. Commun.* **9,** 1109 (2018).
117. Scott, B. L. *et al.* Membrane bending occurs at all stages of clathrincoat assembly and defines endocytic dynamics. *Nat. Commun.* **9,** (2018).
118. Anantharam, A., Axelrod, D. & Holz, R. W. Polarized TIRFM reveals changes in plasma membrane topology before and during granule fusion. *Cell. Mol. Neurobiol.* **30,** 1343–1349 (2010).
119. Galic, M., Begemann, I., Viplav, A. & Matis, M. Force-control at cellular membranes. *Bioarchitecture* **4,** 164–168 (2014).
120. Galic, M. *et al.* External push and internal pull forces recruit curvature-sensing N-BAR domain proteins to the plasma membrane. *Nat. Cell Biol.* **14,** 874–881 (2012).
121. Zhao, W. *et al.* Nanoscale manipulation of membrane curvature for probing endocytosis in live cells. *Nat. Nanotechnol.* **94720,** 1–18 (2017).
122. Elkhatib, N. *et al.* Tubular clathrin/AP-2 lattices pinch collagen fibers to support 3D cell migration. *Science* **356,** (2017).
123. Yamauchi, Y. & Helenius, A. Virus entry at a glance. *J. Cell Sci.* **126,** 1289–1295 (2013).
124. Schneider-Schaulies, J. Cellular receptors for viruses: links to tropism and pathogenesis. *J. Gen. Virol.* **81,** 1413–1429 (2000).
125. Bergelson, J. M. *et al.* Isolation of a common receptor for Coxsackie B viruses and adenoviruses 2 and 5. *Science* **275,** 1320–1323 (1997).
126. Tomko, R. P., Xu, R. & Philipson, L. HCAR and MCAR: the human and mouse cellular receptors for subgroup C adenoviruses and group B coxsackieviruses. *Proc. Natl. Acad. Sci. U. S. A.* **94,** 3352–3356 (1997).
127. Staunton, D. E. *et al.* A cell adhesion molecule, ICAM-1, is the major surface receptor for rhinoviruses. *Cell* **56,** 849–853 (1989).

128. Hofer, F. *et al.* Members of the low density lipoprotein receptor family mediate cell entry of a minor-group common cold virus. *Proc. Natl. Acad. Sci. U. S. A.* **91,** 1839–1842 (1994).

129. Bochkov, Y. A. *et al.* Cadherin-related family member 3, a childhood asthma susceptibility gene product, mediates rhinovirus C binding and replication. *Proc. Natl. Acad. Sci. U. S. A.* **112,** 5485–5490 (2015).

130. Boulant, S., Stanifer, M. & Lozach, P.-Y. Dynamics of virus-receptor interactions in virus binding, signaling, and endocytosis. *Viruses* **7,** 2794–815 (2015).

131. Mercer, J., Schelhaas, M. & Helenius, A. Virus Entry by Endocytosis. *Annu. Rev. Biochem.* **79,** 803–833 (2010).

132. Rust, M. J., Lakadamyali, M., Zhang, F. & Zhuang, X. Assembly of endocytic machinery around individual influenza viruses during viral entry. *Nat. Struct. Mol. Biol.* **11,** 567–573 (2004).

133. Skehel, J. J. & Wiley, D. C. Receptor binding and membrane fusion in virus entry: the influenza hemagglutinin. *Annu. Rev. Biochem.* **69,** 531–569 (2000).

134. Cureton, D. K., Harbison, C. E., Cocucci, E., Parrish, C. R. & Kirchhausen, T. Limited Transferrin Receptor Clustering Allows Rapid Diffusion of Canine Parvovirus into Clathrin Endocytic Structures. *J. Virol.* **86,** 5330–5340 (2012).

135. SABIN, A. B. Reoviruses. A new group of respiratory and enteric viruses formerly classified as ECHO type 10 is described. *Science* **130,** 1387–1389 (1959).

136. Mann, M. A., Knipe, D. M., Fischbach, G. D. & Fields, B. N. Type 3 reovirus neuroinvasion after intramuscular inoculation: direct invasion of nerve terminals and age-dependent pathogenesis. *Virology* **303,** 222–231 (2002).

137. Tardieu, M., Powers, M. L. & Weiner, H. L. Age dependent susceptibility to Reovirus type 3 encephalitis: role of viral and host factors. *Ann. Neurol.* **13,** 602–607 (1983).

138. Tyler, K. L. *et al.* Isolation and molecular characterization of a novel type 3 reovirus from a child with meningitis. *J. Infect. Dis.* **189,** 1664–1675 (2004).

139. Metcalf, P. The symmetry of the reovirus outer shell. *J. Ultrastruct. Res.* **78,** 292–301 (1982).

140. Dryden, K. A. *et al.* Early steps in reovirus infection are associated with dramatic

changes in supramolecular structure and protein conformation: analysis of virions and subviral particles by cryoelectron microscopy and image reconstruction. *J. Cell Biol.* **122,** 1023–1041 (1993).

141. Liemann, S., Chandran, K., Baker, T. S., Nibert, M. L. & Harrison, S. C. Structure of the reovirus membrane-penetration protein, Mu1, in a complex with is protector protein, Sigma3. *Cell* **108,** 283–295 (2002).
142. Chappell, J. D., Prota, A. E., Dermody, T. S. & Stehle, T. Crystal structure of reovirus attachment protein σ1 reveals evolutionary relationship to adenovirus fiber. *EMBO J.* **21,** 1–11 (2002).
143. Fraser, R. D. *et al.* Molecular structure of the cell-attachment protein of reovirus: correlation of computer-processed electron micrographs with sequence-based predictions. *J. Virol.* **64,** 2990–3000 (1990).
144. Furlong, D. B., Nibert, M. L. & Fields, B. N. Sigma 1 protein of mammalian reoviruses extends from the surfaces of viral particles. *J. Virol.* **62,** 246–256 (1988).
145. Strong, J. E., Leone, G., Duncan, R., Sharma, R. K. & Lee, P. W. Biochemical and biophysical characterization of the reovirus cell attachment protein sigma 1: evidence that it is a homotrimer. *Virology* **184,** 23–32 (1991).
146. Barton, E. S. *et al.* Junction adhesion molecule is a receptor for reovirus. *Cell* **104,** 441–451 (2001).
147. Barton, E. S. *et al.* Utilization of sialic acid as a coreceptor is required for reovirus-induced biliary disease. *J. Clin. Invest.* **111,** 1823–1833 (2003).
148. Maginnis, M. S. *et al.* Beta1 integrin mediates internalization of mammalian reovirus. *J. Virol.* **80,** 2760–2770 (2006).
149. Barton, E. S., Connolly, J. L., Forrest, J. C., Chappell, J. D. & Dermody, T. S. Utilization of sialic acid as a coreceptor enhances reovirus attachment by multistep adhesion strengthening. *J. Biol. Chem.* **276,** 2200–2211 (2001).
150. Bass, D. M. *et al.* Intraluminal proteolytic activation plays an important role in replication of type 1 reovirus in the intestines of neonatal mice. *J. Virol.* **64,** 1830–1833 (1990).
151. Bodkin, D. K., Nibert, M. L. & Fields, B. N. Proteolytic digestion of reovirus in

the intestinal lumens of neonatal mice. *J. Virol.* **63,** 4676–4681 (1989).

152. Ivanovic, T. *et al.* Peptides released from reovirus outer capsid form membrane pores that recruit virus particles. *EMBO J.* **27,** 1289–1298 (2008).
153. Zhang, L., Chandran, K., Nibert, M. L. & Harrison, S. C. Reovirus mu1 structural rearrangements that mediate membrane penetration. *J. Virol.* **80,** 12367–12376 (2006).
154. Danthi, P. *et al.* in (ed. Johnson, J. E.) 91–119 (Springer Berlin Heidelberg, 2010). doi:10.1007/82_2010_32
155. Schelling, P. *et al.* The reovirus sigma1 aspartic acid sandwich: a trimerization motif poised for conformational change. *J. Biol. Chem.* **282,** 11582–11589 (2007).
156. Liu, Y. *et al.* Human junction adhesion molecule regulates tight junction resealing in epithelia. *J. Cell Sci.* **113 (Pt 1,** 2363–2374 (2000).
157. Martin-Padura, I. *et al.* Junctional adhesion molecule, a novel member of the immunoglobulin superfamily that distributes at intercellular junctions and modulates monocyte transmigration. *J. Cell Biol.* **142,** 117–127 (1998).
158. Campbell, J. A. *et al.* Junctional adhesion molecule a serves as a receptor for prototype and field-isolate strains of mammalian reovirus. *J. Virol.* **79,** 7967–7978 (2005).
159. Prota, A. E. *et al.* Crystal structure of human junctional adhesion molecule 1: implications for reovirus binding. *Proc. Natl. Acad. Sci. U. S. A.* **100,** 5366–5371 (2003).
160. Antar, A. A. R. *et al.* Junctional adhesion molecule-A is required for hematogenous dissemination of reovirus. *Cell Host Microbe* **5,** 59–71 (2009).
161. Gentsch, J. R. & Pacitti, A. F. Effect of neuraminidase treatment of cells and effect of soluble glycoproteins on type 3 reovirus attachment to murine L cells. *J. Virol.* **56,** 356–364 (1985).
162. Paul, R. W., Choi, A. H. & Lee, P. W. The alpha-anomeric form of sialic acid is the minimal receptor determinant recognized by reovirus. *Virology* **172,** 382–385 (1989).
163. Reinisch, K. M., Nibert, M. L. & Harrison, S. C. Structure of the reovirus core at 3.6 A resolution. *Nature* **404,** 960–967 (2000).

164. Ruoslahti, E. RGD AND OTHER RECOGNITION SEQUENCES FOR INTEGRINS. *Annu. Rev. Cell Dev. Biol.* **12,** 697–715 (1996).

165. Boulant, S. *et al.* Similar uptake but different trafficking and escape routes of reovirus virions and infectious subvirion particles imaged in polarized Madin-Darby canine kidney cells. *Mol. Biol. Cell* **24,** 1196–1207 (2013).

166. Laniosz, V., Holthusen, K. A. & Meneses, P. I. Bovine papillomavirus type 1: from clathrin to caveolin. *J. Virol.* **82,** 6288–6298 (2008).

167. Querbes, W., O'Hara, B. A., Williams, G. & Atwood, W. J. Invasion of host cells by JC virus identifies a novel role for caveolae in endosomal sorting of noncaveolar ligands. *J. Virol.* **80,** 9402–9413 (2006).

168. Panyam, J. & Labhasetwar, V. Biodegradable nanoparticles for drug and gene delivery to cells and tissue. *Adv. Drug Deliv. Rev.* **55,** 329–347 (2003).

169. Chen, J., Guo, Z., Tian, H. & Chen, X. Production and clinical development of nanoparticles for gene delivery. *Mol. Ther. Methods Clin. Dev.* **3,** 16023 (2016).

170. Wu, L., Xu, F. & Reinhard, B. M. Nanoconjugation prolongs endosomal signaling of the epidermal growth factor receptor and enhances apoptosis. *Nanoscale* **8,** 13755–13768 (2016).

171. Wang, J., Tian, S., Petros, R. A., Napier, M. E. & Desimone, J. M. The complex role of multivalency in nanoparticles targeting the transferrin receptor for cancer therapies. *J. Am. Chem. Soc.* **132,** 11306–11313 (2010).

172. Yang, H. *et al.* Amino Acid-Dependent Attenuation of Toll-like Receptor Signaling by Peptide-Gold Nanoparticle Hybrids. *ACS Nano* **9,** 6774–6784 (2015).

173. Paviolo, C., Chon, J. W. M. & Clayton, A. H. A. Inhibiting EGFR clustering and cell proliferation with gold nanoparticles. *Small* **11,** 1638–1643 (2015).

174. Kah, J. C. Y. *et al.* Protein coronas on gold nanorods passivated with amphiphilic ligands affect cytotoxicity and cellular response to penicillin/streptomycin. *ACS Nano* **8,** 4608–4620 (2014).

175. Patel, S., Yin, P. T., Sugiyama, H. & Lee, K.-B. Inducing Stem Cell Myogenesis Using NanoScript. *ACS Nano* **9,** 6909–6917 (2015).

176. Rosi, N. L. *et al.* Oligonucleotide-modified gold nanoparticles for intracellular

gene regulation. *Science* **312,** 1027–1030 (2006).

177. Mahmoudi, M. *et al.* Cell 'vision': complementary factor of protein corona in nanotoxicology. *Nanoscale* **4,** 5461–5468 (2012).
178. Verma, A. & Stellacci, F. Effect of surface properties on nanoparticle-cell interactions. *Small* **6,** 12–21 (2010).
179. Rejman, J., Oberle, V., Zuhorn, I. S. & Hoekstra, D. Size-dependent internalization of particles via the pathways of clathrin- and caveolae-mediated endocytosis. *Biochem. J.* **377,** 159–69 (2004).
180. Chithrani, B. D., Ghazani, A. A. & Chan, W. C. W. Determining the size and shape dependence of gold nanoparticle uptake into mammalian cells. *Nano Lett.* **6,** 662–668 (2006).
181. Shang, L., Nienhaus, K. & Nienhaus, G. U. Engineered nanoparticles interacting with cells: size matters. *J. Nanobiotechnology* **12,** 5 (2014).
182. Harush-Frenkel, O., Debotton, N., Benita, S. & Altschuler, Y. Targeting of nanoparticles to the clathrin-mediated endocytic pathway. *Biochem. Biophys. Res. Commun.* **353,** 26–32 (2007).
183. Cho, E. C., Xie, J., Wurm, P. A. & Xia, Y. Understanding the role of surface charges in cellular adsorption versus internalization by selectively removing gold nanoparticles on the cell surface with a I2/KI etchant. *Nano Lett.* **9,** 1080–1084 (2009).
184. Massol, R. H., Boll, W., Griffin, A. M. & Kirchhausen, T. A burst of auxilin recruitment determines the onset of clathrin-coated vesicle uncoating. *Proc. Natl. Acad. Sci. U. S. A.* **103,** 10265–10270 (2006).
185. Wilcox, M. E. *et al.* Reovirus as an Oncolytic Agent Against Experimental AND. 903–912
186. Ivanovic, T. *et al.* Recruitment of cellular clathrin to viral factories and disruption of clathrin-dependent trafficking. *Traffic* **12,** 1179–1195 (2011).
187. Shah, P. N. M. *et al.* Genome packaging of reovirus is mediated by the scaffolding property of the microtubule network. 1–15 (2017). doi:10.1111/cmi.12765
188. Kolb, H. C., Finn, M. G. & Sharpless, K. B. Click Chemistry: Diverse Chemical Function from a Few Good Reactions. *Angew. Chemie - Int. Ed.* **40,** 2004–2021

(2001).

189. Schenk, F. C., Boehm, H., Spatz, J. P. & Wegner, S. V. Dual-functionalized nanostructured biointerfaces by click chemistry. *Langmuir* **30,** 6897–6905 (2014).
190. Ferguson, J. P. *et al.* Deciphering dynamics of clathrin-mediated endocytosis in a living organism. *J. Cell Biol.* **214,** 347–358 (2016).
191. Morris, A. J., Frohman, M. A. & Engebrecht, J. Measurement of phospholipase D activity. *Anal. Biochem.* **252,** 1–9 (1997).
192. van der Schaar, H. M. *et al.* Dissecting the cell entry pathway of dengue virus by single-particle tracking in living cells. *PLoS Pathog.* **4,** e1000244 (2008).
193. Kastritis, P. L. *et al.* Capturing protein communities by structural proteomics in a thermophilic eukaryote. *Mol. Syst. Biol.* **13,** 936 (2017).
194. Bates, M., Huang, B., Dempsey, G. T. & Zhuang, X. Multicolor super-resolution imaging with photo-switchable fluorescent probes. *Science* **317,** 1749–1753 (2007).
195. Bottanelli, F. *et al.* Two-colour live-cell nanoscale imaging of intracellular targets. *Nat. Commun.* **7,** 10778 (2016).
196. Srivastava, A., Lusby, E. W. & Berns, K. I. Nucleotide sequence and organization of the adeno-associated virus 2 genome. *J. Virol.* **45,** 555–564 (1983).
197. Bartlett, J. S., Wilcher, R. & Samulski, R. J. Infectious entry pathway of adeno-associated virus and adeno-associated virus vectors. *J. Virol.* **74,** 2777–2785 (2000).
198. Samulski, R. J. & Muzyczka, N. AAV-Mediated Gene Therapy for Research and Therapeutic Purposes. *Annu. Rev. Virol.* **1,** 427–451 (2014).
199. Summerford, C. & Samulski, R. J. Membrane-associated heparan sulfate proteoglycan is a receptor for adeno-associated virus type 2 virions. *J. Virol.* **72,** 1438–1445 (1998).
200. Pillay, S. *et al.* An essential receptor for adeno-associated virus infection. *Nature* **530,** 108–112 (2016).
201. Robinson, M. S. Forty Years of Clathrin-coated Vesicles. *Traffic* **16,** 1210–1238 (2015).
202. Soto, C. M. *et al.* Fluorescent signal amplification of carbocyanine dyes using

engineered viral nanoparticles. *J. Am. Chem. Soc.* **128,** 5184–5189 (2006).

203. Wang, Q. *et al.* Chemical modification of M13 bacteriophage and its application in cancer cell imaging. *Bioconjug. Chem.* **21,** 1369–77 (2010).
204. Banerjee, D., Liu, A. P., Voss, N. R., Schmid, S. L. & Finn, M. G. Multivalent display and receptor-mediated endocytosis of transferrin on virus-like particles. *ChemBioChem* **11,** 1273–1279 (2010).
205. Kwak, E.-A. & Jaworski, J. Controlled surface immobilization of viruses via site-specific enzymatic modification. *J. Mater. Chem. B* **1,** 3486–3493 (2013).
206. Sakin, V., Paci, G., Lemke, E. A. & Müller, B. Labeling of virus components for advanced, quantitative imaging analyses. *FEBS Lett.* **590,** 1896–1914 (2016).
207. Borsa, J. *et al.* Two modes of entry of reovirus particles into L cells. *J. Gen. Virol.* **45,** 161–170 (1979).
208. Maginnis, M. S. *et al.* NPXY Motifs in the 1 Integrin Cytoplasmic Tail Are Required for Functional Reovirus Entry. *J. Virol.* **82,** 3181–3191 (2008).
209. Chithrani, B. D. & Chan, W. C. W. Elucidating the mechanism of cellular uptake and removal of protein-coated gold nanoparticles of different sizes and shapes. *Nano Lett.* **7,** 1542–1550 (2007).
210. Ferguson, J. P. *et al.* Mechanoregulation of clathrin-mediated endocytosis. *J. Cell Sci.* **130,** 3631–3636 (2017).
211. Sheetz, M. P. Cell control by membrane-cytoskeleton adhesion. *Nat. Rev. Mol. Cell Biol.* **2,** 392–396 (2001).
212. McDonald, D. *et al.* Recruitment of HIV and its receptors to dendritic cell-T cell junctions. *Science* **300,** 1295–1297 (2003).
213. Arrighi, J.-F. *et al.* DC-SIGN-mediated infectious synapse formation enhances X4 HIV-1 transmission from dendritic cells to T cells. *J. Exp. Med.* **200,** 1279–1288 (2004).
214. Daecke, J., Fackler, O. T., Dittmar, M. T. & Krausslich, H.-G. Involvement of clathrin-mediated endocytosis in human immunodeficiency virus type 1 entry. *J. Virol.* **79,** 1581–1594 (2005).
215. Jing, S. Q. & Trowbridge, I. S. Nonacylated human transferrin receptors are rapidly internalized and mediate iron uptake. *J. Biol. Chem.* **265,** 11555–11559

(1990).

216. Summerford, C., Bartlett, J. S. & Samulski, R. J. AlphaVbeta5 integrin: a co-receptor for adeno-associated virus type 2 infection. *Nat. Med.* **5,** 78–82 (1999).

217. Kashiwakura, Y. *et al.* Hepatocyte growth factor receptor is a coreceptor for adeno-associated virus type 2 infection. *J. Virol.* **79,** 609–614 (2005).

218. Wood, L. A., Larocque, G., Clarke, N. I., Sarkar, S. & Royle, S. J. New tools for "hot-wiring" clathrin-mediated endocytosis with temporal and spatial precision. *J. Cell Biol.* 1–15 (2017).

219. Haver, T. O. *A Pragmatic Introduction to Signal Processing*. *University of Maryland at College Park* (2014). doi:ISBN: 9781533372857